Diverse Approaches to Developing Combination Therapies for NF1-Mutant Cancers

Diverse Approaches to Developing Combination Therapies for *NF1*-Mutant Cancers

A dissertation presented

by

Clare Felicity Malone

to

The Division of Medical Sciences

In partial fulfillment of the requirements
for the degree of
Doctor of Philosophy
in the subject of
Genetics

Harvard University
Cambridge, Massachusetts

April 2015

Dissertation Advisor: Karen Cichowski, PhD Clare Felicity Malone

Diverse Approaches to Developing Combination Therapies for *NF1*-Mutant Cancers

Abstract

The *NF1* tumor suppressor is lost or mutated in a variety of sporadic cancers, as well as in the hereditary cancer predisposition syndrome neurofibromatosis type 1 (NF1). NF1 patients have an 8-13% risk of developing a malignant peripheral nerve sheath tumor (MPNST), which are lethal when they cannot be surgically resected. There are currently no effective therapies for *NF1*-mutant cancers. This dissertation focuses on the development of combination therapies using two distinct approaches: inhibiting specific oncogenic signaling pathways activated by *NF1* mutation (or loss), and exploiting cellular stresses in cancer cells.

NF1 encodes a RAS GTPase activating protein. Therefore, when NF1 is lost, RAS pathway signaling is hyper-activated. However, the signaling node or nodes most critical for tumor growth were not known. Here, we report that p110α and mTORC1 are essential for NF1-deficient proliferation, while AKT and mTORC2 are dispensable. Moreover, we demonstrate that sustained inhibition of both the mTORC1 and MEK/ERK pathways is required for MPNST regression. To identify molecular biomarkers of combined target inhibition we performed transcriptional profiling. *GLUT1*, which encodes a glucose transporter, is significantly repressed when both mTORC1 and MEK are inhibited. ^{18}F-FDG uptake is also suppressed, indicating that FDG-PET imaging could be a useful biomarker. A clinical trial based on these findings is being developed.

We have previously found that the combination of ER-stress inducing agents and rapamycin causes MPNST regression. Here, we show that the combination of the histone deacetylase inhibitor vorinostat with rapamycin exploits this same vulnerability and promotes

tumor regression. This effect is dependent on activation of the unfolded protein response and production of reactive oxygen species. The thioredoxin interacting protein TXNIP is upregulated by combined treatment and appears to be a driver of cell death in this context. These studies suggest that the combination of two FDA-approved drugs, rapamycin and vorinostat, could be rapidly translated to clinical trials.

In summary, we have identified two promising combination therapies for *NF1*-mutant cancers. These studies highlight the therapeutic utility of exploiting both signaling and stress vulnerabilities in cancer. These findings have promising clinical applications, and provide a framework for future therapeutic and mechanistic exploration.

Table of Contents

List of Figures

Chapter 1: Introduction

Chapter 2: Defining Key Signaling Nodes and Therapeutic Biomarkers in *NF1*-Mutant Cancers

Chapter 3: HDAC and mTOR Inhibition Cooperate to Drive Irreversible Cell Stress and Tumor Regression

Chapter 4: Conclusions and Future Directions

Appendix A: Effective combination of a next-generation HSP90 inhibitor and an mTOR inhibitor in Malignant Peripheral Nerve Sheath Tumors

Appendix C: Supplementary Materials For Chapter 2

List of Tables

Acknowledgments

First, and foremost, I would like to thank my thesis advisor, Dr. Karen Cichowski. Karen not only guided me in my science, but she also inspired me—I was never more excited about my work than after a meeting with her, and for that I am truly grateful. I have learned so much from her, both professionally and personally.

I would also like to thank the entire Cichowski lab for their friendship and support. I particularly want to thank Sara McLaughlin who taught me almost everything I know, was an excellent rotation advisor and baymate, and continues to be a wonderful friend. I want to thank Pablo Hollstein for his constant enthusiasm about all things science, and for entertaining us all with his “Pablo-isms.” Thomas De Raedt and Ophélia Maertens shared endless knowledge about both NF1 and Belgium with me, for which I am very grateful. I want to thank my afternoon baymate Abby Miller and my honorary morning baymate Becky Lock for many helpful discussions about both science and life. I want to thank Masha Enos for being a loving friend and for letting me get to know her beautiful family. I want to thank Rachel Ingraham for her awesome dancing, and for being a voice of encouragement and reason when I need one. And of course, I want to thank my fellow graduate students: Ryan Kuzmickas, Naomi Olsen, and Steph Guerra. I had so much fun being “senior grad student” to you guys.

I want to thank my dissertation advisory committee: Dr. Alex Toker, Dr. Nathanael Gray, Dr. Brendan Manning, and Dr. Lewis Cantley for their advice along the way, and my thesis defense committee: Dr. Alex Toker, Dr. Kevin Haigis, Dr. David Kwiatkowski, and Dr. Michael Hemann for reading this thesis and carrying out my defense examination.

I would like to thank my roommates, Adrianna San Roman, Amy Rohlfing, and Joanna Hoffmann. I had the most fun living with you guys, and the memories we made at Ellery St will

always be the highlight of my grad school years. I also want to thank my BBS classmates: Ryan Lee, Matt Owen, Ben Morris, Peter Wang, Diane Shiao, Leah Silverstein, Quinn Sievers, and especially Leah Liu. The friendships I gained in grad school are as valuable to me as my PhD. I particularly want to acknowledge Matt Owen for organizing our weekly Thursday lunch. I also want to thank the BBS program office: Kate, Maria, and Danny. You guys are the best part of the BBS program. And of course, I would like to thank my fellow Penguinites and the staff at Penguin Pizza, especially Niall, Christina, and Andrew. It was so important to know we had a reserved table and friendly bartenders when we needed to celebrate the good times or take our minds off the failed experiments.

I want to thank Stephanie Waters: my kindred spirit, my book club, and my longest friend. She has been supporting my dream to be a scientist and listening to me talk about science for the past 15 years and I really appreciate it. I also want to thank Lindsay Rosshirt, who has been an incredible best friend, and who put so much effort into sustaining our friendship even when we were both unbelievably busy.

Above all, I want to thank my incredible family. My parents, Anne and Michael Malone, gave me their constant love and support, and more tangibly, made so many sacrifices to give me the best education I could get. I would not be here without the opportunities they gave me, and the conviction they instilled in me from a young age that higher education is the greatest gift you can receive. I'm so lucky to have parents like you. I want to thank my sister Nora Malone and my brother-in-law Ryan Tetrick. There is research that suggests that the high bar Nora set contributes to my own success, and that's probably true. But more importantly, since the day I was born, Nora has been, and continues to be, my best friend and my biggest role model.

Finally, I want to dedicate this thesis to the memory of Bernard Bénier. He was the kindest *père-d'accueil*. I hope that this body of work honors his memory.

Chapter 1: Introduction

The NF1 tumor suppressor is mutated in a familial cancer syndrome as well as a large number of sporadic cancers. Currently there are no effective therapies for any *NF1*-mutant tumors. Therefore, treatment for NF1-deficient tumors represents a huge unmet clinical need and the focus of this work is to identify novel therapeutic approaches for these tumors. This chapter will provide background on normal NF1 function and regulation of the RAS pathway, and the role of NF1 in disease pathogenesis. Additionally, this chapter will provide information on downstream RAS effector pathways, proteotoxic stress, and oxidative stress, which are three important topics related to the work in this dissertation.

NEUROFIBROMATOSIS TYPE 1

Germline loss of *NF1* causes the inherited cancer predisposition syndrome neurofibromatosis type 1 (NF1). NF1 is an autosomal dominant disorder that affects about 1 in every 3500 births, making it one of the most common monogenic disorders. Approximately 50% of these cases involve *de novo* mutations in *NF1,* while the other half are familial (Huson et al., 1989). NF1 has a penetrance of nearly 100% although the symptoms occur on a spectrum with some patients only mildly affected while others experience significant morbidity and mortality.

Clinical Features of NF1

Patients with NF1 can develop a variety of symptoms (Table 1–1). One of the hallmarks of NF1 is the development of café-au-lait spots. Café-au-lait spots are flat areas of hyper-pigmentation, typically light brown in color, which gives them their name. While they can be associated with a number of inherited disorders including McCune-Albright syndrome, Legius syndrome, and tuberous sclerosis, over 99% of NF1 patients have café-au-lait spots (Ferner et al., 2007). Thus, the number of café-au-lait spots is an important diagnostic feature of NF1.

Table 1–1. Major Clinical Features of NF1. Shown is the frequency (%), and age of onset for the major clinical manifestations of NF1. Adapted from Ferner et al., 2007.

Clinical Manifestation	Frequency (%)	Age of Onset
Café-au-lait patches	>99	Birth to 12 years
Skin-fold freckling	85	3 years to adolescence
Lisch nodules	90-95	> 3 years
Cutaneous neurofibromas	>99	>7 years, usually late adolescence
Plexiform neurofibromas	30-50	Birth to 18 years
Disfiguring facial plexiform neurofibromas	3-5	Birth to 5 years
Malignant peripheral nerve sheath tumor	2-5 (8-13% lifetime risk)	5-75 years
Scoliosis	10	Birth to 18 years
Scoliosis requiring surgery	5	Birth to 18 years
Pseudoarthrosis of tibia	2	Birth to 3 years
Renal artery stenosis	2	Lifelong
Pheochromocytoma	2	>10 years
Severe cognitive impairment (IQ <70)	4-8	Birth
Learning problems	30-60	Birth
Epilepsy	6-7	Lifelong
Optic pathway glioma	15	Birth to 30 years
Cerebral glioma	2-3	Lifelong
Sphenoid wing dysplasia	<1	Congenital

These spots can be present at birth and typically occur within the first five years of life, so they are frequently the first clinical manifestation of NF1. In addition to café-au-lait spots, NF1 patients typically display Lisch Nodules, impaired cognitive development, optic gliomas, and, most commonly, peripheral neurofibromas.

Neurofibromas are benign peripheral nerve tumors and are the defining feature of NF1. They can occur on nerves anywhere in the peripheral nervous system and can be disfiguring, although they are typically not life-threatening. Neurofibromas can be further subdivided into

two classes: (1) dermal neurofibromas and (2) plexiform neurofibromas. Dermal neurofibromas occur in more than 99% of NF1 patients and can range in size from 0.1cm to >3 cm in diameter. NF1 patients frequently have a large number of neurofibromas, which can arise all over the body. Plexiform neurofibromas are less common, but are one of the most debilitating features of NF1 and can result in significant morbidity. Plexiform neurofibromas are larger and more extensive than dermal neurofibromas. They invade nearby tissue and organs causing significant disfigurement, pain, and loss of nerve or body function (Korf, 1999). While these tumors are benign, unlike dermal neurofibromas, plexiform neurofibromas can undergo malignant transformation into malignant peripheral nerve sheath tumors (MPNST), which are discussed in detail below (Ferner et al., 2007).

NF1-Associated Tumors

In addition to the neurofibromas discussed above, NF1 patients develop a number of other tumor types at a higher rate than the general population. Optic pathway gliomas are one of the most common lesions associated with NF1, occurring in 15% of NF1 patients (Ferner et al., 2007). These gliomas are typically low grade and many are asymptomatic, however in more than a third of cases patients will experience visual impairment or blindness (Balcer et al., 2001). NF1 patients are also at elevated risk for developing gastrointestinal stromal tumors (GIST) and pheochromocytomas (Erem et al., 2007; Maertens et al., 2006). Several myeloproliferative disorders also occur at an increased rate in NF1 patients, most notably juvenile myelomonocytic leukemia (JMML) (Lauchle et al., 2006). NF1 patients have an 8–13% lifetime risk of developing a malignant peripheral nerve sheath tumor (MPNST), which is a significantly elevated risk relative to that of the general population where the lifetime risk is approximately 0.001% (Evans et al., 2002). Indeed, MPNSTs represent 10% of all sarcomas, and more than 50% of MPNSTs occur in NF1 patients (Doorn et al., 1995). Furthermore, the average age at diagnosis in the NF1 population is only 26 years, compared with 62 years in the

general population (Evans et al., 2002). MPNSTs, which are the focus of this dissertation and are described in detail below, are the leading cause of death in NF1-patients and represent a huge unmet clinical need for this population.

MALIGNANT PERIPHERAL NERVE SHEATH TUMORS

MPNSTs are soft tissue sarcomas that develop along peripheral nerves. The cell of origin of MPNSTs appears to be a Schwann cell precursor cell type (Chen et al., 2014; Gupta and Maniker, 2007). Histologically, MPNSTs are poorly differentiated and exhibit a wide range of potential features, but most typically they contain whorling spindle-like cells (Gupta and Maniker, 2007). MPNSTs can arise from major or minor nerve branches or from the nerve sheath, and can be associated with many nerves although the most common nerve of origin is the sciatic nerve (Ducatman et al., 1986). MPNSTs are poorly encapsulated and locally invasive, often extending along the axis of the nerve and into neighboring soft tissue (Kumar et al., 2009). They can arise anywhere on the body: 46% arise on the trunk, 34% arise on extremities, and 19% arise in the head/neck region (Ducatman et al., 1986). MPNSTs are extremely aggressive tumors, and frequently metastasize. As discussed below, MPNSTs do not significantly respond to conventional chemotherapy, and MPNSTs remain the leading cause of death among NF1-patients (Evans et al., 2002; Porter et al., 2009; Zehou et al., 2013).

Diagnosis and Clinical Management of MPNSTs

In NF1 patients, MPNSTs can arise from pre-existing non-malignant plexiform neurofibromas, or they can arise spontaneously (Ducatman et al., 1986). Early detection of an MPNST is critical for patient outcome, as the size of the MPNST at diagnosis is one of the biggest predictors of prognosis (Gupta and Maniker, 2007). However, the diagnosis of an MPNST is complicated by the presence of non-malignant peripheral nerve tumors in NF1 patients. Plexiform neurofibromas must be monitored carefully for potential malignant

transformation. MPNSTs are more metabolically active than non-malignant pre-cursor tumors, so ^{18}F-fluorodeoxyglucose (^{18}F-FDG) uptake measured by positron emission tomography (PET) imaging is an important clinical tool for distinguishing between benign and malignant tumors. Elevated SUV_{max}, a quantitative readout of FDG-uptake, is significantly correlated with MPNSTs and has an 89% sensitivity and a 95% specificity (Benz et al., 2010). The characteristic high glucose uptake of MPNSTs is important for findings in Chapter 2 of this thesis.

Unfortunately at the time of presentation most MPNSTs are already quite large (>5cm in size) and in up to 50% of cases have already metastasized (Farid et al., 2014). As treatment options are limited, patients with MPNSTs have a poor 5-year survival ranging between 15-50% (Farid et al., 2014). Complete surgical resection with clear margins remains the treatment of choice for MPNSTs, although MPNSTs are not always resectable (Widemann, 2009). Even in cases where MPNSTs can be resected, there is local recurrence in 32–65% of cases after an average of 5 to 32.2 months (Baehring et al., 2003; Doorn et al., 1995; Ducatman et al., 1986; Gupta and Maniker, 2007). Unfortunately when complete resection is not achieved, which occurs in about 70% of cases, MPNSTs are uniformly lethal (Evans et al., 2002; Zehou et al., 2013). Conventional chemotherapy can prolong progression free survival but does not appear to improve overall survival (Porter et al., 2009). Treatment options remain limited for metastatic, unresectable, or recurrent MPNSTs, although several investigational agents, many from our laboratory, are in clinical trials and will be discussed in detail later in this chapter.

MPNST Pathogenesis

Inactivation of both *NF1* alleles seems to be an early and requisite step in tumorigenesis. Benign neurofibromas display loss of heterozygosity (LOH) of *NF1,* and progression to an MPNST requires further alterations, most notably those involved in cell cycle control. Loss of *p53* is frequent in MPNSTs, through both mutation and deletion, and this is not observed in benign neurofibromas (Birindelli et al., 2001; Frahm et al., 2004; Jhanwar et al.,

1994; Koga et al., 2002; Legius et al., 1994; Leroy et al., 2001; Liapis et al., 1999; Menon et al., 1990; Rasmussen et al., 2000). Mutations in *CDK2NA*, the gene encoding both $p16^{INK4A}$ and $p19^{ARF}$, are also reported at high levels, with mutations in 75% and 60% of MPNSTs, respectively (Berner et al., 1999; Kourea et al., 1999). Loss of other cell cycle genes including *RB1, MDM2, CDK4, CDKN2B,* and *CCND2* are also reported in MPNSTs, demonstrating that loss of cell cycle regulation is an important step in malignant transformation (Berner et al., 1999). The tumor suppressor PTEN may also contribute to tumorigenesis as protein levels are low in many human MPNSTs (Gregorian et al., 2009).

Mouse Models of MPNSTs

Genetically engineered mouse models of MPNSTs have provided further insight into cooperating mutations and provide pre-clinical models for therapeutic testing. Unlike humans, mice that are heterozygous for *Nf1* (*$Nf1^{+/-}$*) do not develop MPNSTs (Brannan et al., 1994; Jacks et al., 1994). Homozygous deletion of *Nf1* is embryonic lethal, and chimeric *$Nf1^{-/-}Nf1^{+/+}$* mice develop plexiform neurofibromas, but not MPNSTs (Cichowski et al., 1999). Similarly, mouse models with floxed *Nf1* and Cre driven by Plp, Dhh, and Krox20 develop plexiform neurofibromas but not MPNSTs (Mayes et al., 2011; Wu et al., 2008; Zhu et al., 2002) This is likely due to the fact that mutation in a secondary pathway is required for MPNST development, as benign lesions in humans are *NF1* null as well. Mice that are heterozygous for both *Nf1* and *p53* develop MPNSTs with an average latency of 5 months, but only when these deletions are *in cis,* as *Nf1* and *p53* are closely linked in the mouse. These mice (NPcis mice) consistently lose both of the wild type *Nf1* and *p53* alleles in the tumors they develop, therefore they genetically and histologically recapitulate human MPNSTs (Cichowski et al., 1999). The tumors develop with a relatively short latency (5 months) and the tumors are very aggressive (on average they reach maximal size within 10-15 days). Therefore the NPcis model is a useful pre-clinical tool, and pre-clinical testing of therapies using this model is a major focus of this

dissertation. Another mouse model of MPNSTs has since been developed, which demonstrates that other "second-hit" mutations can also contribute to MPNST pathogenesis. About 26% of mice that are heterozygous for *Nf1* and deficient for both *Ink4a* and *Arf* (*Nf1*$^{+/-}$ *Ink4a/Arf*$^{-/-}$) develop MPNSTs with a latency similar to the NPcis model (Joseph et al., 2008).

THE NF1 TUMOR SUPPRESSOR

The 350 kb gene encoding human NF1 is located on chromosome 17 (chromosomal region 17q11.2). *NF1* encodes a relatively large protein of 2839 amino acids known as neurofibromin (Figure 1–1). The RAS GAP related domain (GRD) is a 332 amino acid stretch

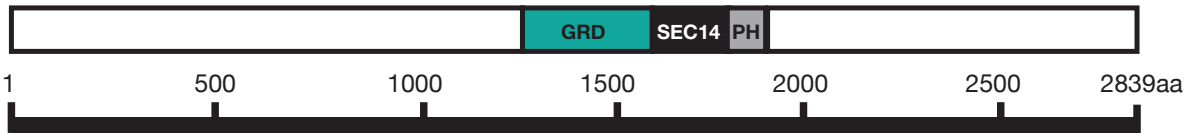

Figure 1–1. Schematic of NF1 Protein Domains. NF1 is a 2839 amino acid protein with a GAP-related domain (GRD), a SEC14-like lipid-binding domain (SEC14), and a plekstrin homology domain (PH). Adapted from Bernards et al., 2003.

near the middle of the protein (Bernards, 2003). This domain directly interacts with RAS and promotes RAS hydrolysis of GTP to GDP, which is discussed in detail below (Martin et al., 1990). Neighboring the GRD, there is a SEC14-like lipid-binding domain (SEC14), followed by a plekstrin homology domain (PH), which is thought to be involved in membrane localization, but the majority of the protein contains regions of unknown function. Expression of the GRD in many contexts is sufficient to restore tumor suppressive function, suggesting that many of the effects of NF1-loss may be mediated by RAS, as discussed below (Hiatt et al., 2001; Johannessen et al., 2008). Moreover, missense point mutations in the GRD are found in NF1

patients and are sufficient to cause disease (Klose et al., 1998). Nevertheless, it is possible that NF1 has other functions that have not been discovered yet.

NF1 was originally described as a tumor suppressor in the context of neurofibromatosis type 1, however it is now clear that NF1 also functions as a tumor suppressor in sporadic cancer. *NF1* mutations have now been reported in a wide variety of human cancers (Figure 1–2, TCGA). While these mutations may not all be inactivating mutations, further studies in

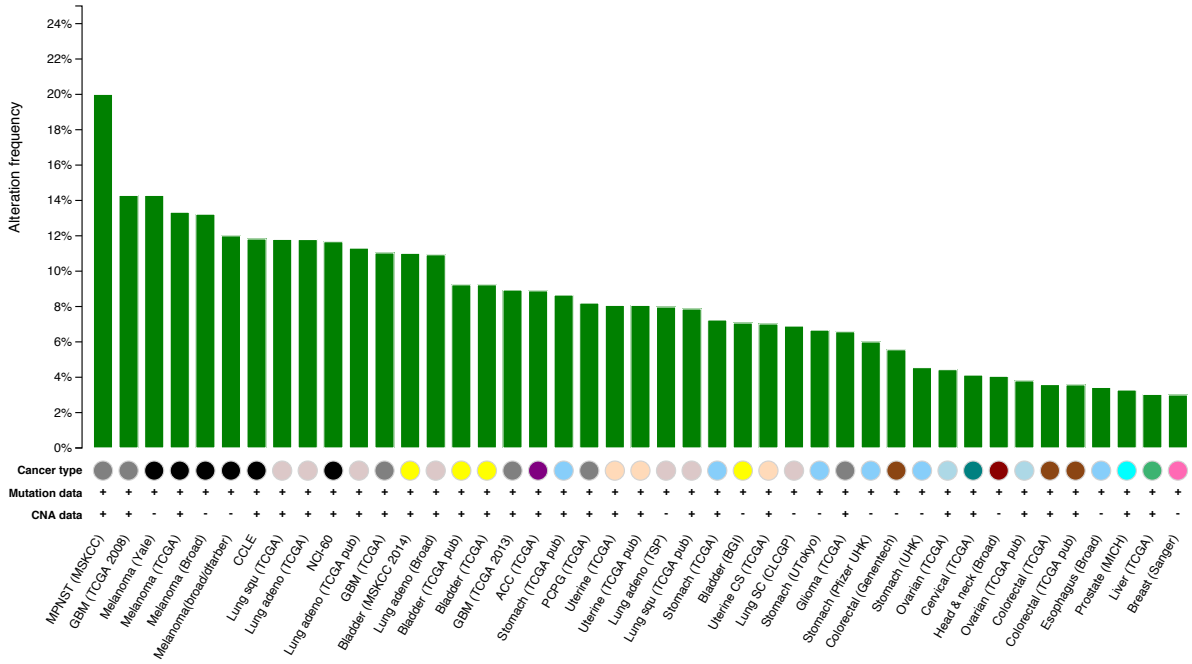

Figure 1–2. *NF1* Mutations across Cancer Types. Graph shows the frequency of NF1 mutations in various cancers. Data sets with lower than a 3% mutation rate are not shown. Data are from the TCGA and cBioPortal (Cerami et al. 2012, Gao et al. 2013).

glioblastoma, non-small cell lung cancer (NSCLC), and melanoma demonstrate that NF1 does function as a tumor suppressor (Boudry-Labis et al., 2013; Ding et al., 2008; Hölzel et al., 2010; Maertens et al., 2013; McGillicuddy et al., 2009; Parsons et al., 2008). Importantly, NF1 expression can also be regulated by non-genetic mechanisms including proteosomal degradation, which is frequently observed in glioblastoma (McGillicuddy et al., 2009). Therefore

the number of mutations shown in Figure 1-2 may under-represent the frequency of *NF1* inactivation in sporadic cancer.

Nearly 1500 point mutations in *NF1* capable of causing NF1 have been identified, as well as single or multiple exon deletions, micro deletions, micro insertions, and large insertions (Abramowicz and Gos, 2014). Mutations in *NF1* are relatively evenly spread throughout the protein from exon 3 to intron 47, with no known mutational hotspots (Jeong et al., 2006; Ko et al., 2013). Interestingly, sporadic mutations in *NF1* are also distributed throughout the gene without any clear hotspot mutations (Figure 1-3).

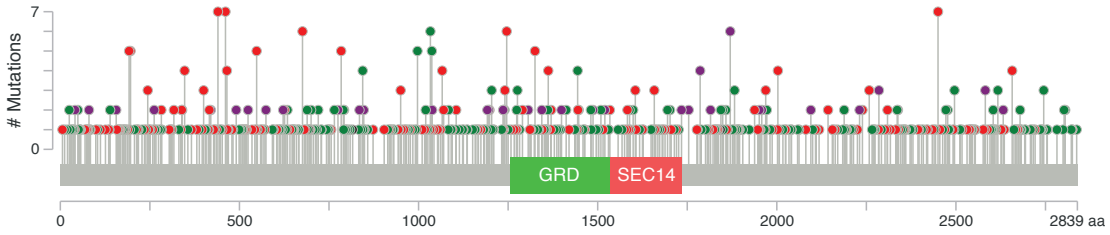

Figure 1–3. Spectrum of *NF1* Mutations in Human Cancer. Shown are the sites of mutations identified in human cancer. Red circles indicate truncating mutations, green circles indicate missense mutations, black circles indicate in-frame mutations, and purple circles indicate sites that are affected by different mutation types at the same frequency. The y-axis indicates the number of mutations identified at a given residue. The green box indicates the general location of the GRD. The red box indicates the general location of the SEC14 domain. Figure is adapted from the cBio Portal and data is from the TCGA database (Cerami et al. 2012, and Gao et al. 2013).

NEUROFIBROMIN AND THE RAS PATHWAY

NF1 is a negative regulator of the RAS pathway. The RAS pathway is a critical regulator of normal cell growth and homeostasis, linking extracellular growth signals to intracellular effector pathways. The RAS superfamily contains approximately 150 low molecular weight GTPases. There are over thirty *RAS* genes, however only three of these, HRAS, KRAS, and NRAS have an established role in cancer.

The RAS proteins have critical roles in normal growth and proliferation. Therefore their activity must be tightly regulated. RAS itself is a small GTPase, which switches between a GDP-bound inactive state, and a GTP bound active state, with the GDP/GTP state essentially functioning as an on/off switch. Two classes of proteins control RAS activity: the RAS guanine exchange factors (RAS GEFs), and the RAS GTPase activating proteins (RAS GAPs). The RAS GEFs promote the exchange of GDP for GTP, allowing RAS to become activated (Figure 1–4). Conversely, the RAS GAPs catalyze the GTPase activity of RAS allowing hydrolysis of GTP to GDP and effectively turning off RAS activity.

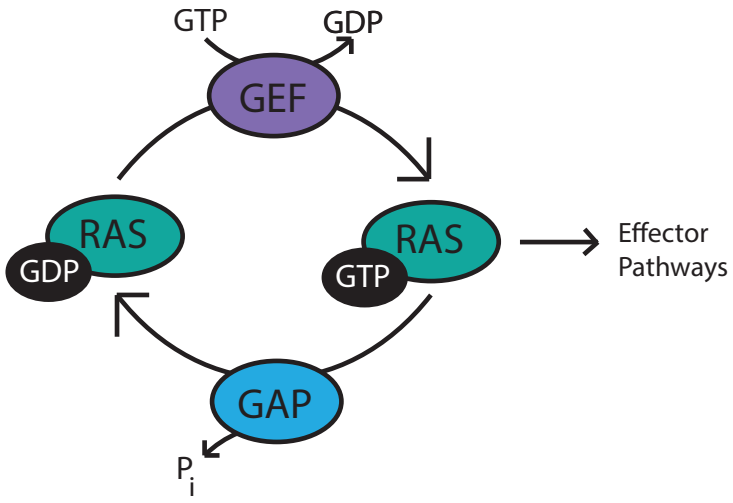

Figure 1–4. Regulation of RAS Activity by RAS GEFs and RAS GAPs RAS switches between an inactive GDP-bound state and an active-GTP bound state. The conversion of GTP to GDP is catalyzed by RAS GAPs, inactivating RAS. Conversely, RAS GEFs promote the exchange of GDP for GTP, activating RAS and allowing RAS to signal to downstream effectors.

RAS Pathway Deregulation in Human Cancer

The RAS pathway is one of the most frequently altered pathways in human cancer. Mutations in the H-, K-, and NRAS isoforms occur in approximately 20-30% of all human cancers, with mutation rates exceeding 90% in certain subtypes of cancer such as pancreatic cancer. Most mutations in *RAS* itself fall into two classes of mutations, point mutations

affecting codons 12 or 13, and point mutations in codon 61. Both classes are considered activating mutations, although the mechanism is distinct. Mutations in codons 12 and 13 do not affect the active site of RAS, but instead impairs RAS binding to GAPs, and GAP binding can no longer promote GTPase activity. As intrinsic RAS GTPase activity is limited, this effectively leads to constitutive activation of RAS with no regulation by the RAS GAPs. Codon 61 is located in the active site of RAS and mutations in this codon impair the catalytic site and block GTPase activity. While mutations in *RAS* itself are common, upstream regulators of RAS and downstream effectors of RAS are also frequently mutated in human cancer.

In addition to mutations in *RAS* itself, it has been proposed that RAS GEFs and RAS GAPs could function as oncogenes and tumor suppressors respectively. Inherited mutations in SOS1, a RAS GEF, cause a congenital disorder called Noonan syndrome. Noonan syndrome patients are at an elevated risk for some type of cancer including JMML. However, to date no mutations in RAS GEFs have been identified in sporadic cancers, suggesting that the oncogenic potential of these proteins is limited. In contrast, there is a growing body of evidence to suggest that a number of RAS GAPs can and do function as tumor suppressors in human cancer.

As discussed above, NF1 is an established tumor suppressor, both for its role in the inherited cancer predisposition syndrome neurofibromatosis type 1, and in sporadic cancer. In addition to NF1, our lab has shown that DAB2IP and RASAL2 function as tumor and metastasis suppressors in prostate cancer and breast cancer, respectively (McLaughlin et al., 2013; Min et al., 2010).

RAS EFFECTOR PATHWAYS

Because NF1 is a negative regulator of RAS, the pathogenesis of NF1-deficient tumors is driven, at least in part, through aberrant activation of the RAS pathway. RAS mediates its

effects through activation of a variety of downstream pathways that affect cell growth, proliferation, and survival among other critical processes (Figure 1–5). RAS has been demonstrated to regulate many effector pathways, but the extracellular signal-regulated kinase (ERK) and phosphotidylionsitol 3-kinase (PI3K) pathways appear most critical for the pathogenesis of human cancer.

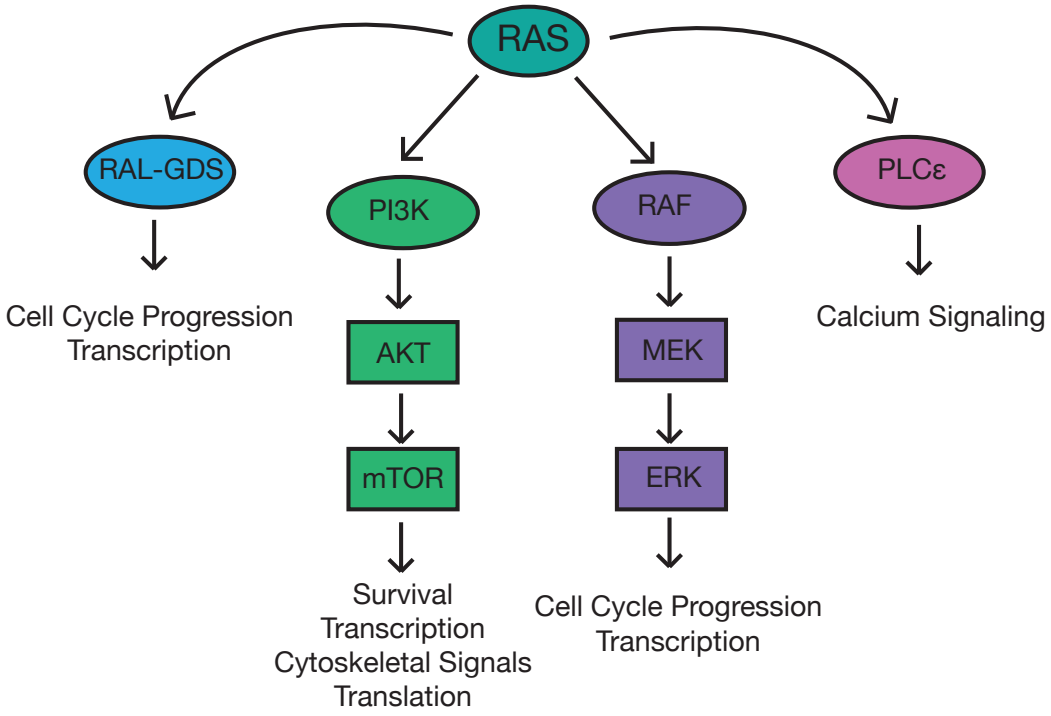

Figure 1–5. RAS Effector Pathways Regulate Cellular Growth and Proliferation. Schematic showing the main downstream effector pathways activated by RAS, RAL-GDS, PI3K, RAF and PLCε, which jointly regulate cell cycle progression, transcription, survival, and calcium signaling, among other processes. Adapted from Downward et al., 2003.

PI3K/AKT/mTOR Signaling

PI3K consists of a p110 catalytic subunit and a p85 regulator subunit. There are three Class IA catalytic isoforms of PI3K: p110α, p110β and p110δ which are encoded by distinct genes: *PIK3CA, PIK3CB, and PIK3CD,* respectively. p110α and p110β are ubiquitously expressed, while p110δ shows a more limited expression pattern, mostly limited to white blood

cells and neurons (Bi et al., 1999; 2002; Chantry et al., 1997; Eickholt et al., 2007; Geering et al., 2007; Hu et al., 1993; Vanhaesebroeck et al., 1997). *PIK3CA* is mutated in approximately 15% of human cancers with higher incidence in specific cancer subtypes (Karakas et al., 2006). Overexpression studies and gene deletion experiments have demonstrated that hotspot mutations in *PIK3CA* are in fact oncogenic as they induce transformation of primary fibroblasts, allow anchorage independent growth, and promote tumor formation in animal models (Bader et al., 2006; Ikenoue et al., 2005; Isakoff et al., 2005; Kang et al., 2005; Samuels et al., 2005; Zhao and Vogt, 2008). Somatic mutations in *PIK3CB* and *PIK3CD* are notably absent from human cancer (Thorpe et al., 2015). However, overexpression of wild type p110β and p110δ is sufficient to induce cellular transformation (Kang et al., 2006), in contrast to wild type p110α, which is not a sufficient oncogenic signal in primary fibroblasts suggesting that mutations may not be necessary for p110β and p110δ to act as oncogenes, which is supported by their frequent over expression in human cancer (Thorpe et al., 2015).

The enzymatic activity of all three isoforms is identical, however they appear to have non-redundant roles in human cancer. As described, *PIK3CA* mutations are relatively common. However, it was recently shown that p110β appears to be the primary isoform responsible for oncogenic activity in the context of *PTEN* deficiency (Jia et al., 2008). Furthermore, p110δ activity appears to be the primary isoform functioning in hematopoietic cancers, as p110δ-specific inhibitors show profound anti-cancer activity in B-cell malignancy cell lines (Herman et al., 2010; Hoellenriegel et al., 2011; Ikeda et al., 2010; Lannutti et al., 2011; Meadows et al., 2012). Isoform-specific inhibitors against all three isoforms are being developed and are likely to have unique applications in human cancer.

RAS drives the PI3K signaling pathway through direct interaction with the p110 catalytic subunit (Pacold et al., 2000; Rodriguez-Viciana et al., 1994). This interaction leads to conformational changes and the translocation of PI3K to the cellular membrane where it can

phosphorylate phosphtidylinostiol-4,5-biphosphate (PIP_2) resulting in the formation of phosphatidylinositol-3,4,5-triphosphate (PIP_3). PIP_3 can be converted back into PIP_2 by the phosphatase PTEN. In addition to activating mutations in *PIK3CA* and over-expression of p110β and p110δ, loss of *PTEN* is also common in human cancer, including MPNSTs as discussed above.

When activated, PIP_3 interacts with a large number of downstream proteins, but most notably leads to activation of AKT by PDK1 through binding to AKT at the plasma membrane allowing PDK1 to phosphorylate AKT on threonine 308 (T308). This phosphorylation event is sufficient for AKT phosphorylation of many target proteins, but full activation of AKT requires a second phosphorylation event on serine 473 (S473) by mTORC2 (Loewith et al., 2002; Sarbassov et al., 2005). This second phosphorylation event allows AKT to activate its full spectrum of target proteins.

One of the key substrates of activated AKT is tuberous sclerosis protein 2, or tuberin (TSC2) (Manning et al., 2002). There are at least five known AKT phosphorylation sites on TSC2, and phosphorylation of all five is necessary for full mTORC1 activation (Inoki et al., 2002; Manning et al., 2002; Potter et al., 2002). TSC2, together with tuberous sclerosis protein 1, or hamartin (TSC1) forms a complex that negatively regulates mTORC1 signaling (Tee et al., 2002). Phosphorylation of TSC2 by AKT releases the suppression of the TSC complex on mTORC1, thus leading to activated mTORC1 signaling. Phosphorylation of TSC2 releases it from the lysosomal membrane where mTORC1 and RHEB are located (Menon et al., 2014). When TSC2, a RHEB-GAP, is present, RHEB is maintained in an inactive state and cannot activate mTORC1, but once TSC2 is released from the membrane more RHEB is in the active GTP-bound state, which in turn activates mTORC1. NF1 loss leads to hyperactivation of mTORC1, which is critical for NF1-deficient cell growth, underscoring the importance of this pathway (Johannessen et al., 2008; 2005).

mTOR Complex 1 and mTOR Complex 2

mTOR exists in two distinct complexes: mTOR complex 1 (mTORC1) and mTOR complex 2 (mTORC2) (Figure 1–6). While mTOR is the catalytic subunit of both complexes,

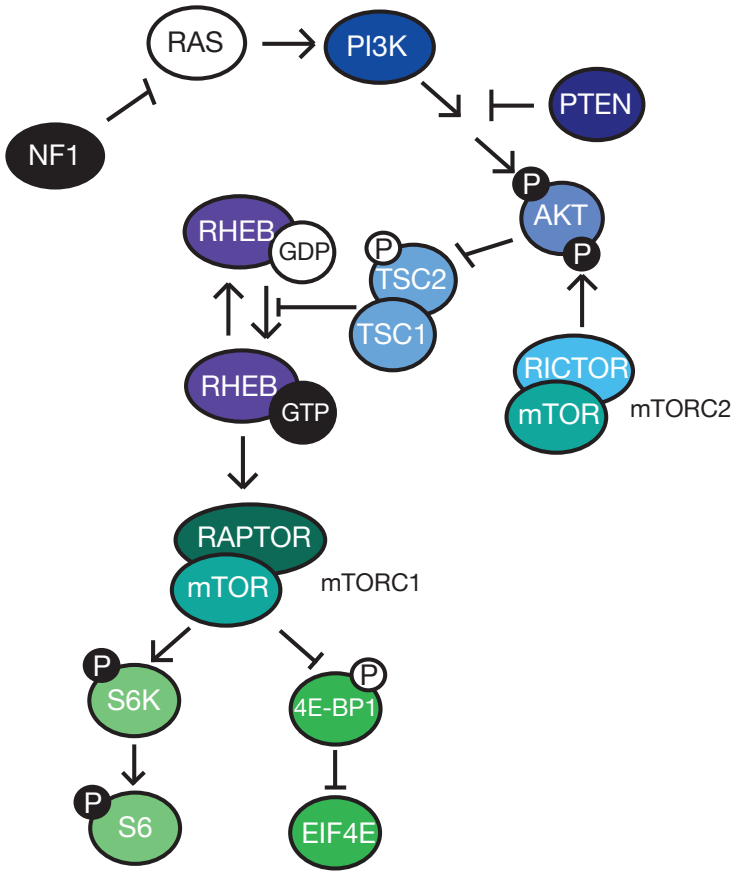

Figure 1–6. mTORC1 and mTORC2 are Functionally Distinct Complexes. Shown is a diagram of mTORC1 and mTORC2 functions. mTORC2 phosphorylates AKT on S473, allosterically activating AKT. mTORC1 phosphorylates S6Kinase (S6K) and 4E-BP1, activating S6K and inhibiting 4E-BP1 function. Activating phosphorylation events are shown in black and inhibitory phosphorylation events are shown in white. For simplicity, a single phosphorylation event is shown, although in many cases there are multiple phosphorylation sites. Also for simplicity, only RAPTOR and RICTOR component proteins of mTORC1 and mTORC2 are shown.

each complex contains distinct obligate subunits and has distinct functions (Loewith et al., 2002). mTORC1 consists of RAPTOR and mLST8/GβL. PRAS40 and DEPTOR can also interact with mTORC1, but appear to be recruited to the complex to suppress mTORC1 activity and thus are not essential for catalytic function (Peterson et al., 2009; Thedieck et al., 2007). The

exact role of RAPTOR and mLST8 is still unclear, but RAPTOR is required for proper mTORC1 function. mTORC1 activity is directly regulated by RHEB and TSC2 as discussed above. In addition to regulation by growth factors through RAS and PI3K, mTORC1 activity is also regulated by nutrient and energy levels.

mTORC1 is a master regulator of cellular growth and metabolism. mTORC1 positively regulates protein translation, lipid synthesis, and mitochondrial metabolism, and negatively regulates autophagy (Düvel et al., 2010; Fingar and Blenis, 2004; Hay and Sonenberg, 2004; Laplante and Sabatini, 2009; Morita et al., 2015). mTORC1 regulates these processes by phosphorylating a number of targets, including ULK1, 4-EBP1, and p70S6kinase (Hara et al., 1997; Kim et al., 2011; Park et al., 2002; Price et al., 1992). mTORC1 activation also leads to the phosphorylation of eIF4G, although this may be indirect (Raught et al., 2000). The phosphorylation of 4-EBP1 releases eIF4E from 4-EBP1 suppression allowing cap-dependent protein translation to occur (Ma and Blenis, 2009). On the other hand, the phosphorylation of p70S6kinase is an activating event that allows p70S6kinase to phosphorylate its targets including ribosomal protein S6 (Fingar et al., 2004).

mTORC2 is comprised of RICTOR, SIN1, and mLST8/GβL. DEPTOR, PROTOR, and PRR5L have also been found to associate with mTORC2 (Pearce et al., 2007; Peterson et al., 2009; Thedieck et al., 2007; Woo et al., 2007). mTORC2 phosphorylates AGC kinases such as AKT, PKC, and SGK and allosterically activates them. This phosphorylation event is in addition to a catalytically activating phosphorylation event by PDK1 on AGC kinases, and is required for these kinases to interact with their full spectrum of substrates (Oh and Jacinto, 2011). mTORC2 seems to regulate a number of critical cellular processes including protein synthesis, cellular survival, and actin organization, although the mechanism of how mTORC2 regulates some of these processes remains elusive (Jacinto et al., 2004; Oh and Jacinto, 2011; Oh et al., 2010; Sarbassov et al., 2004).

The ERK Pathway

The first identified RAS effector protein is the serine/threonine kinase RAF (Moodie et al., 1993; Vojtek et al., 1993; Warne et al., 1993; Zhang et al., 1993). There are three closely related RAF isoforms: ARAF, BRAF, and CRAF. When RAS is in its active GTP-bound state, it can directly bind RAF and leads to translocation of RAF to the plasma membrane, which contributes to activation of RAF. RAF activation induces a kinase phosphorylation cascade, beginning with the phosphorylation of its direct targets, the mitogen activated kinase kinases 1 and 2 (MEK1 and MEK 2), which in turn phosphorylate and activate extracellular signal-regulated kinases 1 and 2 (ERK1 and ERK2), which are also referred to as the mitogen activated kinases 1 and 2 (Kolch, 2005). ERK has a wide variety of substrates that are both nuclear and cytoplasmic. ERK can directly phosphorylate a number of transcription factors including ETS-1, c-MYC, and c-JUN. Through this direct transcription factor phosphorylation, as well as indirect regulation such as the phosphorylation of RSK, which then activates the transcription factor CREB, ERK activation drives a transcriptional program that promotes cell-cycle progression. ERK is also hyper-activated in *NF1*-mutant tumors, as discussed in detail below.

TARGETING RAS AND RAS EFFECTOR PATHWAYS IN CANCER

Given its role in human cancer, there has been much interest in RAS inhibition. Ablation studies have demonstrated that many cancers have a dependency on RAS signaling, validating RAS as a therapeutic target (Chin et al., 1999; Fisher et al., 2001; Singh et al., 2009; Ying et al., 2012). RAS has a picomolar affinity for GTP, and cellular concentrations of GTP are very high, so developing inhibitors that can outcompete for GTP binding has not been possible (John et al., 1990). Recently two inhibitors of KRAS with the G12C mutation have been identified: an allosteric inhibitor that alters RAS affinity for GTP and a covalent irreversibly binding GDP

analogue (Lim et al., 2014; Ostrem et al., 2013). These inhibitors rely on the unique ability of cysteine to interact with molecules that contain disulfide, and thus are only effective on the mutations that cause an amino acid change to cysteine, but not wild type RAS or mutations that lead to other amino acid changes. To date, there are no inhibitors that can directly target wild type RAS.

An alternative approach has focused on post-translational modification of RAS. RAS must be localized at the cellular membrane in order to have oncogenic activity (Willumsen et al., 1984). RAS prenylation is required for translocation of RAS to the membrane and activation of many effector pathways. Farnesyl transferase inhibitors have been developed, but unfortunately they have not proved to be clinically useful, likely because while HRAS appears to be inhibited, both KRAS and NRAS can be geranylgeranylated when farnesyl transferases are inhibited and this still yields proper cellular localization of these RAS isoforms.

The farnesyl transferase inhibitor Tipifarnib was tested in a clinical trial in children and young adults with NF1 and plexiform neurofibromas, but, as with most FTIs that have been tested clinically, this did not prolong time to progression likely because they are not inhibiting all RAS isoforms (Widemann et al., 2014). Because effectively targeting RAS itself has not yet proved possible, a large number of agents targeting RAS effector pathways have been developed, many of which are in clinical trials.

Inhibitors are either approved or in clinical development for all members of the PI3K/AKT/mTOR pathway (Table 1–2). The p110δ-specific inhibitor idelalisib is the only clinically approved PI3K inhibitor, but both pan-PI3K inhibitors as well as isoform-specific inhibitors against p110α, p110β, and p110δ are currently in clinical trials for a variety of oncology indications. A number of AKT inhibitors have also been developed and are in early stage clinical trials. Allosteric inhibitors against mTORC1 including rapamycin (sirolimus) and the rapalogs (everolimus, temsirolimus, ridaforlimus) are FDA-approved for a variety of

Table 1–2. Inhibitors for the PI3K/AKT/mTOR Pathway in Clinical Development. Shown are inhibitors against PI3K, AKT, and mTOR and their current stage in clinical trials. Compiled from the NCI Drug Encyclopedia and clinicaltrials.gov.

Agent	Target(s)	Clinical Status
mTOR INHIBITORS		
Sirolimus (rapamycin)	mTORC1 (allosteric)	FDA-approved
Everolimus	mTORC1 (allosteric)	FDA-approved
Temsirolimus	mTORC1 (allosteric)	FDA-approved
Ridaforolimus	mTORC1 (allosteric)	FDA-approved
MLN0128/INK128	mTORC1/2	Phase I
OSI-027	mTORC1/2	Phase II
CC-223	mTORC1/2	Phase II
DS-3078a	mTORC1/2	Phase I
AZD 2014	mTORC1/2	Phase II
PI3K INHIBITORS		
Buparlisib (BKM120)	Pan-PI3K (class 1)	Phase III
Copanlisib (BAY80-6946)	Pan-PI3K (class 1)	Phase III
Pictilisib (GDC-0941)	Pan-PI3K (class 1)	Phase II
SAR245408	Pan-PI3K (class 1)	Phase II
ZSTK474	Pan-PI3K (class 1)	Phase I
BYL719	PI3K p110α	Phase I/II
MLN1117/INK1117	PI3K p110α	Phase I
AZD 8835	PI3K p110α	Phase I
Taselisib	PI3K p110α	Phase I
BAY1082439	PI3K p110α/β	Phase I
GSK2636771	PI3K p110β	Phase I/II
SAR260301	PI3K p110β	Phase I/II
Idelalisib (CAL-101)	PI3K p110δ	FDA-approved
INCB040093	PI3K p110δ	Phase I
AMG 319	PI3K p110δ	Phase I
TGR 1202	PI3K p110δ	Phase I
IPI-145	PI3K p110δ/γ	Phase III
RP6530	PI3K p110δ/γ	Phase I
DUAL INHIBITORS		
SAR245409	PI3K/mTORC1/2	Phase I/II
GDC-0980	PI3K/mTORC1/2	Phase II
VS-5584	PI3K/mTORC1/2	Phase I
PKI-587/ PF-05212384	PI3K/mTORC1/2	Phase I/II
DCBCI0901	PI3K/mTORC1/2	Phase I
DS-7423	PI3K (p110α)/mTORC1/2	Phase I
AKT INHIBITORS		
MK-2206	Pan-AKT	Phase II
Afuresertib (GSK2110183)	Pan-AKT	Phase II
Ipatasertib (GDC-0068)	Pan-AKT	Phase II
ARQ 092	Pan-AKT	Phase I
BAY1125976	AKT1/2	Phase I
RX-0201	AKT1	Phase I/II
AZD-5363	Pan-AKT	Phase II
GSK 2141795	Pan-AKT	Phase II
LY-2780301	AKT/p70S6K	Phase I/II

indications. Rapamycin and other rapalogs function by creating a complex with the mTOR binding protein FKBP12, which then binds to mTORC1 near the catalytic site of mTOR, exclusively inhibiting mTORC1 kinase activity. mTOR kinase inhibitors, which are active against mTORC1 and mTORC2 are in clinical development. Finally, dual-specificity inhibitors that target the kinase activity of both PI3K and mTOR are also being investigated clinically, although none have been approved to date.

The PI3K/AKT/mTOR axis is known to be hyper-activated when NF1 is lost (Johannessen et al., 2005). Furthermore, mTORC1 has been demonstrated to be critical for proliferation of *NF1*-deficient MPNSTs, and mTORC1 inhibition has a cytostatic effect on MPNSTs in a genetically engineered mouse model (Johannessen et al., 2008). Currently mTOR inhibitors are being evaluated in clinical trials for plexiform neurofibromas (NCT00652990, NCT01365468). While the results of these trials are not yet published, they have been presented publically and indicate that mTOR inhibitors seem to be producing a cytostatic response, as was seen in the mouse model. An additional trial combining everolimus and the angiogenesis inhibitor bevacizumab is entering Phase II as a result of observations in our lab that tumors treated with mTOR inhibitors long-term become highly de-vascularized. (NCT01661283).

These data suggest that the components of this pathway are potentially good therapeutic targets, however it remains unclear which signaling nodes represent the most critical therapeutic targets. Given the large number and variety of agents being investigated clinically, a better understanding of the pathway components and their relative contribution to the pathogenesis of *NF1*-mutant cancer is critical for selecting the best therapeutic combinations. This problem is the focus in Chapter 1 of this thesis.

The ERK pathway is similarly hyper-activated when NF1 is lost. As with the PI3K/AKT/mTOR pathway, a number of clinical agents targeting these signaling nodes have been or are being

clinically developed (Table 1–3). The RAF inhibitors sorafenib, dabrafenib, and vemurafenib have been FDA-approved, and more recently the MEK inhibitor trametinib was approved for use in combination with dabrafenib in melanoma. More recently, ERK inhibitors have been identified and they are actively being explored in clinical trials now, although none are FDA-approved yet.

Table 1–3. Inhibitors for the ERK Pathway in Clinical Development. Shown are inhibitors against RAF, MEK, and ERK and their current stage in clinical trials. Compiled from the NCI Drug Encyclopedia and clinicaltrials.gov.

Agent	Target(s)	Clinical Status
RAF INHIBITORS		
Sorafenib	CRAF/BRAF	FDA-approved
Dabrafenib	BRAF/BRAF^{v600E}/CRAF	FDA-approved
Vemurafenib	BRAF^{v600E}	FDA-approved
Encorafenib	BRAF^{V600}	Phase III
RAF265	BRAF/VEGFR2	Phase II
CEP-32496	BRAF/ BRAF^{v600E}/CRAF	Phase I/II
MEK INHIBITORS		
Trametinib	MEK 1/2	FDA-approved
Cobimetinib	MEK 1/2	Phase III
Binimetinib (MEK 162)	MEK 1/2	Phase I/II
PD-0325901	MEK 1/2	Phase II
Selumetinib (AZD6244)	MEK 1/2	Phase I/II
ERK INHIBITORS		
BVD-523	ERK 1/2	Phase I/II
GDC-0994	ERK 1/2	Phase I
CC-90003	ERK 1/2	Phase I

Pre-clinical evidence strongly supports a role for both the mTOR pathway and the ERK pathway in NF1-deficient tumorigenesis. *NF1*-mutant tumor cell lines and primary tissue display RAF/MEK/ERK hyper-activation (Donovan et al., 2002; Ingram et al., 2000; Jessen et al., 2013; Lau et al., 2000). Furthermore, *NF1* –null cells show increased proliferation in an ERK-dependent manner, and expression of the NF1 GAP-related-domain (GRD) can rescue this effect, indicating that ERK activation contributes to the pathogenesis of *NF1*-deficient cancers (Donovan et al., 2002; Hiatt et al., 2001; Ingram et al., 2000). Inhibition of the MAPK pathway

using the MEK inhibitor PD-0325901 has been shown to have a profound cytotoxic effect in a mouse model of neurofibromas, demonstrating that this pathway is also critical to NF1-deficient pathogenesis (Jessen et al., 2013). A phase II clinical trial using PD-0325901 in NF1-adolescents with plexiform neurofibromas is currently enrolling, and preliminary results, which have been presented publically, are promising (NCT02096471, clinicaltrials.gov).

While there is ample evidence that both the PI3K/AKT/mTOR pathway and the ERK pathway are hyperactivated when *NF1* is lost, it is unlikely that inhibition of either of these pathways will be sufficient to induce tumor regression as monotherapies. Inhibitors directed against both pathways are currently in clinical trials as monotherapies, but MPNST mouse models have shown cytostatic responses at best to mTOR inhibitors and MEK inhibitors (Jessen et al., 2013; Johannessen et al., 2008). To date, no single agent has shown clinical efficacy in this aggressive tumor type. Therefore, it is likely that a combination therapy will be necessary to achieve tumor regression, as is addressed in both Chapter 2 and Chapter 3 of this thesis.

THE STRESS PHENOTYPE OF CANCER

Mutations in oncogenes and tumor suppressors are the causal events in cancer leading to the well-described hallmarks of cancer: self sufficiency in growth signals, insensitivity to anti-growth signals, evading apoptosis, limitless replicative potential, increased angiogenesis, and tissue invasion and metastasis (Hanahan and Weinberg, 2000). Targeting the specific alterations that give cancer these properties, as discussed above, is the focus of Chapter 2 of this thesis. However, it has recently been appreciated that many other pathways in the cell may be activated in a response to the tumorigenic state to allow cancer cell survival and that these processes may also represent potential therapeutic targets. This increased dependence of a

cancer cell on the activity of a normal gene is called *non-oncogene addiction*. Thus, in addition to the canonical hallmarks induced by oncogenes and tumor suppressors, several new hallmarks related to the stress phenotype of cancer have been proposed: DNA damage and replicative stress, proteotoxic stress, mitotic stress, metabolic stress, and oxidative stress (Luo et al., 2009). While these alterations are not causative of tumorigenesis they are characteristics present in most, if not all, tumors and are essential to maintaining the tumorigenic state. Chapter 3 of this thesis will focus on exploiting the oxidative and proteotoxic stress of cancer cells to develop therapies, so these specific types of stress are discussed in detail below.

PROTEOTOXIC STRESS

Most tumors are highly aneuploid and have a large number of gene copy number changes (Holland and Cleveland, 2009). These alterations can promote tumor growth by altering the balance between positive and negative regulators of proliferation and survival. However, these imbalances can also change the transcriptional stoichiometry of cellular complexes leading to an increased number of misfolded proteins and protein aggregates that the cellular machinery that regulates protein folding and degradation must attenuate. Studies of aneuploid mouse embryonic fibroblast cells observe high levels of chaperone protein expression, suggesting that aneuploidy puts a strain on the protein folding capabilities of the cell (Oromendia and Amon, 2014; Sheltzer et al., 2012; Williams et al., 2008). Further, a large number of aneuploid cell lines have been characterized and regardless of specific genetic alterations, they share a common set of expression alterations termed the environmental stress response, which is indicative of proteotoxic stress (Sheltzer et al., 2012).

Aneuploidy leads to slower growth in most contexts, despite the fact that 90% of solid tumors are aneuploid (Williams et al., 2008). MPNSTs in particular are known to have a complex karyotype with numerous chromosomal alterations and frequent aneuploidy (Bridge et

al., 2004). Thus cancer cells must adapt to maintain an increased proliferative rate despite the presence of aneuploidy (Torres et al., 2010). Cancer cells may be more reliant on the protein chaperone machinery responsible for attenuating proteotoxic stress, and similarly hyper-sensitive to any further induction of proteotoxic stress.

The Unfolded Protein Response

The unfolded protein response (UPR) is a cellular stress response primarily responsible for attenuating endoplasmic reticulum stress (ER stress). This process is inherently connected to proteotoxic stress as the ER is the site of cellular protein folding. When misfolded or unfolded proteins accumulate in the lumen of the ER, this leads to induction of the UPR, which is initially a protective response but will trigger apoptosis in the case of irresolvable ER stress. As will be discussed later in this thesis, we have found that induction of ER stress and modulation of the UPR can induce tumor regression. Therefore, a detailed description of the UPR is included, which will be important for Chapter 3.

BIP (or GRP78) is an ER luminal protein, which is the initial trigger for the UPR. BIP is a protein chaperone, which can assist in the folding of unfolded proteins. When no unfolded proteins are present, BIP is bound to the three main effectors of the UPR: Inositol requiring protein 1 (IRE1), Protein kinase RNA-like endoplasmic reticulum kinase (PERK), and activating transcription factor 6 (ATF6), and prevents their activation. However, as the number of unfolded proteins in the ER lumen rises, BIP is recruited away from the UPR initiators to refold these proteins. This releases these proteins to trigger activation of downstream UPR effector proteins (Figure 1–7). There is some evidence that unfolded proteins can also directly activate IRE1α and PERK. The three canonical sensors of ER stress, IRE1α, PERK, and ATF6, and their direct effectors are discussed in detail below, however in reality there is a large amount of cross-talk and integration of these pathways.

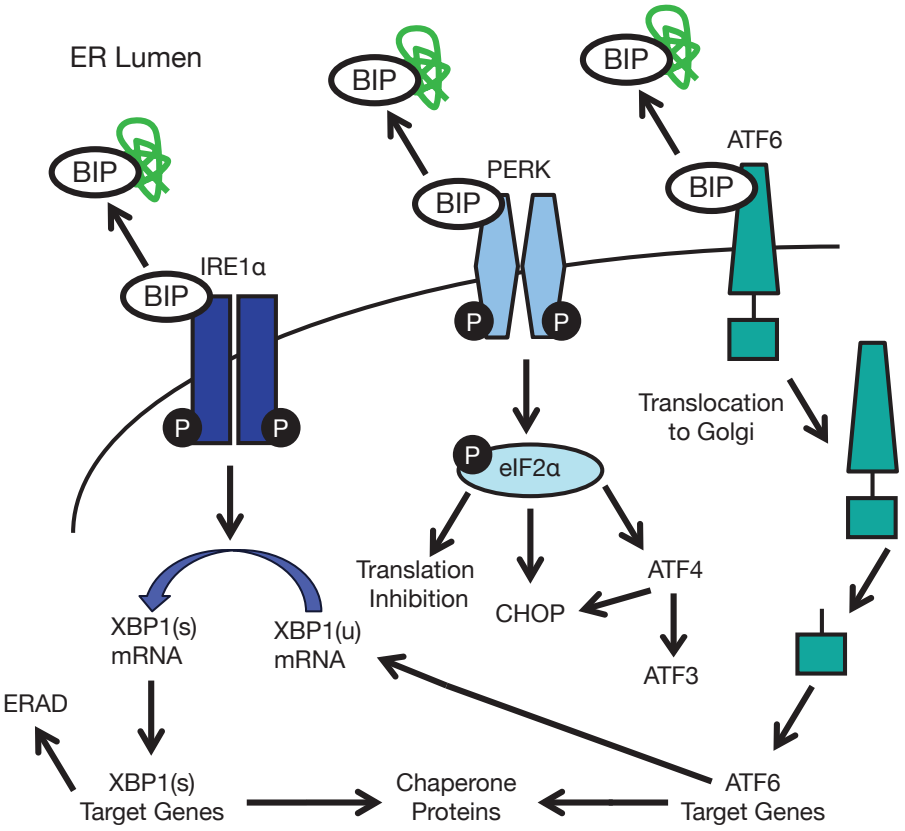

Figure 1–7. The Unfolded Protein Response (UPR). The three main transducers of the UPR—IRE1α, PERK, and ATF6 are all activated in response to the presence of unfolded proteins in the ER lumen. In an unstressed ER, the protein chaperone BIP binds to these transducers and keeps them inactive. When unfolded proteins are present, they recruit BIP away, and release IRE1α, PERK, and ATF6. There is also evidence that unfolded proteins can directly activate at least IRE1α and PERK. IRE1α auto-phosphorylates and then splices XBP1 mRNA to produce XBP1(s), which can activate a number of genes involved in the stress response. PERK phosphorylates eIF2α, which blocks global translation. When BIP releases ATF6, ATF6 translocates to the Golgi where it is cleaved, which allows ATF6 to then activate a number of UPR genes in the nucleus.

IRE1α

IRE1α is a serine/threonine protein kinase as well as an endonuclease. IRE1α is a luminal transmembrane protein that contains an ER luminal portion that can sense the presence of unfolded proteins, and a cytoplasmic kinase domain-containing portion that can signal to effector pathways to alter protein transcription and translation in response to ER

stress (Sidrauski and Walter, 1997). When unfolded proteins are present, IRE1α oligomerizes and auto-phosphorylates. IRE1α is unusual amongst transmembrane kinases, as this autophosphorylation does not lead to a phosphorylation cascade—the only known substrate of IRE1α is itself. Instead, activation and autophosphorylation of IRE1α allows IRE1α to perform its other function: endonucleolytic cleavage of X-box binding protein-1 (XBP1). IRE1α cuts XBP1 in two locations, removing an intron, and the remaining pieces are ligated creating a spliced mRNA. This spliced version of XBP1 encodes a transcriptional activator of a number of UPR effectors (Sidrauski and Walter, 1997). IRE1α may also have endonuclease activity against other mRNAs, but this activity seems to lead to their degradation (Hollien and Weissman, 2006; Hollien et al., 2009).

PERK

Similar to IRE1α, PERK is a transmembrane protein with a luminal stress-sensing domain, and a cytoplasmic kinase-containing domain. PERK also oligomerizes under stressful conditions, and autophosphorylates. However, in contrast to IRE1α, PERK can phosphorylate eIF2α. This phosphorylation event is an inhibitory phosphorylation signal, and reduces eIF2α activity, which leads to a suppression in translation, to prevent a further increase in the number of proteins requiring folding in the ER lumen (Harding et al., 1999; Shi et al., 1998). In addition to suppression of translation, it seems that PERK activation can also regulate the transcription of some UPR-associated genes, including *CHOP*, *ATF3*, and *ATF4* (Teske et al., 2011). In cells where PERK has been knocked out, the transcription of a number of UPR effector genes is impaired (Harding et al., 2000; 2003; Teske et al., 2011), and a similar effect was observed in cells containing an eIF2α Ser51Ala mutation, suggesting that most of the transcriptional effects of PERK activation are mediated through eIF2α phosphorylation (Scheuner et al., 2001).

ATF6

The third main arm of the unfolded protein response is through ATF6, a transmembrane transcription factor. ATF6 is normally retained in the ER lumen through interaction with BIP, however as BIP is recruited away by unfolded proteins, ATF6 is released from the ER and moves to the Golgi (Chen et al., 2002). ATF6 is processed in the Golgi by the serine protease site-1 protease (S1P) and the metalloprotease site-2 (S2P) to release a soluble transcription factor, which regulates a number of UPR-associated genes. In the nucleus, ATF6 recognizes ER stress response elements, UPR elements, and cAMP response elements in gene promoters leading to transcription of a program of genes to mediate cellular survival and the production of proteins involved in ER associated-degradation to promote the clearance and degradation of accumulated misfolded proteins (Kokame et al., 2001; Yoshida et al., 1998; 2001).

UPR-Mediated Cell Death

While most aspects of the unfolded protein response are directed at protecting the cell from further damage by halting translation to relieve stress and promoting degradation of misfolded proteins and aggregates, the unfolded protein response can also trigger apoptosis in the face of irremediable ER stress. Several UPR-regulated factors have been implicated in the induction of ER-stress induced apoptosis. IRE1α can activate Apoptotic Signaling Kinase 1 (ASK1), which causes activation of a phosphorylation cascade that can promote apoptosis (Kim et al., 2008). CHOP activation has also been implicated in ER-stress mediated apoptosis, as CHOP seems to promote transcription of apoptotic genes such as BIM. However, CHOP is clearly not the only path to ER-stress induced apoptosis as $CHOP^{-/-}$ cells are only partially resistant to ER-stress induced death and $PERK^{-/-}$ cells are not resistant to apoptosis despite low levels of CHOP (Oyadomari and Mori, 2004). A third mechanism by which ER-stress can induce apoptosis is through calcium release from the ER lumen, which is mediated by BAX and BCL-2 (Sano and Reed, 2013).

The exact signals that cause the UPR to switch from an adaptive response to a terminal response remain unclear. However, recently, increased expression of thioredoxin interacting protein (TXNIP) has been implicated in the switch to an apoptotic fate, at least in the setting of pancreatic β-cells (Anthony and Wek, 2012; Lerner et al., 2012; Oslowski et al., 2012). In these studies, TXNIP expression was increased in conditions of ER stress through PERK and IRE1α, and suppression of TXNIP promoted cell survival in these conditions. This role for TXNIP is particularly interesting, as TXNIP is also an important factor in the oxidative stress response as discussed below. TXNIP induction by the UPR thus connects both proteotoxic and oxidative signals with an apoptotic cellular fate.

OXIDATIVE STRESS

Oxidative stress refers to the imbalance of naturally occurring reactive oxygen species (ROS) and the endogenous systems that detoxify the ROS and repair any resulting damage. In cancer cells this balance is typically disturbed for a variety of reasons. Cancer cells exhibit an accelerated metabolism as well as a high proliferative rate, both of which contribute to the elevated production of ROS. In order to attenuate this increased oxidative stress, cancer cells often upregulate cellular ROS scavenging systems, producing a paradoxical situation in which cancer cells have higher levels of ROS than normal cells, despite a much higher antioxidant capacity. Importantly, there is an interdependent relationship between oxidative stress and proteotoxic stress: oxidative stress results in misfolded proteins and induces proteotoxic stress, and proteotoxic stress results in mitochondrial damage and oxidative stress. This link between proteotoxic and oxidative stress is discussed in detail later, and is critical for Chapter 3 of this thesis.

Reactive Oxygen Species

The term ROS refers to any oxygen-containing chemical species that has reactive properties. This includes a number of different free radicals and non-radical molecules. Mitochondria are the major source of cellular ROS. Approximately 3–5% of the oxygen consumed by mitochondria is converted to ROS (Finkel, 2012). Different levels of ROS produce different physiological effects, so the regulation of redox balance is critical for cellular homeostasis. At low levels, ROS function as important signaling molecules within the cell, regulating proliferation and differentiation (Janssen-Heininger et al., 2008). At moderate levels, ROS will induce cellular stress responses to promote cellular survival, but at high levels ROS can damage DNA, RNA, proteins, and lipids (Veskoukis et al., 2012). Excessive ROS will ultimately lead to cell death (Gorrini et al., 2013).

Antioxidant Systems

There are two thiol-dependent anti-oxidant systems that promote the detoxification of ROS: the glutathione (GSH) system and the thioredoxin (TRX) system. Generally, these systems can scavenge ROS either directly or indirectly through enzymatic reactions, reducing the level of ROS present in the cell. These two systems are described in detail below.

Glutathione System

Reduced glutathione (GSH) is the main cellular defense against ROS. Glutathione contains a reducing thiol group (-SH), which becomes oxidized when it reacts with oxidized molecules. Oxidized glutathione quickly reacts with another reduced glutathione producing glutathione disulfide (GSSG). Glutathione disulfide can be converted back into reduced glutathione in an NADPH-dependent manner by glutathione reductase (GR). In normal cells, 90% of the GSH is reduced, and only 10% is oxidized, providing a large buffering capacity for the cell. One combination therapy our lab has developed, which is discussed in detail later, functions in part by decreasing the level of reduced GSH present in the cell.

Thioredoxin System

The thioredoxin (TRX) system is very similar to the GSH system. TRX contains two reducing thiol groups, which can reduce target molecules resulting in oxidized thioredoxin. Thioreductase (TrxR) then reduces thioredoxin in an NADPH-dependent fashion (Lu and Holmgren, 2014). There are two thioredoxin proteins, thioredoxin 1 (TRX1) which is predominantly cytoplasmic and nuclear, and thioredoxin 2 (TRX2), which is mitochondrial. The TRX system can directly induce apoptosis via activation of apoptosis regulating signal 1 (ASK1). Reduced TRX directly binds ASK1, and inhibits ASK1 activity. When TRX is oxidized, this causes the dissociation of TRX and ASK1, releasing ASK1 to initiate apoptosis. The thioredoxin interacting protein (TXNIP) regulates this interaction. TXNIP is an inhibitor of reduced TRX; TXNIP blocks the reducing capabilities of TRX via a direct binding. When TXNIP is bound to TRX, this similarly causes a dissociation of ASK1, and allows apoptosis initiation (Lu and Holmgren, 2012).

Crosstalk between the ER and the Mitochondria during Stress

While proteotoxic and oxidative stress can arise for distinct reasons, the cellular response pathways are interconnected, linking the ER and the mitochondria in a complex and interdependent manner. Activation of the unfolded protein response results in a release of calcium from the ER, which depolarizes the mitochondrial membrane and leads to increased ROS production, which in turn can further impair protein folding (Malhotra and Kaufman, 2007). Conversely, oxidative stress can induce protein misfolding, which will engage the UPR, and again, lead to further mitochondrial damage and ER stress (Eletto et al., 2014). At moderate levels of stress the cell can engage compensatory mechanisms such as the UPR and the GSH and TRX systems that will attenuate the ER stress and ROS, and the cell will survive. However, if the stress is insurmountable, or the adaptive pathways are impaired, this will result in a

vicious cycle of damage between the ER and the mitochondria, ultimately resulting in cell death (Kim et al., 2008).

TARGETING THE STRESS PHENOTYPE IN MPNSTS

The elevated proteotoxic and oxidative stress observed in cancer cells could make them more sensitive to inducers of stress or modulators of stress responses (Figure 1–8). MPNSTs in a genetically engineered mouse model display high levels of ER stress, and MPNST cell lines are sensitive to a number of ER-stress inducing agents *in vitro*, including thapsigargin, tunicamycin, and HSP90 inhibitors. However, these agents do not induce tumor shrinkage as a monotherapy *in vivo* (De Raedt et al., 2011). When ER stress inducing agents are combined with the mTOR inhibitor rapamycin, which is cytostatic as a monotherapy, they convert the cytostatic response to a cytotoxic response (De Raedt et al., 2011; Johannessen et al., 2008). Interestingly, this effect was shown to be dependent on ROS, as ER stress inducing agents increased ROS levels, and the ROS scavenger ascorbic acid could block this effect (De Raedt et al., 2011). ER stress inducing agents alone induce ER stress and ROS, but the cell is able to attenuate this stress by activating stress response pathways. However, we found that mTOR inhibitors reduce activity of the pentose phosphate pathway—one of the key sources of NADPH in the cell (De Raedt et al., 2011; Düvel et al., 2010). The glutathione system is dependent on NADPH to maintain reduced GSH; when mTOR inhibitors are added to ER stress inhibitors the cell can no longer attenuate the oxidative stress resulting from the ER stress, and a vicious cycle of ER and mitochondrial damage is triggered (Figure 1–9) (De Raedt et al., 2011).

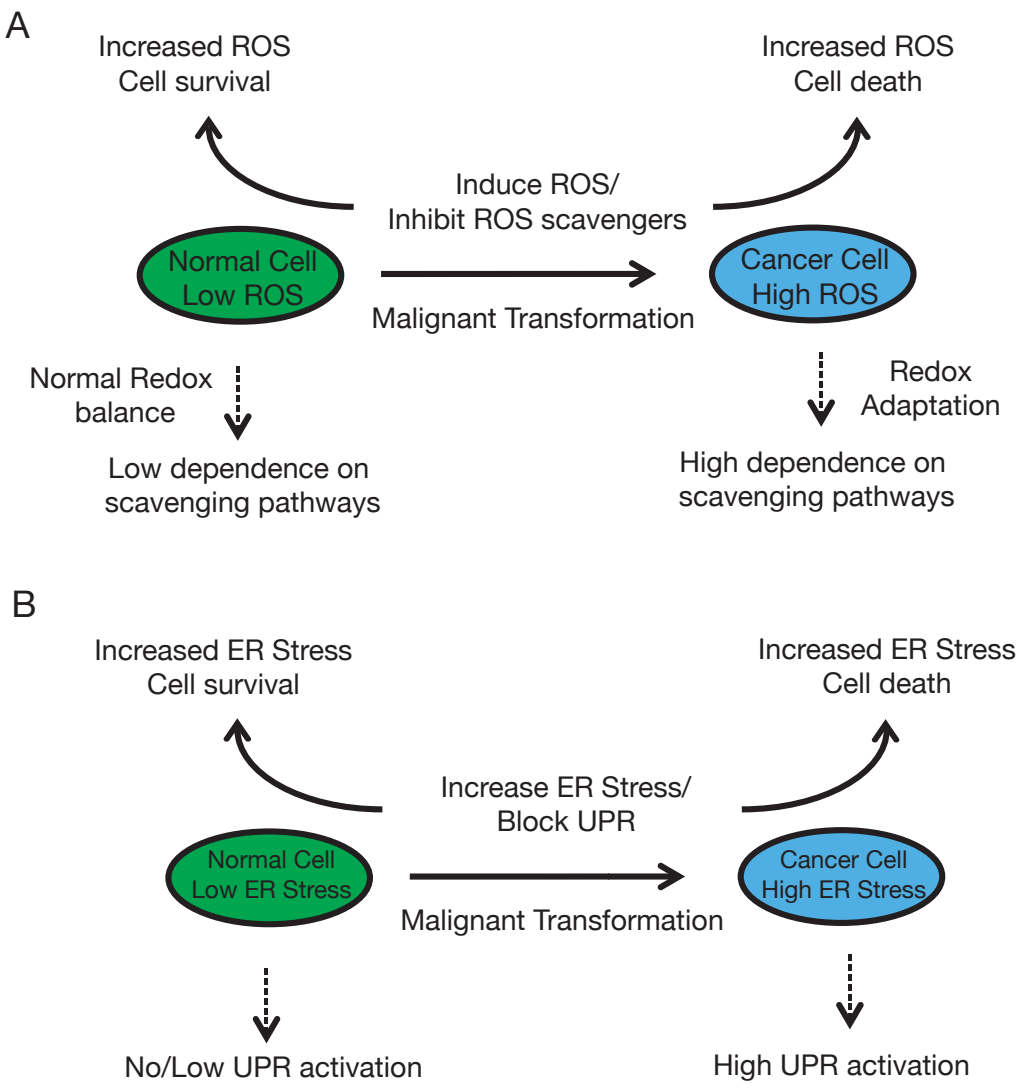

Figure 1–8. Diagram of Cancer Susceptibility to Modulators of Proteotoxic and Oxidative Stress. A, Cancer cell display increased ROS relative to normal cells. Agents that increase ROS or impair ROS scavenging systems will push the ROS level beyond the threshold for survival in cancer cells, while normal cells can accommodate the increased ROS. **B,** Similar to A, cancer cells have elevated ER stress so ER stress inducers or agents that impair the UPR will further increase the ER stress levels in cancer cells beyond the threshold of acceptable stress, while normal cells can attenuate the increased stress and survive.

The combination of ER stress inducing agents and mTOR inhibitors is the first combination discovered that reduces tumor size in this aggressive mouse model of MPNSTs. Of the ER stress inducing compounds included in that study, only HSP90 inhibitors are being

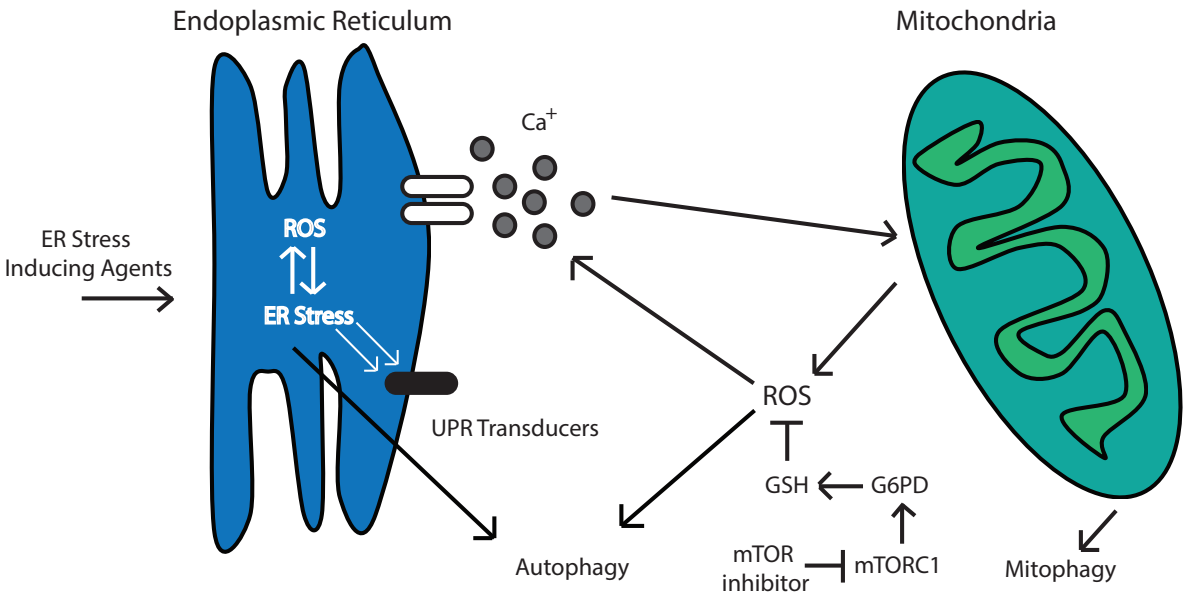

Figure 1–9. Model for Synergy between ER Stress Inducers and mTOR Inhibitors. Schematic of the proposed mechanism of synergy between ER Stress Inhibitors and mTOR inhibitors. ER Stress inducers activate the UPR and cause a release of calcium from the ER, triggering ROS production in the mitochondria. mTOR inhibitors reduce the cell's ROS scavenging abilities through a reduction in levels of reduced glutathione, and a vicious cycle is activated.

clinically developed. A Phase I/II trial of restapimycin (IPI-504) and everolimus (an mTOR inhibitor) was recently completed in patients with KRAS-mutant non-small cell lung cancer, however study results are not yet public (NCT01427946). A Phase I/II of second-generation HSP90 inhibitor ganetespib (STA-9090) and sirolimus in MPNST patients is currently enrolling (NCT02008877). To date however, there are no FDA-approved HSP90 inhibitors, and it remains possible that a tolerable therapeutic window for this particular combination will not be identified. However, given the proposed mechanism of synergy, a large number of ER stress modulators or ROS modulators could potentially induce the same process in combination with mTOR inhibitors. Chapter 2 of this thesis explores an alternative approach to exploiting tumor stress in MPNSTs by combining the histone deacetylase inhibitors with mTOR inhibitors.

HISTONE DEACETYLASE INHIBITORS

The histone deacetylase (HDAC) inhibitor vorinostat is FDA-approved for use in cutaneous t-cell lymphoma (CTCL), and is known to induce ER stress and ROS (Kahali et al., 2010; Petruccelli et al., 2011). Vorinostat is a pan-HDAC inhibitor with activity against all Zn^{2+}-dependent HDACs. Histone deacetylases received their name because they enzymatically remove acetyl groups from lysines on histones, counteracting the activity of histone acetyl-transferases. However, this is a bit of a misnomer as HDACs also have important roles deacetylating proteins and indeed some HDACs, such as HDAC6, are entirely cytoplasmic and have no known role in the nucleus. Thus inhibition of HDACs affects function of acetylated proteins, which become hyper-acetylated in the context of HDAC inhibition, as well as global gene transcription through modulation of histone acetylation.

Vorinostat induces the unfolded protein response, and this activation has been shown to contribute to its antitumor effect in some settings (Kahali et al., 2010; 2011). The mechanism for this effect on the unfolded protein response remains unclear. A primary proposed mechanism has focused on HDAC6 inhibition. HDAC6 is a cytoplasmic HDAC that has been shown to deacetylate HSP90 (Kekatpure et al., 2009). When HSP90 is acetylated, it cannot act as a chaperone for target proteins (Scroggins et al., 2007), effectively inhibiting HSP90 activity. Thus HDAC inhibition could represent an alternative way of inducing ER stress through HSP90 inhibition. Alternatively, it has been proposed that BIP is also acetylated, and that this acetylation event prevents BIP from binding the UPR transducers in the ER lumen, releasing them to activate the UPR (Choudhary et al., 2009; Kahali et al., 2012). The class I HDACs (1-3), as well as HDAC6, are implicated in the deacetylation of BIP (Kahali et al., 2012; Rao et al., 2010). Vorinostat has also been shown to increase ROS (Ungerstedt et al., 2012). This effect is thought to be through modulation of the TRX system. Vorinostat induces an upregulation of

TXNIP, a negative regulator of TRX, thus limiting one of the key ROS scavenging pathways (Butler et al., 2002; Ungerstedt et al., 2005).

OVERVIEW OF THESIS

Malignant peripheral nerve sheath tumors (MPNSTs) are the leading cause of death among patients with NF1 and current treatment options are limited. Loss of the tumor suppressor NF1 is a critical component of MPNST pathogenesis, and is also a common event in a wide variety of sporadic cancers. Thus, therapies for NF1-deficient cancers represent an important clinical need. During my dissertation research, I aimed to better understand the signaling and stress vulnerabilities of this tumor type. I identify two novel combination therapies that I hope can be translated to meaningful clinical benefit for patients.

In Chapter 2, I dissect key signaling nodes downstream of NF1 loss to identify a combination therapy and describe a therapeutic biomarker of effective target inhibition. In a panel of NF1-deficient cell lines we show that p110α and mTORC1 are the key signaling nodes downstream of NF1 loss. Conversely, we find that p110β, p110δ, mTORC2, and AKT are not necessary for proliferation or sustained mTORC1 signaling. Using a genetically engineered mouse model of MPNSTs we show that combined inhibition of mTORC1 and MEK promotes tumor regression, but only when target inhibition is sustained. Transcriptional profiling of the tumors unexpectedly identified the glucose transporter *GLUT1* as a biomarker of dual target inhibition. We show that early changes in FDG-PET uptake correlate with eventual tumor regression, suggesting that this could serve as a non-invasive proxy measurement for target inhibition.

In Chapter 3, I describe a combination of two FDA-approved agents that exploits proteotoxic and oxidative stress vulnerabilities in MPNSTs. We find that the pan-HDAC inhibitor vorinostat induces ER stress in MPNSTs, and that MPNST cell lines are sensitive to

HDAC inhibition *in vitro*. I demonstrate that addition of an mTOR inhibitor sensitizes cells to vorinostat *in vitro*, and that the combination of vorinostat and rapamycin leads to MPNST regression *in vivo.* I further show that HDAC6 inhibition alone is not sufficient. I identify modulation of the unfolded protein response, oxidative stress, and the thioredoxin system as one mechanism likely contributing to the therapeutic efficacy of this combination.

In Appendix A, I report the effective combination of a second-generation HSP90 inhibitor STA-1474 and rapamycin in MPNSTs. In Appendix B, I reprint a publication from the laboratory that describes the effective combination of ER stress inducers and mTOR inhibitors in MPNSTs. This work, to which I contributed, provides the basis for the studies described in Chapter 3. Appendix C contains supplemental materials for Chapter 2.

Chapter 2: Defining Key Signaling Nodes and Therapeutic Biomarkers in *NF1*-Mutant Cancers

Defining Key Signaling Nodes and Therapeutic Biomarkers in *NF1*-Mutant Cancers

Clare F. Malone[1,2], Jody A. Fromm[1,2], Ophélia Maertens[1,2], Thomas DeRaedt[1,2,3], Rachel Ingraham[1,2], Karen Cichowski[1,2,3]

[1]Genetics Division, Department of Medicine, Brigham and Women's Hospital, [2]Harvard Medical School, Boston MA 02115, [3]Ludwig Center at Dana-Farber/Harvard Cancer Center, Boston, MA 02115

Author Attributions

Clare F. Malone: Performed all experiments not attributed to others and with KC planned the project and wrote the manuscript.

Jody A. Fromm: Assisted CFM with experiments shown in 2-2 C, D, and E along with OM, RI, and TDR. Performed experiments shown in 2-3 A and B and 2-4 jointly with CFM. Performed experiments shown in 2-3 C and D.

Ophélia Maertens: Performed experiment 2-2 A. Performed experiment 2-2 B jointly with CFM. Assisted CFM in experiments shown in 2-2 C, D, and E along with JAF, RI, and TDR.

Thomas DeRaedt: Assisted CFM in experiments shown in 2-2 C, D, and E along with JAF, RI, and OM.

Rachel Ingraham: Assisted CFM in experiments shown in 2-2 C, D, and E along with JAF, TDR, and OM.

Karen Cichowski: Supervised and developed the project, and wrote the manuscript with CFM.

The text and figures of this chapter were published, as presented here, in the following manuscript:

Defining key therapeutic signaling nodes and therapeutic biomarkers for *NF1*-mutant cancers.

Clare F. Malone*, Jody A. Fromm*, Ophélia Maertens, Thomas DeRaedt, Rachel Ingraham, Karen Cichowski. *Cancer Discovery*. Vol 4 (9) pp. 1062-1073. September 2014. *co-first authors.

INTRODUCTION

The *NF1* tumor suppressor is mutated or suppressed in a variety of sporadic cancers including glioblastoma, neuroblastoma, melanoma and non-small cell lung cancer (Ding et al., 2008; Maertens et al., 2013; McGillicuddy et al., 2009; Parsons et al., 2008; The et al., 1993). *NF1* mutations also underlie the familial cancer syndrome, neurofibromatosis type 1 (NF1) (Cawthon et al., 1990; Martin et al., 1990). NF1 patients exhibit a variety of tumorigenic and non-tumorigenic manifestations but the most common cause of death is malignant peripheral nerve sheath tumors (MPNSTs). These highly aggressive tumors are lethal in approximately 70% of patients, and conventional chemotherapy and radiation do not reduce mortality in individuals with inoperable tumors (Evans et al., 2002; Porter et al., 2009; Zehou et al., 2013). Therefore, developing effective targeted therapies for these individuals represents an important and unmet clinical need. Moreover, an effective therapy for this tumor type may be more broadly applicable to other sporadic *NF1*-mutant cancers.

The *NF1* tumor suppressor gene encodes a RAS GAP, which inactivates RAS by catalyzing the hydrolysis of RAS-GTP (Cawthon et al., 1990; Martin et al., 1990). As such, when *NF1* is mutated or suppressed, RAS and downstream effectors become hyperactivated (DeClue et al., 1992). Both the PI3K/mTOR and MEK/ERK pathways have been shown to be important in various *NF1*-mutant tumors and therefore components of these pathways represent potential therapeutic targets (Endo et al., 2013; Johannessen et al., 2008; Parkin et al., 2010; See et al., 2012). However, given the plethora of available drugs that target these pathways we set out to genetically and chemically deconstruct the most important signaling nodes in *NF1*-mutant MPNSTs. Together with preclinical studies in a genetically engineered mouse tumor model, we found that mTORC1 is the key PI3K pathway component in these *NF1*-mutant malignancies, AKT and TORC2 are dispensable, and only sustained mTORC1 and MEK inhibition promotes tumor regression.

Several combined PI3K/MEK pathway trials are in development or are being considered for other cancers (Britten, 2013). However, the clinical challenge will be to identify a drug combination and dose that effectively suppresses both pathways, while minimizing toxicity. It is currently unclear how dosing can be adjusted while confirming that both targets are sufficiently inhibited in real time, especially given that the duration of inhibition appears to be an important determinant of efficacy. Thus, establishing a tractable biomarker for effective, combined target inhibition would greatly facilitate this effort. By performing transcriptional profiling and imaging studies we unexpectedly identified *GLUT1*, which mediates ^{18}F-fluorodeoxyglucose (^{18}F-FDG) uptake, as a key gene that is suppressed prior to tumor regression but only when both pathways are effectively inhibited. Moreover, we show that ^{18}F-FDG uptake is a reliable readout of combined target inhibition. This insight can be directly applied to the design of clinical trials in *NF1* mutant cancers and may also have broader utility in other RAS-driven tumors.

RESULTS

p110α and mTORC1 are the Key Effectors in NF1-Mutant Nervous System Malignancies

We previously showed that loss or inactivation of *NF1* triggers the aberrant activation of PI3K/mTORC1 signaling in human and mouse MPNSTs (Johannessen et al., 2005). However, it is currently unclear which specific components within this pathway represent the best therapeutic targets. Such insight would reveal which drugs should be preferentially evaluated or excluded in clinical trials. Therefore, we sought to genetically and chemically deconstruct this pathway in *NF1*-mutant MPNSTs. There are three Class 1A catalytic PI3K isoforms: p110α, p110β, and p110δ. While p110α is frequently mutated in human cancer, p110β has been shown to play an essential role in *PTEN* mutant cancers and p110δ is critical in chronic lymphocytic leukemia (Herman et al., 2010; Jia et al., 2008; Samuels et al., 2004). To identify

which catalytic isoform(s) are essential in *NF1*-mutant nervous system malignancies, we first assessed the biological effects of isoform-specific ablation in human MPNST cells derived from NF1 patients. While all three isoforms were present in MPNSTs, genetic ablation of p110α, but not p110β or p110δ, dramatically impaired the proliferation of both tumor lines (Figure 2–1A). Similarly, *NF1*-mutant gliblastoma (GBM) cells were exclusively sensitive to siRNA-mediated depletion of p110α, but not p110β or p110δ, suggesting that p110α may play a more general role in *NF1*-deficient cancers (Figure 2–1A). To complement these findings, we utilized PI3K isoform-specific inhibitors: the p110α- specific inhibitor A66-(S), the p110β-specific inhibitor AZD-6284, and the p110δ-specific inhibitor CAL-101, as well as GDC-0941, a pan-PI3K inhibitor (Folkes et al., 2008; Jamieson et al., 2011; Lannutti et al., 2011; Nylander et al., 2012). The reported specificities of each drug are outlined in Appendix C (Table C–1). In human MPNST cell lines, the p110α-specific inhibitor A66-(s) and GDC-0941 potently inhibited the phosphorylation of AKT and S6; however, the p110β- or p110δ-specific inhibitors, AZD-6284 and CAL-101 respectively, did not suppress the phosphorylation of either protein (Figure 2–1B). Accordingly, A66-(S) was the only isoform-specific inhibitor that suppressed proliferation in these cells (Figure 2–1C; $p=0.039$ in 90-8TLs and $p=0.0006$ in S462s). Together, these observations suggest that p110α is the primary catalytic subunit responsible for pro-proliferative PI3K signaling in *NF1*-mutant nervous system malignancies.

mTOR functions in two distinct complexes: the rapamycin-sensitive complex mTORC1, which phosphorylates 4E-BP1 and S6 kinase, and the relatively rapamycin-insensitive complex mTORC2, which phosphorylates AKT at serine 473 (Loewith et al., 2002; Sarbassov et al., 2005). *NF1*-deficient MPNSTs have been shown to be sensitive to rapamycin, indicating that mTORC1 plays a role in this tumor type; however, the contribution of mTORC2 activity, if any, to MPNST growth is unknown (Johannessen et al., 2005; 2008). We genetically targeted

Figure 2–1. p110α and mTORC1 are Critical for the Proliferation of *NF1*-Deficient Tumor Cells. A, S462, 90-8TL, and LN-229 cells were transfected with pooled siRNAs targeting *PIK3CA*, *PIK3CB*,*PIK3CD*, or non-targeting siRNA. Bar graphs, relative change in cell number from day 0 to 96 hours as compared with control cells transfected with the non-targeting siRNA. Data points, triplicate averages ± SD. Immunoblots depict p110α, p110β, and p110δ protein levels 72 hours after transfection with the indicated siRNA. Actin serves as a loading control. *, $P < 0.002$. **B,** Immunoblots showing pAKT and pS6 levels in S462 cells following treatment with indicated inhibitors (4 hours; 500 nmol/L). AKT, S6, and actin serve as controls. **C,** Bar graphs of S462 and 90-8TL cells treated inhibitors as specified. Numbers represent the relative change in cell number from day 0 to 96 hours as compared with vehicle-treated control cells. Data points, triplicate averages ± SD. *, $P < 0.04$. **D,** S462 and 90-8TL cells were transfected with pooled siRNAs targeting *MTOR*, *RAPTOR*, *RICTOR*, or non-targeting siRNA. Bar graphs, relative change in cell number from day 0 to 96 hours as compared with control cells transfected with the non-targeting siRNA. Data points, triplicate averages ± SD. Immunoblots show mTOR, Raptor, Rictor, pAKT, and pS6 levels 72 hours after transfection with the indicated siRNA. AKT, S6, and actin levels serve as controls. *, $P < 0.02$. **E,** S462 cells were treated with the rapamcyin (Rap) at 100 nmol/L, Torin1 at 250 nmol/L, or MK-2206 (concentration indicated). Bar graph, relative change in cell number from day 0 to 96 hours as compared with vehicle-treated control cells. Data points, triplicate averages ± SD. Immunoblots show $pAKT^{T308}$, $pAKT^{S473}$, $pTSC2^{T1462}$, pS6, and 4E-BP1 levels in the presence of the specified inhibitors. AKT, TSC2, S6, and actin serve as controls. *, $P < 0.0001$. **F,** S462 cells treated with either rapamycin at 100 nmol/L, MK-2206 at 5 μmol/L, or both drugs together. Bar graphs, relative change in cell number from day 0 to 96 hours as compared with vehicle-treated control cells. Data points, triplicate averages ± SD. p, phosphorylated.

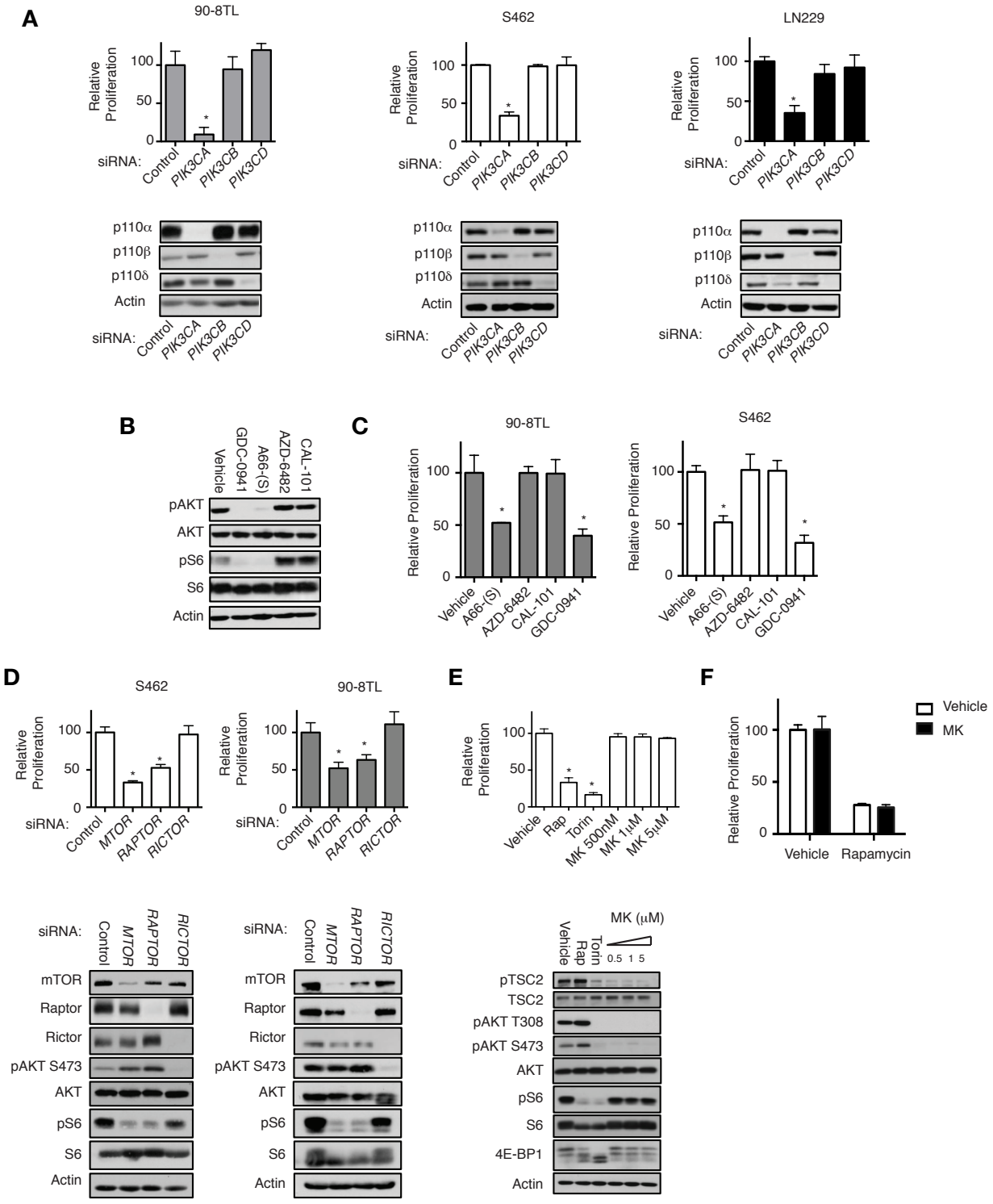

Figure 2–1 (Continued)

essential component proteins of each complex in order to evaluate the relative contribution of these two complexes. RAPTOR, is an essential component of mTORC1, but is not present in mTORC2, while RICTOR, a primary component protein of mTORC2, is not a member of the mTORC1 complex (Huang and Manning, 2009; Sarbassov et al., 2004) As expected, siRNA-mediated-loss of RAPTOR or mTOR suppressed S6 phosphorylation and led to impaired proliferation of MPNST cell lines (Figure 2–1D). However, loss of RICTOR had no effect on MPNST proliferation, despite the effective suppression of phosphorylation of the mTORC2 target AKT (Figure 2–1D).

To further evaluate a role for AKT, or lack thereof, tumors cells were treated with the allosteric AKT inhibitor MK-2206 (Hirai et al., 2010). MK-2206 suppressed the phosphorylation of AKT at S473 and T308, and effectively inhibited AKT kinase activity as confirmed by the loss of TSC2 phosphorylation on T1462 (Figure 1–1E and Appendix C Figure C–1). However, unlike rapamycin, MK-2206 had no effect on the proliferation of *NF1*-mutant MPNST cells (Figure 2–1E). The mTOR kinase inhibitor Torin1 inhibits both the mTORC1 and mTORC2 complexes. Notably, Torin1 has been reported to more effectively inhibit mTORC1, as compared to rapamycin, and in particular more potently suppresses 4E-BP1 phosphorylation, as observed in these studies (Figure 2–1E and Apppendix C Figure C–1). Accordingly, Torin1 potently suppressed the proliferation of *NF1* mutant cells and did so better than rapamycin ($p < 0.02$). As noted, both MK-2206 and Torin1 equivalently and potently suppressed AKT phosphorylation and activity, although only Torin1 suppressed MPNST cell proliferation. Moreover, MK-2206 did not enhance the anti-proliferative effects of rapamycin (Figure 2–1F). Taken together, these results suggest that mTORC1 is a critical effector in *NF1*-mutant cancers and that mTORC2 and AKT are dispensable in these tumor cells.

Selection of an Effective PI3K/mTOR Pathway Inhibitor

These *in vitro* studies suggested that pan-PI3K inhibitors, p110a-specific inhibitors or mTORC1 inhibitors should suppress the growth of *NF1*-mutant MPNSTs. Therefore, we first evaluated the *in vivo* effects of GDC-0941 and rapamycin in a genetically engineered mouse MPNST model. Like human MPNSTs, tumors from these animals harbor compound mutations in *Nf1* and *p53,* and develop with an average latency of five months. These MPNSTs are highly aggressive, and mice survive for an average of 10.7 days after tumors are detected, thus recapitulating the aggressive nature of human tumors (Cichowski et al., 1999). As previously shown, rapamycin suppressed the growth of *Nf1/p53* mutant MPNSTs ($p<0.0001$) (Johannessen et al., 2008); however, GDC-0941 did so significantly less well ($p=0.0021$) (Figure 2–2A). Notably, the maximum tolerated dose of GDC-0941 (150mg/kg) inhibited the phosphorylation of AKT, S6 and 4E-BP1 in tumors within 1 hour, however these pathways were reactivated within 4 hours after treatment (Figure 2–2B). In contrast, rapamycin suppressed S6 and 4E-BP1 phosphorylation for at least 18 hours, consistent with the observed enhanced efficacy and the demonstrated importance of mTORC1 is these tumors. It should be noted that AKT is not activated by relief of feedback mechanisms in this model, as we have previously shown (Figure 2–2B) (De Raedt et al., 2011; Johannessen et al., 2008). Several other PI3K/mTOR pathway inhibitors including BEZ-235, Torin2, and INK-128 were evaluated in these animals (data not shown); however we were unable to identify an inhibitor that exhibited better pharmacodynamics or growth inhibition than rapamycin at tolerable doses in these animals. Therefore, rapamycin was selected for further studies.

Combined, Sustained Inhibition of mTORC1 and MEK Promotes MPNST Regression in vivo

Although mTORC1 is a critical signaling node in *NF1* mutant tumors, mTORC1 inhibition exerted only cytostatic effects on MPNSTs *in vitro* and *in vivo* (Figure 2–1D, E, 2–2A) (Johannessen et al., 2008). Therefore, we evaluated the effects of rapamycin combined with a

Figure 2–2. Therapeutic Effects of PI3K and MEK Pathway Inhibitors *in vivo*. A, Waterfall plot depicting change in tumor volume in *NPcis* mice after 10 days of treatment with vehicle (black), GDC-0941 (blue), or rapamycin (green). The left *y*-axis indicates the $\log_2$ of the fold change in volume after 10 days. The right *y*-axis indicates the percent change in tumor volume relative to day 0. **B,** pAKT/pS6/4E-BP1 immunoblots of tissue from animals exposed to GDC-0941 or rapamycin for the indicated amount of time. AKT, S6, and vinculin serve as controls. **C,** Waterfall plot depicting change in tumor volume after 10 days of treatment with PD-0325901 (yellow) or rapamycin and PD-0325901 (Rap–PD) in combination (purple). Vehicle and rapamycin (gray) are reprinted from A for reference. The left *y*-axis indicates the $\log_2$ of the fold change in volume after 10 days. The right *y*-axis indicates the percent change in tumor volume relative to day 0. **D,** Immunoblots showing pERK levels in tissue after treatment with PD-0325901 once daily (top) or twice daily (bottom). Hours, number of hours from initial treatment. Representative samples from three biologic replicates are shown. Vinculin and ERK serve as controls. **E,** Waterfall plot depicting change in tumor volume after 10 days of treatment with PD-0325901 twice daily or PD-0325901 twice daily in combination with rapamycin. The left *y*-axis indicates the $\log_2$ of the fold change in tumor volume relative to day 0 and the right *y*-axis indicates the percent change in tumor volume**.**

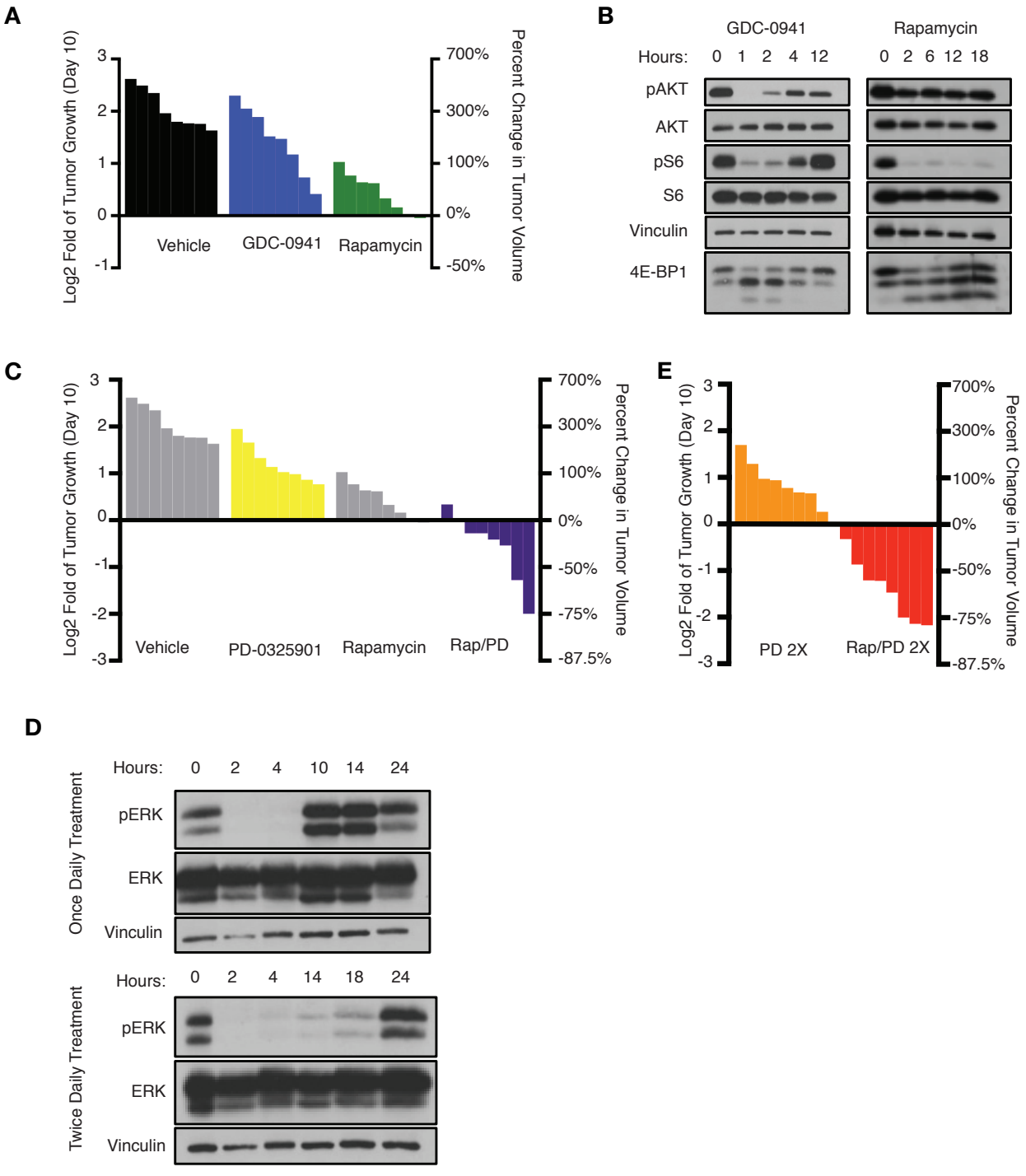

Figure 2–2 (Continued)

MEK inhibitor, which targets a second critical RAS effector pathway. Tumor-bearing mice were treated with vehicle, the MEK inhibitor PD-0325901, rapamycin, or the combination of rapamycin and PD-0325901. As a monotherapy, PD-0325901 slightly attenuated the growth of MPNSTs, but did so less than rapamycin (Figure 2–2C). However, combined PD-0325901 and rapamycin treatment induced tumor regression in these mice (Figure 2–2C). Interestingly, these observations differ from effects observed in benign *NF1*-deficient peripheral nervous system tumors and myeloid malignancies, where MEK appears to function as the dominant RAS-effector pathway and MEK inhibitors exert cytotoxic effects alone, suggesting that different tumor types harboring the same initial driving genetic lesion may rely on different downstream signals (Chang et al., 2013; Jessen et al., 2013). Nevertheless, upon examining the pharmacodynamics of PD-0325901 at this dose, we found that ERK phosphorylation was inhibited for only 4–6 hours, whereas sustained inhibition could be achieved by dosing with PD-0325901 twice daily (Figure 2–2D). As such, we hypothesized that a revised dosing schedule might exert more potent therapeutic effects. Twice-daily PD-0325901 treatment did not promote tumor regression as a monotherapy, however when combined with rapamycin, twice daily PD-0325901 treatment improved the therapeutic response (Figure 2–2E). All mice treated with this combination responded, and more than half of the tumors regressed 50% or more, with several shrinking 75% or more. Together, these observations indicate that the duration of both MEK and mTORC1 inhibition is a critical determinant of the therapeutic response.

Identifying GLUT1 as a Component of the Therapeutic Signature that is Suppressed Prior to Tumor Regression

Pharmocodynamic markers in tumors are often not examined during clinical trials, and when they are, the kinetics of suppression are difficult to evaluate. Therefore, if a treatment does not show efficacy, especially in cases of dose de-escalation, it is often unclear whether

the target or targets were sufficiently inhibited. Therefore, we sought to identify a molecular change that might serve as a functional biomarker of effective, combined inhibition of mTORC1 and MEK pathways. The transcriptional profiles of tumors from animals treated with vehicle, rapamycin, PD-0325901 (twice daily), or the combination of rapamycin and PD-0325901 were evaluated. Importantly, tissues were collected after 14 hours of treatment: a time point that would capture transcriptional changes caused by sustained target inhibition but occurring prior to tumor regression. Using a gene expression class comparison, we identified a gene set that was exclusively regulated by combined rapamycin and PD-0325901 treatment (Figure 2–3A). Interestingly *Slc2a1*, which encodes a glucose transporter and is commonly referred to as *Glut1,* was identified as one of the uniquely suppressed genes in rapamycin/PD-0325901 treated tumors (Figure 2–3A) Effective mTORC1 and MEK target inhibition in tumor tissue was verified (Figure 2–3B). Q-PCR analysis confirmed that *Glut1* levels were reduced 64% after only 14 hours of treatment compared to vehicle treated tumors and that neither rapamycin nor PD-0325901 exerted suppressive effects alone (Figure 2–3C). A dramatic decrease in GLUT1 protein levels was further confirmed by evaluating its expression in tumor biopsies taken before and 3 days after treatment (Figure 2–3D). These findings differ from observations in *VHL* and *LKB1* mutant tumors, where *GLUT1* mRNA and consequently protein expression is primarily regulated by mTOR and HIF1a, and its expression can be suppressed by mTORC1 inhibitors alone (Shackelford et al., 2009; Thomas et al., 2006). However in these *Nf1*-mutant MPNSTs, suppression of both mTORC1 and the MEK/ERK pathways are required. This finding resolves a longstanding observation that rapamycin is not sufficient to suppress the expression of GLUT1, or other HIF-1a target genes *in vitro* or *in vivo* in this tumor type (Johannessen et al., 2008). Together, these results demonstrate that GLUT1 is suppressed in MPNSTs only after combined mTORC1 and MEK inhibition, which could be exploited for developing an imaging biomarker of combined target inhibition.

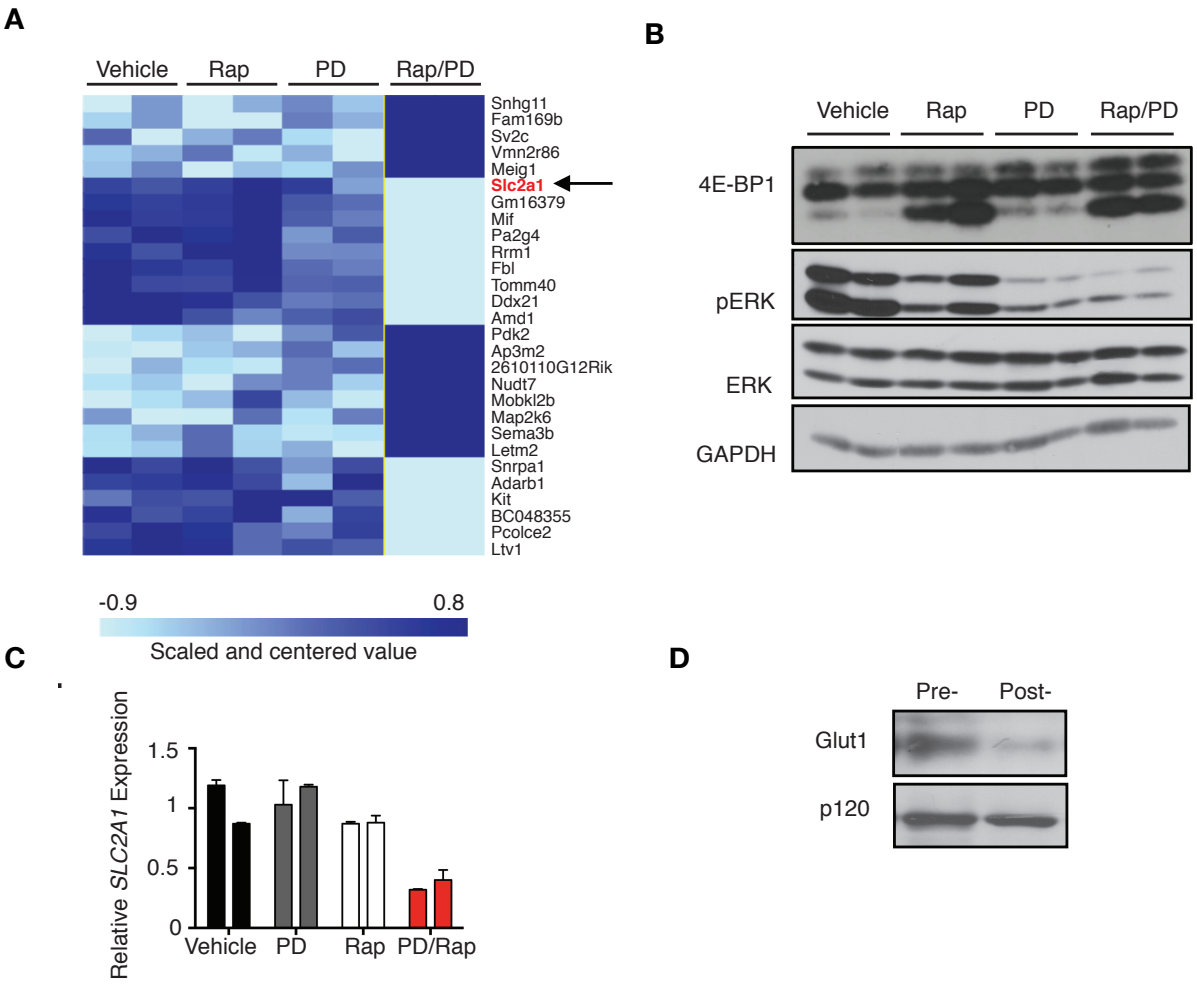

Figure 2–3. GLUT1 is an Early Biomarker of Effective Combined MEK–mTORC1 Inhibition. A, Microarray analysis of mouse tumors 14 hours after treatment with vehicle, rapamycin, PD-0325901 (PD), or both rapamycin and PD-0325901 (Rap–PD). Heat map depicts the uniquely upregulated genes (dark blue) or downregulated genes (light blue) from tumors in mice treated with Rap–PD as compared with all other groups reaching a significance level of $P = 0.001$. The arrow denotes *Slc2a1*(encoding GLUT1), highlighted in red, as one gene of particular interest within this signature. **B**, Immunoblot of pERK and 4E-BP1 levels in individual tumors as described in **A**. ERK and GAPDH serve as a control. **C**, Quantitative PCR showing*Slc2a1* transcript levels in individual tumors described in **A**. **D**, Immunoblot showing GLUT1 levels in a pretreatment biopsy sample, and in the same tumor after treatment with PD-0325901 (twice daily) and rapamycin. p120 serves as a control.

Only combined, effective suppression of mTORC1 and MEK inhibit ^{18}F-FDG uptake

GLUT1 is a membrane bound glucose transporter that is frequently over-expressed in tumors, in part, because altered tumor metabolism requires increased glucose uptake (Amann et al., 2009; Grover-McKay et al., 1998; Sakashita et al., 2001; Younes et al., 1997b). This metabolic activity can be measured by positron emission tomography (PET) scans designed to quantify ^{18}F-FDG uptake (Som et al., 1980). GLUT1 has been shown to regulate ^{18}F-FDG uptake in a variety of tumor types (Avril, 2004; Smith, 2001). MPNSTs are generally FDG-PET positive, and enhanced ^{18}F-FDG uptake is used to diagnose a conversion to malignancy, as MPNSTS often arise from benign precursor lesions (Benz et al., 2010). Because human MPNSTs exhibit a strong FDG-PET signal, and because GLUT1 was specifically suppressed in tumors treated with combined rapamycin and PD-0325901, we hypothesized that the substantial reduction in GLUT1 mRNA and protein might inhibit ^{18}F-FDG uptake in these tumors. To evaluate this possibility, FDG-PET imaging was performed on tumor bearing mice. As expected, MPNSTs were FDG-PET positive at baseline, mirroring the behavior of human MPNSTs (Figure 2–4A). Mice were then treated with vehicle, PD-0325901, rapamycin or PD-0325901/rapamycin and PET analysis was performed a second time, 40 hours after the baseline scan. This time point was selected because it represents a time before detectable regression occurs, in order to avoid any confounding change in the FDG-PET signal due to a reduction in tumor size. It should be noted that the initial (64%) decrease in *Glut1* mRNA levels can be detected 14 hours after treatment, however given the dramatic decrease in GLUT1 protein after 72 hours this repression is sustained and perhaps enhanced, Animals treated with vehicle, PD-0325901, or rapamycin, did not have a significant change in ^{18}F-FDG uptake after treatment (Figure 2–4A,B); however, animals treated with both PD-0325901 and rapamycin exhibited a significant decrease in SUVmax values ($p<0.004$) (Figure 2–4A,B). Importantly, while hexokinase and other GLUT genes can regulate glucose uptake in some settings

Figure 2–4. ^{18}F-FDG Uptake is a Noninvasive Biomarker of Combined MEK–mTORC1 Inhibition. A, Representative images of FDG–PET scans of animals treated with vehicle, PD-0325901, rapamycin, or both (Rap–PD). PD-0325901 was dosed twice daily. Baseline scans are shown at left (pre-), and the right image shows the same view of the same animal 40 hours after treatment with the indicated compound (post-). Arrow, MPNST. Scale bar, relative ^{18}F-FDG uptake, with low uptake in blue and highest uptake in white. **B**, The ^{18}F-FDG uptake by tumors was quantified using SUV_{max}, and the $\log_2$ of the fold change of this number was calculated to indicate the change in ^{18}F-FDG uptake 40 hours after treatment relative to baseline for each animal. The change in combination-treated animals (Rap–PD) is compared with monotherapy and vehicle-treated animals (controls). The *y*-axis indicates the $\log_2$ of the fold change in SUV_{max} relative to baseline. **C**, Representative images of FDG–PET scans of animals treated with 100% PD-0324901–rapamycin, 50%PD-0325901–rapamycin, or 25% PD-0325901–rapamycin. The left image (pre-) shows the baseline scan for each animal and the right (post-) shows the scan 40 hours after treatment with the indicated dose. Again, the tumors are indicated with arrows. Scale bar, relative FDG uptake, with low uptake in blue and highest uptake in white. **D**, Left, a waterfall plot depicting the $\log_2$ fold change of SUV_{max}, a quantification of tumor FDG–PET activity, of selected tumors at 40 hours after treatment with PD-0325901 (25%, 50%, or 100% of the dose) and rapamycin. Right, a waterfall plot depicting the $\log_2$ of fold change in tumor volume of the same mice after 10 days. Individual tumors are graphed in the same order on each plot. **E**, Regression analysis of nine combination-treated mice (100%, $n = 3$; 50%, $n = 3$; 25%, $n = 3$). The *x*-axis represents the $\log_2$ of fold change in tumor volume at 10 days, and the*y*-axis represents the $\log_2$ of fold change in SUV_{max} levels after 40 hours of treatment. Both numbers are relative to day 0 measurements. Line, best-fit linear correlation, and the Pearson coefficient (r) was calculated.

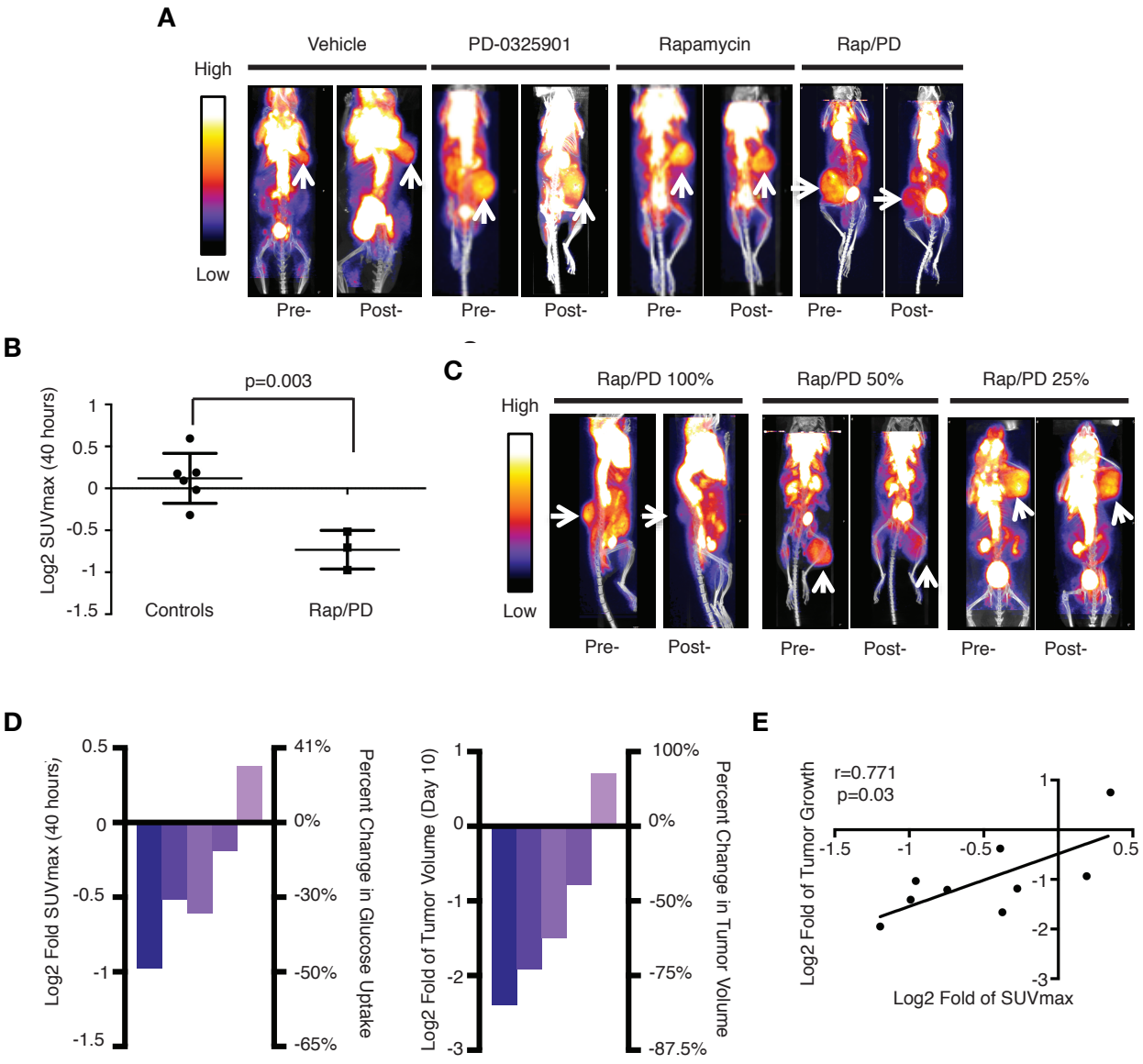

Figure 2–4 (Continued)

(Aloj et al., 1999; Ito et al., 1998; Smith, 2001; Younes et al., 1997a), rapamycin/PD-0325901 treatment did not affect the expression of any of these genes suggesting that GLUT1 may be the rate-limiting step for FDG-PET uptake in MPNSTs (Appendix C, Table C–2).

These observations suggested that FDG-PET imaging could be used as a biomarker of effective combined mTORC1/MEK inhibition in *NF1*-mutant tumors. Such a biomarker would be invaluable in the course of evaluating similar therapies in the clinic and in the course of dose de-escalation/escalation studies. This biomarker would be particularly useful if the early change in FDG-PET imaging were predictive of a later change in tumor size. To experimentally evaluate this possibility, we performed a dose de-escalation study in mice. Mice were treated with rapamycin in combination with 100%, 50%, or 25% of the PD-0325901 dose. As expected, this produced a range of responses in FDG-PET uptake at 40 hours and tumor regression after 10 days (Figure 2–4C,D). Importantly, the suppression of FDG-PET activity at 40 hours, as measured by change in SUVmax, correlated with the ultimate decrease in tumor size after 10 days (Pearson R=0.711, p=0.03) (Figure 2–4D,E). These results suggest that early changes in the FDG-PET signal are indicative of the degree of target inhibition and correlate with eventual tumor regression in MPNSTs treated with combined mTORC1/MEK inhibitors.

DISCUSSION

Numerous PI3K pathway inhibitors have been developed and are being evaluated in clinical trials (Britten, 2013). However in many cancers it is not clear which specific component(s) within this pathway are most critical or to what degree they must be inhibited. Such information would undoubtedly facilitate the selection of the most appropriate drugs for clinical studies. In this study we used a genetic and chemical approach to systematically deconstruct the PI3K signaling pathway in *NF1*-mutant nervous system malignancies. Importantly, we found that mTORC1, which is regulated by p110a in these tumors, is the

minimal, essential PI3K pathway component and that surprisingly AKT and mTORC2 are dispensable. However, while agents that inhibit mTORC1 promote cytostasis in human tumor cells and genetically engineered models, tumor regression requires concomitant suppression of the MEK/ERK pathway.

Notably, there are currently no effective therapies for MPNSTs. As such, these studies reveal a promising therapeutic approach as well as a mechanistic framework for selecting the most appropriate agents for clinical trials. For example, because p110β does not appear to contribute to the therapeutic response in these tumors perhaps p110a-specific, β-sparing PI3K inhibitors could be used with less toxicity (Liu et al., 2009). Alternatively, because mTORC1 appears to be the key PI3K effector in these tumors perhaps rapalogs, which exhibit excellent pharmacokinetic properties, may be suitable for combination therapies. The observation that AKT is not activated in these tumors by feedback inhibition and that AKT inhibitors do not enhance the effects of rapamycin, further alleviates the concern that AKT suppression may be required in this setting. Nevertheless, these studies suggest that successful agents must promote sustained inhibition of both ERK and mTORC1. Importantly, suppression of these same targets results in tumor regression in a mouse model of *NF1*-mutant melanoma, underscoring the importance of these pathways in *NF1*-deficient cancers (Maertens et al., 2013). Nevertheless, establishing the sufficient degree/length of inhibition of both targets that will be required to mediate an efficacious response in patients represents a formidable challenge.

While mouse models are useful for identifying critical therapeutic targets in genetically defined cancers, the ultimate success of a therapy in humans depends on many factors. Certainly, species-specific differences in tumor complexity may limit efficacy or restrict therapeutic responses to a subset of patients. However, perhaps an even more important consideration relates to dosing. One of the primary obstacles in developing combination

therapies, especially when targeting two major signaling pathways, is achieving efficacy while preventing toxicity. As such, even if the correct therapeutic targets have been identified, it may not be possible to sufficiently suppress these targets in humans. MEK inhibitors have been shown to exhibit toxicity in humans at high doses (LoRusso et al., 2010; Renouf et al., 2012). Therefore in this study we used a dose of PD-0325901 that is comparable to the tolerable dose in humans. Similarly, the dose of rapamycin was selected based on a previous preclinical study that led to successful human clinical trial in a number of tuberous sclerosis complex related pathologies, although reported trough plasma levels were somewhat higher than what has been observed in humans (~50ng/ml versus 3–20 ng/ml in humans) (Ando et al., 2013; Franz et al., 2013; Krueger et al., 2013; Meikle et al., 2008). However our preliminary observations suggest that lower doses and/or intermittent dosing of mTOR inhibitors/rapalogs are also effective when combined with MEK inhibitors. Given the differences in toxicity observed between mice and humans, only clinical trials will reveal whether an effective, non-toxic dose can be achieved. As such, another important goal of this study was to develop a biomarker that could be used to guide dosing in the clinic.

Current clinical trial strategies involve dosing up to the Maximum Tolerated Dose of one drug, and adding the second drug to the tolerable dose when possible. However, it is not always clear how dose escalation/de-escalation affects the degree or kinetics of target inhibition or if dosing at the MTD is necessary. As such, we set out to identify a biomarker(s) that would serve as an early downstream readout of effective, combined inhibition of MEK and TORC1. While several genes were identified in these tumors, *GLUT1* stood out as an important and tractable molecular change. Consistent with the documented role of GLUT1 in regulating glucose uptake, we found that ^{18}F-FDG uptake, as measured by FDG-PET, was a reliable readout of effective, combined target inhibition *in vivo*. Importantly, changes in GLUT1 expression and ^{18}F-FDG uptake occurred prior to tumor regression, supporting its role as a

molecular marker of TORC1/MEK suppression rather than a consequence of tumor shrinkage. Interestingly, neither GLUT1 expression nor glucose uptake were suppressed after treatment with either rapamycin or MEK inhibitors alone. This observation differs from findings in a subset of other mTOR-driven tumor types, where HIF1α-dependent *GLUT1* expression is decreased after treatment with rapamycin, as is ^{18}F-FDG uptake (Shackelford et al., 2009; Thomas et al., 2006). We have previously shown that neither GLUT1 nor HIF1α levels are altered in MPNSTs when treated with rapamycin, marking an important distinction between *NF1*-deficient tumors and these other mTOR-driven tumors (Johannessen et al., 2008). Here, we provide an explanation for this difference, as simultaneous inhibition of both the mTORC1 and MEK are required to suppress GLUT1 and ^{18}F-FDG uptake in MPNSTs. It will be interesting to determine whether inhibition of both pathways is required to alter glucose uptake in other tumors, in particular other RAS-driven tumors. Certainly, other factors, such as hexokinase activity or other members of the GLUT family, may contribute to glucose uptake in some cancers and in these instances ^{18}F- FDG uptake might not be an effective biomarker. However our studies suggest that FDG-PET imaging represents a promising, non-invasive means of measuring combined mTORC1/MEK inhibition *in vivo* in these *NF1*-mutant tumors, which can be readily incorporated into clinical trials. Such a tool should help identify the most effective drugs, facilitate dosing, and its utility may extend beyond NF1-mutant cancers.

METHODS

Cell Lines and Reagents

S462s and LN229s were purchased from ATCC. 90-8TLs were generously provided by Dr. Eric Legius (KULeuven). The authors performed no further authentication of the cell lines. Cell lines were cultured in Dulbecco's Modified Eagle Medium (DMEM) supplemented with fetal bovine serum (10%) and L-glutamine. Antibodies were obtained from the following sources:

Cell Signaling Technologies: pAKT (4060), AKT (9272), pERK (4370), ERK (9102), pS6 (2211), S6 (2217), p110α (4255), p110β (3011), Vinculin (4650), 4E-BP1 (9452), mTOR (7C10), Rictor (53A2), Raptor (24C12) pTSC2 (3611), TSC2 (3612) GAPDH (2118); Santa Cruz Biotechnology: p110δ (sc-7176); Trans Labs: p120 (G12920), Sigma: Actin (A2066), Alpha Diagnostics: Glut1 (GT11-A). Torin1, A66-(S), AZD-6284, and CAL-101 were kindly provided by Nathanael Gray (Dana Farber Cancer Institute/Harvard Medical School). MK-2206 was generously provided by D. Wade Clapp (Indiana University). GDC-0941 was provided by Genentech (San Francisco, CA). PD-0325901 was a gift from Kevin Shannon (University of California, San Francisco). Rapamycin was purchased from LC Labs.

RNAi

Non-Targeting and PIK3CA, PIK3CB, PIK3CD, Raptor, Rictor, mTOR siRNA pools were purchased from Dharmacon (D-001810-10, L-003018-00, L-003019-00, L-006775-00, L-004107-00, L-016984-00, L-003008-00, respectively). siRNAs were transfected overnight in antibiotic free medium using RNAiMax lipofectamine from Invitrogen.

Cellular Proliferation Studies

Approximately 125,000 cells per well were seeded in 6-well plates. For siRNA experiments, cells were seeded 12–16 hours after transfection. 24-hours after plating, day 0 counts were taken using a hemocytometer and trypan blue exclusion. For inhibitor experiments, drug treatments were started at this time. Inhibitors were changed once daily, except for PI3K isoform experiments where drugs were replenished twice daily. Final cell counts were taken 96 hours after day 0 counts.

Drug Treatments and Dosing Schedule

Animal procedures were approved by the Center for Animal and Comparative Medicine in Harvard Medical School in accordance with the NIH Guild for the Care and Use of Laboratory Animals and the Animal Welfare Act. C56/BL6 NPcis mice have been previously

described (Cichowski et al., 1999). Mice were treated daily with rapamycin via IP injections at 5 mg/kg, which were prepared as previously described (Johannessen et al., 2008). PD-0325901 was administered at 1.5 mg/kg once or twice daily (10 hours apart) by oral gavage. PD-0325901 was prepared as previously described.(Brown et al., 2007). GDC-0941 was administered at 150mg/kg once daily by oral gavage. GDC-0941 was prepared as previously described (Wallin et al., 2012). Compounds given in combination were administered sequentially.

Biopsy

Tumor biopsy was performed on mice prior to drug treatment using the wedge biopsy technique and snap-frozen. Drug treatment was started 8 hours after initial biopsy. The post-treatment biopsy was performed 3 days after treatment began. The mouse was anesthetized by isoflurane inhalation and given a local block with lidocaine and marcaine while the tumor biopsy was collected.

Tumor Volume Measurements

Mice were started on a treatment when tumor size reached 200–1000 mm3. Tumor size was measured every 2–3 days by Vernier calipers. Tumor volume was calculated using the standard formula $L \times W^2 \times 0.52$. A mouse pathologist confirmed that all tumors in this study are MPNSTs.

^{18}F-FDG-PET Imaging and Analysis

PET/CT scans were performed on the Bioscan NanoPET/CT at the Longwood Small Animal Imaging Facility. This PET scanner is equipped with a dedicated isoflurane anesthesia system, temperature controlled platform, cardiac gating, and respiratory gating. PET scanning was performed on anesthetized animals lying motionless on a table, after Retro-orbital IV injection of 0.1 to 10 mCi of F18-FDG PET radioisotope, while being imaged with a coincidence camera. The mice were imaged after a pre-determined “washout” period (30-60 min). Individual

mice were first scanned pre-treatment and then 40 hours after the treatment regimen was initiated (see dosing schedule methods). For quantitative analysis, the standardized uptake value (SUV) normalized to body weight in the tumor was calculated using SUV= ACvoi (kBq/ml)/(FDGdose(MBq)/BW(kg)) where ACvoi is the average activity concentration in the tumor volume (or the maximum value); FDGdose is the dose of F18-FDG administered; and BW is the body weight. For evaluating tumors the highest SUV in the tumor was taken as the SUVmax.

Microarray

RNA isolated from MPNST tumor samples from NPcis mice treated for 14 hours with vehicle, rapamycin, PD-0325901, or the combination of rapamycin and PD-0325901 For all PD-0325901 treated samples, PD-0325901 was dosed a second time at 10 hours. RNA was isolated with Trizol following the manufactures protocol. RNA clean-up was then performed using Qiagen's RNA easy kit (#74104). The Partners HealthCare Center for Personalized Genetic Medicine core facility hybridized the RNA to the Affymetrics Mouse Gene 1.0 STS. To determine genes differentially expressed in the combination treatment, a class comparison between the combination treated samples and all other samples was performed. Analysis was completed using BRB-Array tools developed by Dr. Richard Simon and the BRB-ArrayTools Development team. Thresholds were set at $p<0.001$. Microarray data can be accessed in the GEO database (accession number: GSE57141).

Acknowledgments

We would like to thank Haley Goodwill, John Frangioni, and the Longwood Small Animal Imaging facility at Beth Israel Hospital for performing the ^{18}F-FDG PET imaging studies. We also thank Roderick T. Bronson for histologic confirmation of all MPNSTs.

Chapter 3: HDAC and mTOR Inhibitors Cooperate to Drive Irreversible Cell Stress and Tumor Regression

HDAC and mTOR Inhibitors Cooperate to Drive Irreversible Cell Stress and Tumor Regression

Clare F. Malone[1,2], Kay F. Macleod[3], Karen Cichowski[1,2,4]

[1]Genetics Division, Department of Medicine, Brigham and Women's Hospital, [2]Harvard Medical School, Boston MA 02115, [3]The Ben May Institute for Cancer Research, The University of Chicago, Chicago, IL 60637 [4]Ludwig Center at Dana-Farber/Harvard Cancer Center, Boston, MA 02115

Author Attributions

Clare F Malone: Performed all experiments, wrote the manuscript, and with KC planned the project.

Kay F Macleod: Analyzed EM samples shown in Figure 3-3.

Karen Cichowski: Supervised and developed the project with CFM, edited the manuscript.

INTRODUCTION

Mutations in the *NF1* tumor suppressor are frequently found in sporadic cancers and cause the familial cancer predisposition syndrome neurofibromatosis type 1 (NF1). NF1 patients experience a variety of symptoms, most commonly café-au-lait spots, benign neurofibromas, and Lisch nodules. However, 8–13% of NF1 patients will develop a malignant peripheral nerve sheath tumor (MPNST) in their lifetime (Evans et al., 2002). These tumors are highly aggressive, readily metastasize, and are the leading cause of death in NF1 patients (Evans et al., 2002; Porter et al., 2009). Complete surgical resection is currently the only effective treatment, as conventional radiation and chemotherapy do not prolong overall survival (Zehou et al., 2013). Therefore, identifying novel therapeutic approaches for these tumors is of critical clinical importance.

We have previously focused on identifying therapies that target specific signaling pathways that become activated upon NF1 loss (Malone et al., 2014). However, in addition to specific mutations in oncogenes and tumor suppressors, which cause the pro-tumorigenic hallmarks of cancer (Hanahan and Weinberg, 2000), there are a number of cellular adaptations that are not sufficient to induce transformation but are nonetheless required for maintenance of the tumorigenic state (Solimini et al., 2007). In particular, cancer cells frequently exhibit high levels of proteotoxic and oxidative stress as a result of aneuploidy, high mutational load, and altered cellular metabolism (Klaunig et al., 2010; Oromendia and Amon, 2014; Williams et al., 2008). Cancer cells are reliant on stress response pathways in order to survive with high levels of unfolded proteins and reactive oxygen species (ROS), and thus targeting the stress phenotype of cancer is an alternative therapeutic approach (Luo et al., 2009). Inhibiting adaptive stress responses or inducing further stress could push the level of stress in cancer cells beyond the survival threshold while neighboring normal cells, which have low levels of basal stress, will survive.

Previously, our lab has shown that MPNSTs are very sensitive to the combination of mTOR inhibitors and agents that induce endoplasmic reticulum stress, which demonstrates that proteotoxic stress can be therapeutically exploited in this context (De Raedt et al., 2011). The combined effects of mTOR inhibition and ER stress induction initiated a vicious cycle of ER and mitochondrial damage leading to destruction of cellular organelles and eventual cell death. Importantly, the production of ROS was critical, and treatment with a ROS scavenger blocked the effects of this combination. ROS was produced after ER stress, and mTOR inhibition lowered the levels of reduced glutathione (GSH), an important ROS scavenger, so that cells could no longer attenuate increased ROS. In particular, that study identified that HSP90 inhibition induced ER stress and could synergize with mTOR inhibition. The combination of ganetespib, an HSP90 inhibitor, and everolimus, an mTOR inhibitor, recently entered clinical trials for MPNSTs (NCT02008877). However, to date there are no approved HSP90 inhibitors, and it remains to be determined whether an acceptable toxicity level can be achieved by combining these two agents.

Therefore, we decided to look for an FDA-approved drug that can also induce ER stress and possibly exploit these same vulnerabilities to promote tumor regression in combination with an mTOR inhibitor. The pan-HDAC inhibitor vorinostat is approved for use in cutaneous T-cell lymphoma (CTCL) and has been shown to induce ER stress in some settings (Kahali et al., 2010). Here, we report that the combination of two FDA-approved agents, vorinostat and rapamycin, effectively promotes MPNST regression in a genetically engineered mouse model of MPNSTs. We further show that this combination exploits both proteotoxic and oxidative stress to promote cell death.

RESULTS

HDAC Inhibition Induces ER Stress and Promotes MPNST cell death

Induction of ER stress leads to activation of the unfolded protein response (UPR). The UPR is initially a cytoprotective process designed to reduce translation and increase chaperone function to attenuate the accumulation of unfolded proteins in the ER lumen. However, if ER stress is prolonged and excessive, the UPR will drive apoptosis (Ron and Walter, 2007). The FDA-approved, pan-HDAC inhibitor vorinostat has been reported to induce ER-stress and the unfolded protein response (Kahali et al., 2010; 2012). Therefore, we were interested in whether vorinostat would induce ER stress in MPNSTs. Treatment with vorinostat induced a number of markers of the UPR, including BIP, EIF2α phosphorylation, spliced XBP1, ATF4, and CHOP, indicating that the UPR was indeed activated by vorinostat treatment (Figure 3–1A). ER-stress inducing agents such as thapsigargin, tunicamyicn, and HSP90 inhibitors are cytotoxic *in vitro* in MPNST cells (De Raedt et al., 2011). Consistent with this, vorinostat has a cytotoxic effect on MPNST cell lines as a monotherapy (Figure 3–1B, C). Importantly, these concentrations are more than 10-fold lower than lethal concentrations reported for non-

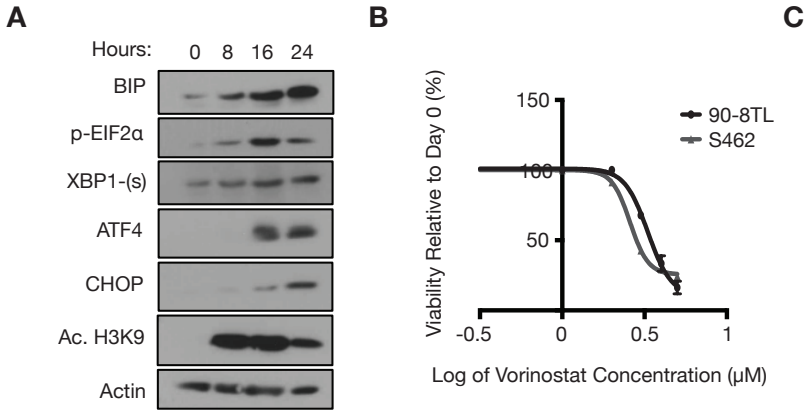

C

Cell Line	LD50 (μM)
S462	2.5
90-8TL	3.3

Figure 3–1. HDAC Inhibition Induces ER Stress and Kills MPSNT Cells *in vitro*. A, immunoblot of UPR markers BIP, p-EIF2α, XBP1-(s), ATF4, and CHOP, as well as Acetylated histone H3K9 after treatment with 2μM vorinostat for the indicated amount of time. Actin serves as a control. **B,** the percent of viable cells relative to day 0 after 72 hours of treatment with vorinostat at the indicated dose. **C,** the experimentally determined dose of vorinostat at which 50% of cells are dead (LD50) for two MPNST cell lines

transformed cells, indicating that MPSNT cell lines are hyper-sensitive to HDAC inhibition (Bolden et al., 2013).

Combined mTOR and HDAC Inhibition Promotes Tumor Regression in vivo

While ER stress inducers, such as the HSP90 inhibitor IPI-504, kill human and mouse MPNST cells *in vitro*, we have shown that they are not sufficient to induce tumor regression *in vivo* as a monotherapy (De Raedt et al., 2011). However, when ER stress inducers are combined with mTOR inhibition, which alone is cytostatic, this induces a profound cytotoxic effect by enhancing lethal ER stress through increased ROS, as discussed above. Therefore, we were interested in whether the addition of an mTOR inhibitor could improve the therapeutic effects of vorinostat *in vitro*. Interestingly, at sub-LD50 doses of vorinostat, treatment with INK-128, an mTOR kinase inhibitor, enhanced the cytotoxic effect of vorinostat, indicating that the combination of these two agents might be an effective therapy (Figure 3–2A).

To test the effects of this combination *in vivo*, we employed a genetically engineered mouse model of MPNSTs. In this model, mice are heterozygous for *Nf1* and *p53*, and the deletions are in *cis* (NPcis), such that mice experience simultaneous loss of heterozygosity for *Nf1* and *p53.* MPNSTs, which genetically and histologically recapitulate human tumors, develop with an average latency of about 5 months and grow aggressively—tumors reach maximal acceptable size within 10–15 days. Tumor bearing animals were treated with vorinostat or the combination of rapamycin and vorinostat. A dose of 100mg/kg of vorinostat was selected as this is a standard pre-clinical dose (Saelen et al., 2012; Xu et al., 2013). Vorinostat alone had no effect on tumor growth ($p=0.35$, Figure 3–2B) in contrast to xenograft models of MPNSTs where HDAC inhibition has a cytostatic effect (Lopez et al., 2011). However, as with other ER-stress inducing agents, when vorinostat and rapamycin were

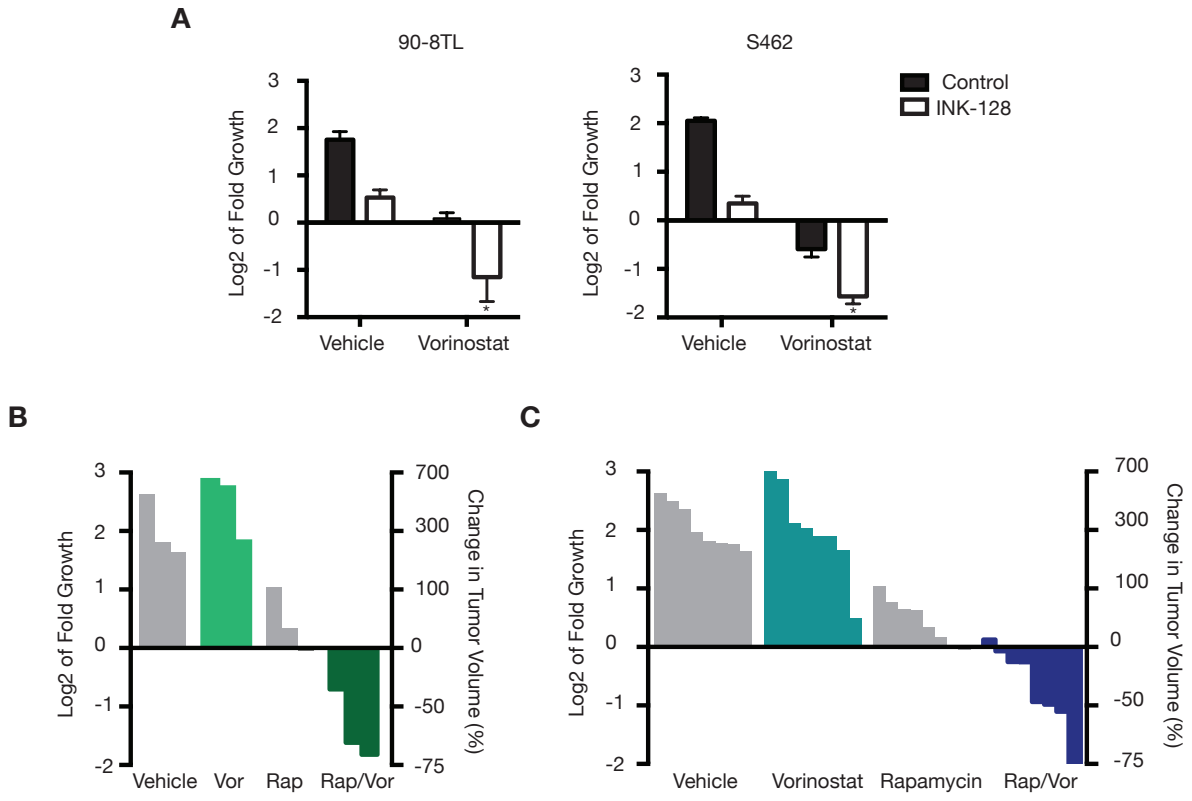

Figure 3–2. Combined mTOR and HDAC Inhibition Kills MPNSTs *in vitro* and *in vivo*. A, MPNST cell lines were treated with vorinostat (2μM) plus vehicle (black) or INK-128 (100nM in 90-8TLs, 200nM in S462s, white) for 72 hours. Bar graphs indicate the log2 of fold change in growth relative to day 0. Data points, triplicate averages ± SD. * $p<0.05$. **B,** waterfall plot depicting the log2 of fold change in MPNST volume after 10 days of treatment with 100mg/kg vorinostat daily (pale green), or vorinostat plus 5mg/kg rapamycin daily (dark green). Vehicle and rapamycin data is reprinted from Figure 2-2 for reference (grey). Left y-axis, log2 fold of tumor growth. Right y-axis, percent change in tumor volume. **C,** waterfall plot depicting the log2 of fold change in tumor volume after 10 days of treatment with 50mg/kg vorinostat (teal) or vorinostat plus 5mg/kg rapamycin (dark blue). Vehicle and rapamycin values are reprinted from figure 2-2 for reference (grey). Left y-axis, log2 fold of tumor growth. Right y-axis, percent change in tumor volume.

administered together, tumors regressed dramatically, with an average 62% decrease in tumor volume (Figure 3–2A). These studies provided proof of principle that dual HDAC and mTOR inhibition is a promising therapeutic strategy for MPNSTs.

However, while this dose of vorinostat (100mg/kg) is commonly used pre-clinically in mouse models, it does not accurately reflect human dosing. To verify the clinical relevance of

this result, we wanted to determine whether a human equivalent dose of vorinostat could also induce tumor shrinkage when combined with rapamycin. To this end, we calculated the mouse equivalent dose using a formula for dose translation based on body surface area (Reagan-Shaw et al., 2008). The standard human dose of vorinostat is 400mg daily, which can be reduced to 300mg daily in the event of toxicity (Mann et al., 2007). A primary concern with any combination therapy is achieving an effective therapeutic dose without inducing toxicity. Therefore, we decided to treat mice with 50mg/kg of vorinostat, a very conservative dose that is even lower than the dose that would recapitulate the lowest human dose of 300mg. Tumor-bearing mice were treated with 50mg/kg vorinostat once a day, either alone or in combination with rapamycin. As with the higher dose, vorinostat alone had no significant effect on tumor growth ($p=0.7768$), but when combined with rapamycin tumors regressed, with half of the tumors shrinking 50% or more. Thus, even at a clinically relevant dose of vorinostat, the combination of these two FDA-approved agents has substantial anti-tumor activity.

Combined HDAC and mTOR Inhibition Promotes ER and Mitochondrial Damage

One of the distinguishing features of HSP90 inhibitors and rapamycin in this model was the ER swelling and mitochondrial swelling observed by transmission electron microscopy (De Raedt et al., 2011). Given that HDAC inhibition induces ER stress in MPNST cells, we sought to determine whether this novel combination was inducing a similar phenotype. Tumors were examined by transmission electron microscopy 16 and 40 hours after treatment with rapamycin and vorinostat. However, at these time points, much of the tumor had already begun to die, leaving very few live cells to examine. In the cells that were still alive, there was visible swelling of the ER and mitochondria (Figure 3–3). This evidence is consistent with the induction of irresolvable ER stress and mitochondrial damage resulting in a catastrophic cycle of organelle damage and cell death, similar to the effect of HSP90 inhibition.

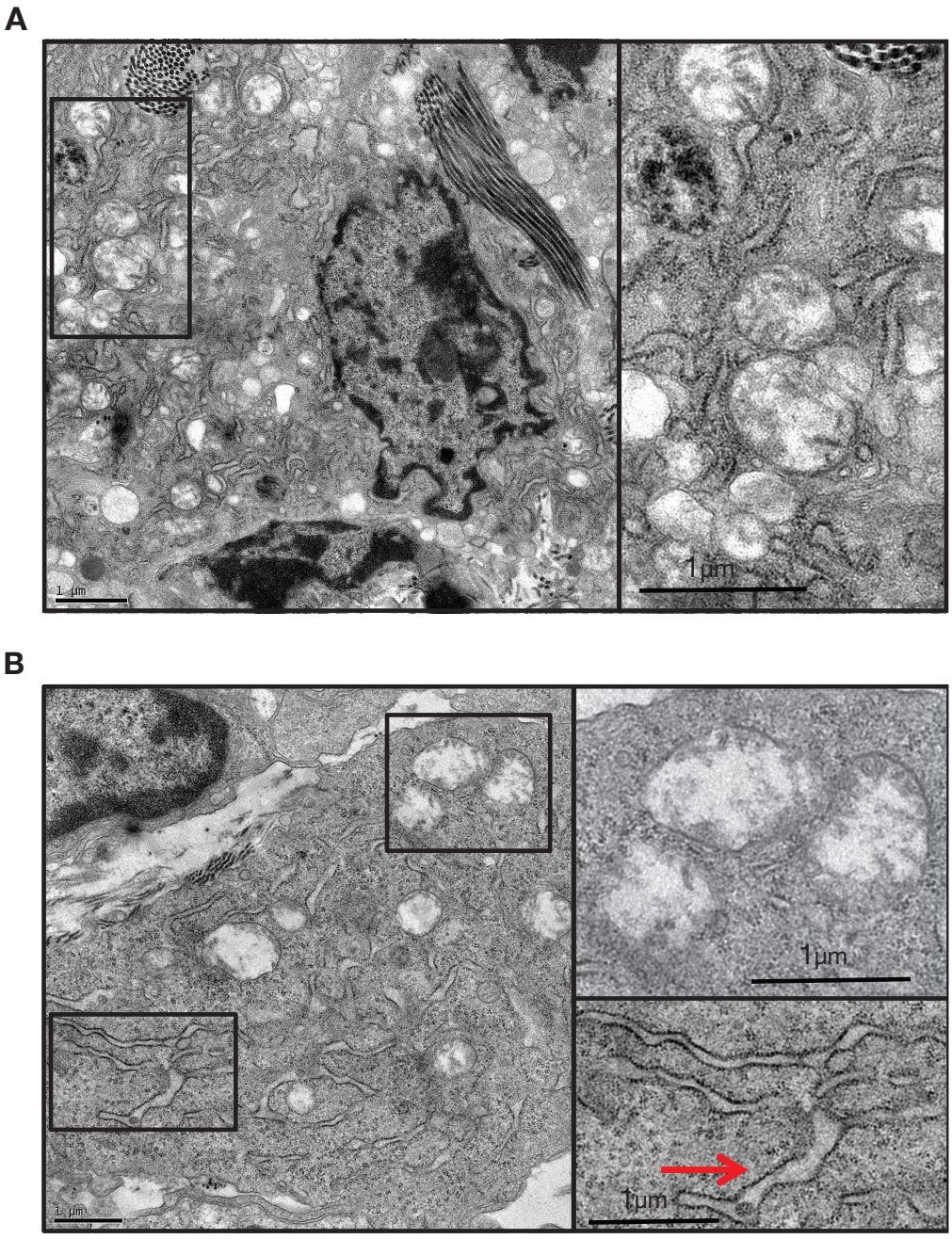

Figure 3–3. Combined HDAC and mTOR Inhibition Causes ER and Mitochondrial Swelling in MPNSTs. A, Transmission electron microscopy of MPNST after 16 hours of treatment with 100mg/kg vorinostat and 5mg/kg rapamycin showing mitochondrial swelling. Boxed area is enlarged at right, showing a number of swollen mitochondria. **B,** Transmission electron microscopy of MPNST after 40 hours of treatment with 100mg/kg vorinostat and 5mg/kg rapamycin. Top box is enlarged on top right, showing swollen mitochondria. Bottom box is enlarged on bottom right, showing swollen ER, indicated with a red arrow.

HDAC6 Suppression is not Sufficient to Synergize with Rapamycin

In order to investigate the mechanism by which vorinostat might be inducing ER stress we examined the connection between HDAC inhibition and HSP90. Vorinostat treatment has been reported to impair HSP90 function in some settings (Rao et al., 2009). Specifically, HDAC6 is the primary deacetylase for HSP90. When HDAC6 is inhibited, HSP90 becomes hyper-acetylated, which blocks its chaperone function (Boyault et al., 2007; Kekatpure et al., 2009; Scroggins et al., 2007). Vorinostat is a pan-HDAC inhibitor with activity against all Zn^{2+}-dependent HDACs, including HDAC6. HSP90 inhibitors are known to induce ER stress and synergize with mTOR inhibition in this tumor model, and we observed a similar cellular phenotype by electron microscopy, so we wanted to determine whether vorinostat was mediating its effects through HDAC6 inhibition and HSP90 hyper-acetylation. To this end, we ablated HDAC6 expression in MPNST cells through siRNA-mediated knockdown, and then treated with the mTOR inhibitor INK-128. There was no difference in response to INK-128 treatment between HDAC6-deficient cells and controls (Figure 3–4A), suggesting that HDAC6 inhibition is not sufficient to synergize with INK-128. Furthermore, treatment with Nexturastat A, a highly specific HDAC6 inhibitor, did not affect MPNST cell growth at concentrations from 0.1 to 1μM (Figure 3–4B). Moreover, the addition of INK-128 did not have any combined effect, in marked contrast to what was observed with vorinostat (Figure 3–4B). Importantly, even at a concentration of 0.1μM, tubulin, an established target of HDAC6, was hyper-acetylated demonstrating effective HDAC6 inhibition. In contrast, histone acetylation was not substantially elevated suggesting that Nexturastat A is indeed HDAC6-specific (Figure 3–4B).

HDAC6 has been reported to be the primary deacetylase for HSP90, but there is some evidence that other HDACs may be able to deacetylate HSP90 as well (Nishioka et al., 2008).

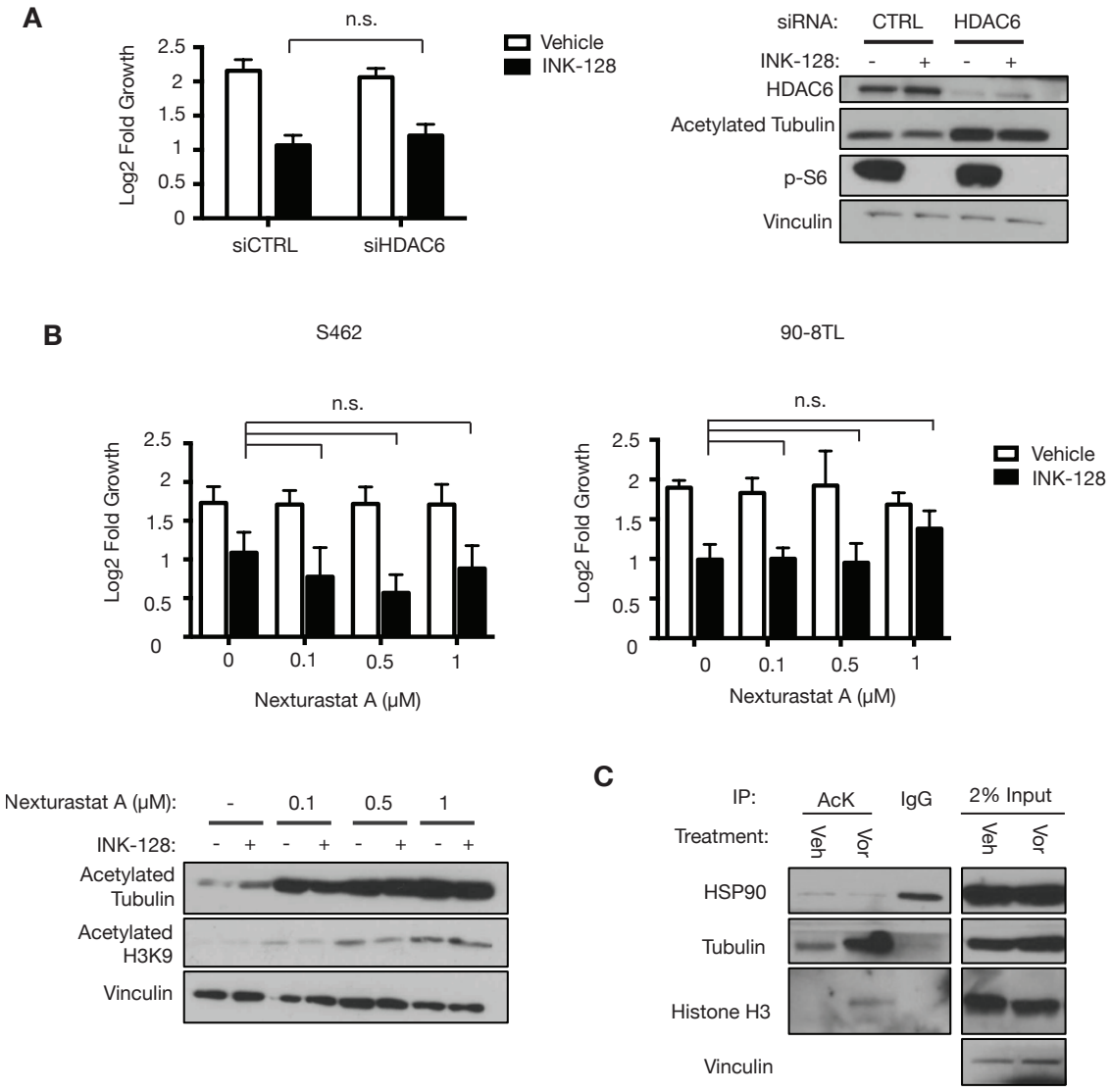

Figure 3–4. HDAC6 Inhibition is not Sufficient to Synergize with mTOR Inhibition. A, 90-8TLs were transfected with pooled siRNA targeting *HDAC6* or non-silencing siRNA and then treated with vorinostat (white) or 100nM INK-128 (black). Data points, triplicate averages ± SD of log2 of fold change relative to day 0 after 72 hours of treatment. Immunoblot shows HDAC6, acetylated tubulin, and phosphorylated S6 48 hours after transfection with indicated siRNA and 24 hours after indicated treatment. Vinculin serves as a control. **B,** MPNSTs were treated with indicated concentration of Nexturastat A, plus vehicle (white) or INK-128 (100nM 90-8TLs, 200nM S462s, black). Immunoblot shows acetylated tubulin and acetylated H3K9 after treatment with indicated concentration of Nexturastat A plus or minus INK-128 as indicated. Vinculin serves as a control. **C,** Acetylated lysine or IgG was precipitated from 90-8Tls after 16 hours of treatment with vehicle (Veh) or 2μM vorinostat (Vor). Immunoblot shows HSP90, tubulin, and Histone H3. Vinculin serves as a control.

Given the strong connection between HSP90 and ER stress, and our previous studies outlining the efficacy of HSP90 inhibitors in combination with mTOR inhibitors, we wanted to determine whether HSP90 was acetylated after treatment with vorinostat. To that end, we treated MPNST cells with vorinostat and then immunoprecipitated acetylated lysine, and probed for HSP90, Histone H3, and Tubulin. As expected, acetylated histone H3 was present in the vorinostat treated cells, as well as acetylated tubulin, which is indicative of successful HDAC 1–3 and HDAC6 inhibition, respectively (Figure 3–4C). However, there was no increase in HSP90 acetylation in vorinostat treated cells. Together, this data demonstrates that HDAC6 inhibition alone is not sufficient and that HSP90 hyper-acetylation does not appear to be a primary contributor to the efficacy of this combination therapy.

Activation of the Unfolded Protein Response Contributes to Cell Death in Combination treated MPNSTs

Modulation of HSP90 activity does not seem to be contributing to the efficacy of vorinostat in this context, so we wanted to determine whether activation of the unfolded protein response is related to the therapeutic effect. The UPR is initially a cell protective response, but when ER stress is unresolved, the UPR can become a driver of apoptosis (Sano and Reed, 2013). Given this dual role for the UPR, we were interested in whether activation of the UPR was protecting against ER stress induced by the combination therapy, or was contributing to the cell death observed after treatment. In order to address this, we used pooled siRNAs to ablate expression of two of key UPR mediators: PERK, which is encoded by the gene *EIF2AK3*, and IRE1α, which is encoded by *ERN1*. We found that ablation of IRE1α had no effect on the efficacy of the combination therapy in either MPNST cell line, suggesting that this arm of the UPR is not significantly protecting against or inducing the observed cell death (Figure 3–5A). However, PERK ablation partially protected both MPNST cell lines from

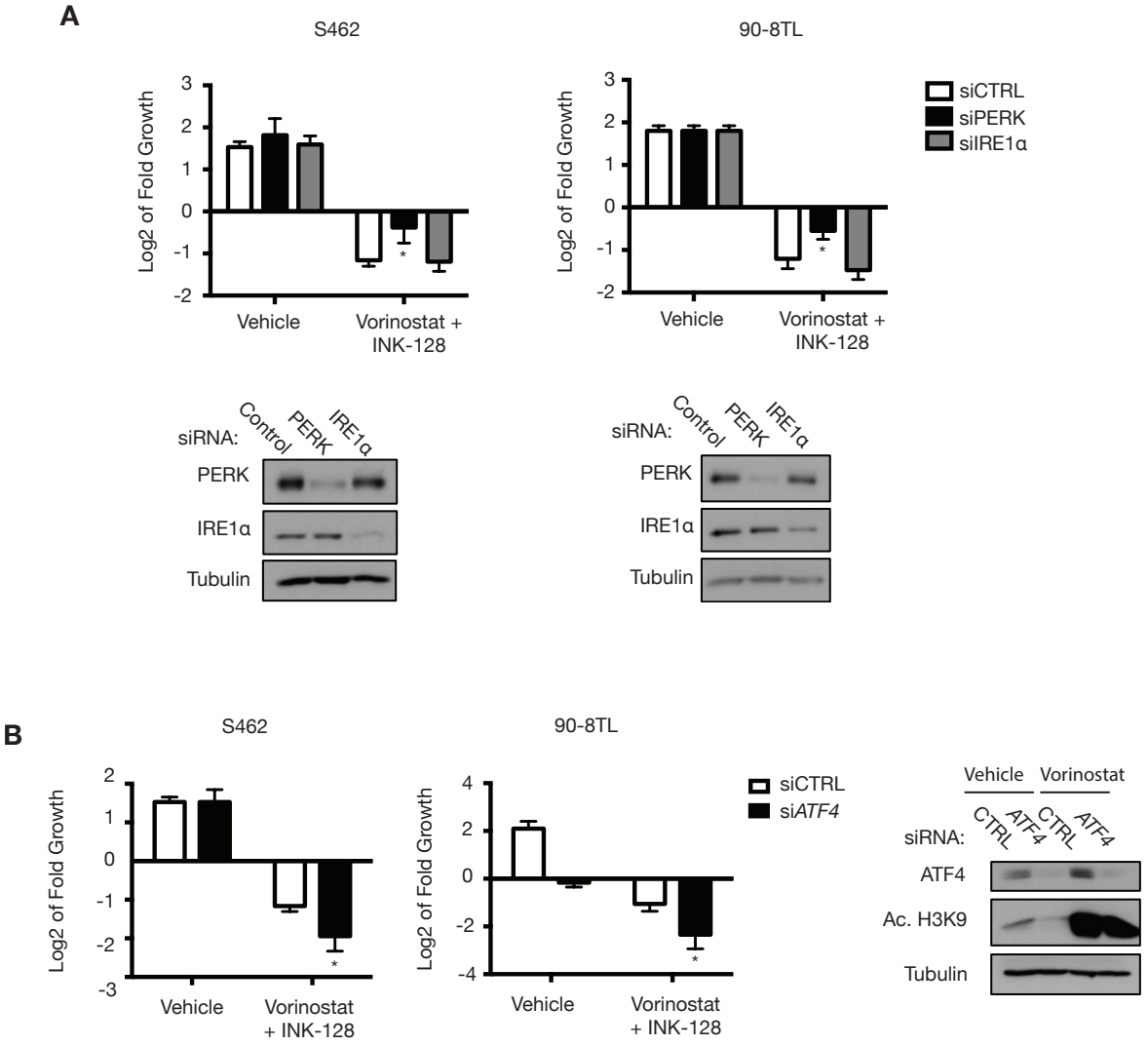

Figure 3–5. The UPR Contributes to Combination Induced Cell Death. A, S462s and 90-8TLs were transfected with pooled siRNAs against *EIF2AK3* (PERK, black) or *ERN1* (IRE1α, grey), or non-silencing (white) and then treated with vehicle or vorinostat (2μM) and INK-128 (200nM S462, 100nM 90-8TLs) as indicated. Bar graphs are triplicate averages ± SD of the log2 of fold change after 72 hours. Below, immunoblot shows PERK and IRE1α protein levels 72 hours after transfection with indicated siRNA. Tubulin serves as a control. **B,** 90-8TLs and S462s were transfected with pooled siRNAs targeting *ATF4* (black) or non-targeting (white) and treated with vehicle or vorinostat and INK-128 as indicated. . Bar graphs are triplicate averages ± SD of the log2 of fold change after 72 hours. At right, immunoblot shows ATF4 and Acetylated H3K9 levels in S462s 72 hours after transfection with either non-targeting siRNA, or si*ATF4*, and treatment with vehicle or 2μM vorinostat as indicated.

combination-induced death (Figure 3–5A), demonstrating that PERK activation in combination treated cells is likely promoting cell death.

PERK canonically drives apoptosis through activation of the transcription factor ATF4, which upregulates CHOP, and together they promote apoptosis (Han et al., 2013; Kim et al., 2008; Sano and Reed, 2013). To determine whether PERK activation was driving cell death through this canonical apoptotic pathway we tested the effect of ATF4 ablation. ATF4 knockdown reduced basal levels of ATF4 and blocked ATF4 upregulation after vorinostat treatment (Figure 3–5B). Unexpectedly, ATF4 knockdown not only failed to rescue the effects of the combination, but in fact ATF4 loss increased the sensitivity of both MPNST cell lines to combination treatment. The increased sensitivity of ATF4-deficient cells suggests that PERK's contribution to cell death is not through ATF4 in this context.

HDAC Inhibition Induces Oxidative Stress which is Essential for Synergy with mTOR inhibition

In order to better understand the mechanism of synergy between mTOR and HDAC inhibition, we performed transcriptional profiling in vehicle, INK-128, vorinostat, or combination treated MPNST cells, after 24 hours of treatment to allow time for epigenetic-mediated changes in transcription to occur. We performed a gene set class comparison to identify gene sets where more genes are differentially expressed than would be expected due to random chance in the combination treated cells relative to the other treatments, using gene sets in the Molecular Signatures Database. As expected, a number of gene sets involved in the unfolded protein response were differentially expressed in the combination treated cells by at least one metric of statistical significance (Figure 3–6A). Interestingly, we also found a number of gene sets related to oxidative stress were altered in the combination treated cells, suggesting a potential mechanistic role for oxidative stress in the therapeutic efficacy of the combination.

Figure 3–6. HDAC Inhibitor Induced Oxidative Stress is Critical for Therapeutic Efficacy. A, a microarray analysis was performed on 90-8TLs treated with vehicle, 100nM INK-128, 2μM vorinostat, or both for 24 hours. Table indicates proteotoxic and oxidative stress-related gene sets with differential expression in the combination treated cells relative to the other treatment groups that reached at least one metric of significance. Significance values for KS permutation, LS permutation, and the Efron-Tibshirani GSA p-value is shown. Values in red reach the cutoff for significance ($p<0.005$). **B,** Representative histogram of fluorescence intensity for S462s treated with vehicle (light grey), 2μM vorinostat (light green), or 1mM H_2O_2 (dark green), and dyed with DCFDA. An un-dyed vehicle-treated control is shown in dark grey. **C,** As in B, S462s were treated with vehicle or 2μM vorinostat and dyed with DCFDA. Bar graph indicates average mean fluorescent intensity from three independent experiments. A ratio-paired student's t-test was performed, and the p-value is shown. **D,** S462s and 90-8TLs were treated with 3μM vorinostat plus (black) or minus (white) 5mM N-acetyl cysteine (NAC). Bar graphs indicate triplicate average ± log2 of fold change after 72 hours of treatment. **E,** S462s were treated with vehicle or 2μM vorinostat as indicated, plus vehicle (white), 200nM INK-128 (black) or 200nM INK-128 and 5mM NAC (INK+NAC, grey). Data points indicate triplicate averages ± SD of log2 fold of tumor growth after 72 hours of treatment. * $p<0.05$.

A

Gene Set	LS Permutation Value	KS Permutation Value	Efron-Tibshirani's GSA test p-value
Oxidative Stress			
KYNG_RESPONSE_TO_H2O2	0.00039	0.00039	0.07
CHUANG_OXIDATIVE_STRESS_RESPONSE_UP	0.00066	0.02977	0.0005
CHUANG_OXIDATIVE_STRESS_RESPONSE_DN	0.00361	0.11379	0.57
WIEGEL_OXIDATIVE_STRESS_BY_TBH_AND_H2O2	0.00933	0.00047	0.36
MOOTHA_ROS	0.09478	0.0017	0.525
GARGALOVIC_RESPONSE_TO_OXIDIZED_PHOSPHOLIPIDS_TURQUOISE_DN	0.0004	0.01311	0.62
GARGALOVIC_RESPONSE_TO_OXIDIZED_PHOSPHOLIPIDS_TURQUOISE_UP	0.00062	0.00005	0.085
Proteotoxic Stress			
REACTOME_UNFOLDED_PROTEIN_RESPONSE	0.00353	0.0029	0.545
REACTOME_ACTIVATION_OF_CHAPERONES_BY_IRE1_ALPHA	0.01542	0.0042	0.32
REACTOME_ACTIVATION_OF_CHAPERONE_GENES_BY_ATF6_ALPHA	0.01644	0.00462	0.06
REACTOME_ACTIVATION_OFCHAPERONES_BY_ATF6_ALPHA	0.02922	0.00488	0.075

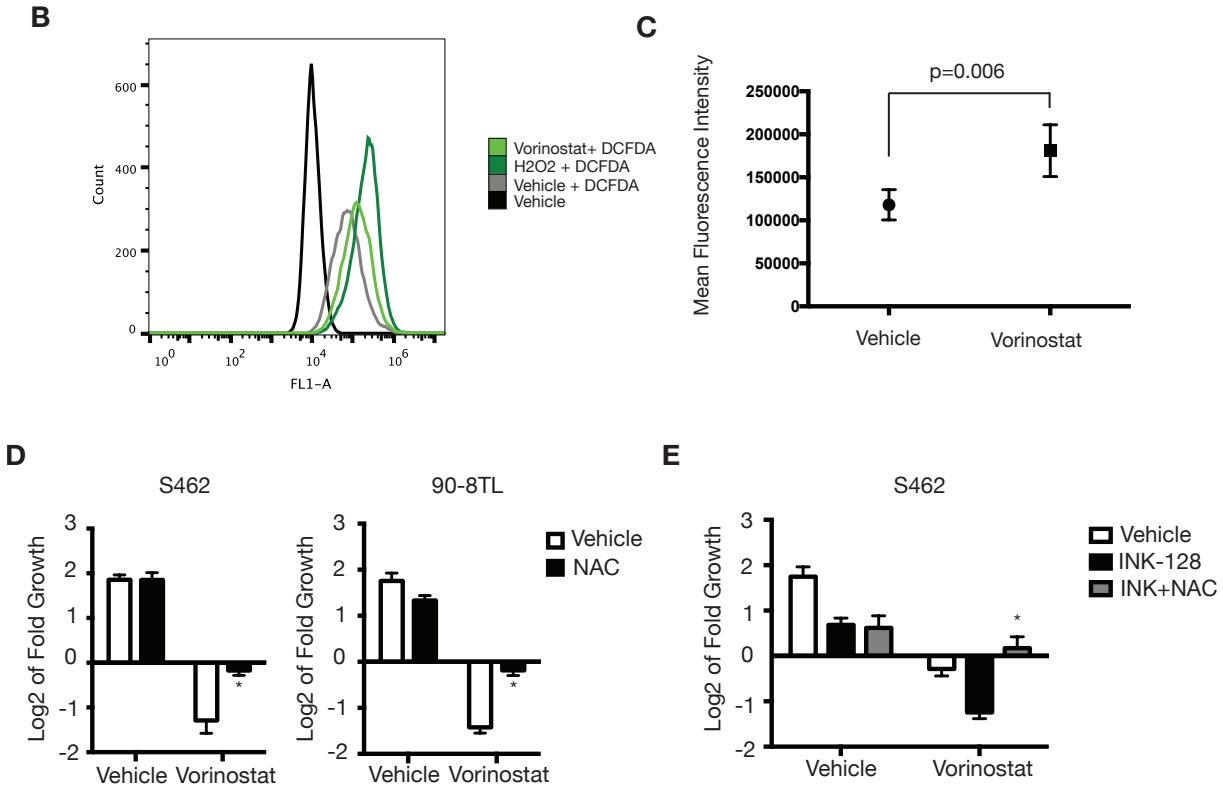

Figure 3–6 (Continued)

This finding was particularly striking because there is a well-established interdependent relationship between ER stress and oxidative stress. Increased oxidative stress promotes protein misfolding, and the accumulation of misfolded proteins causes calcium to be released from the ER, which promotes ROS production in the mitochondria (Eletto et al., 2014; Malhotra and Kaufman, 2007). We have previously found that oxidative stress is critical for the synergy between HSP90 inhibitors and mTOR inhibitors in this tumor type. Inhibition of mTOR lowers levels of the NADPH-dependent ROS scavenger reduced glutathione (GSH) in MPNSTs, sensitizing them to oxidative stress induced by HSP90 inhibitors (De Raedt et al., 2011). Notably, we found that vorinostat treatment increased cellular reactive oxygen species (ROS) by an average of 1.5 fold, as measured by DCFDA fluorescence (Figure 3–6B, C). Furthermore, cells treated with the broad ROS scavenger N-acetyl cysteine (NAC) were resistant to the cytotoxic effects of vorinostat alone, as well as the combination of INK-128 and vorinostat (Figure 3–6D, E) suggesting that oxidative stress is a critical component contributing to the therapeutic effect of this combination.

The Thioredoxin Inhibitor TXNIP is Upregulated by Combination Therapy

To identify specific gene targets that were altered during combination therapy, which might be mechanistically contributing to the oxidative and proteotoxic stress, we performed a gene expression class comparison on our transcriptional profile between combination treated cells and all other treatment groups. One of the most significantly upregulated genes in the combination treated cells was thioredoxin interacting protein (*TXNIP*) (2.47 fold, p=0.0000807, Figure 3–7A). TXNIP expression is modestly, but significantly, elevated by both vorinostat and INK-128 treatment in MPSNT cells (1.4 fold, p=0.0003273, and 1.7 fold, p=0.0000251, respectively) but it is significantly further upregulated in the combined treatment relative to either single treatment (2.3 fold relative to vorinostat p=0.0000187, and 1.95 fold relative to INK-128 p=0.0000012). Protein levels of TXNIP also increased modestly after treatment with

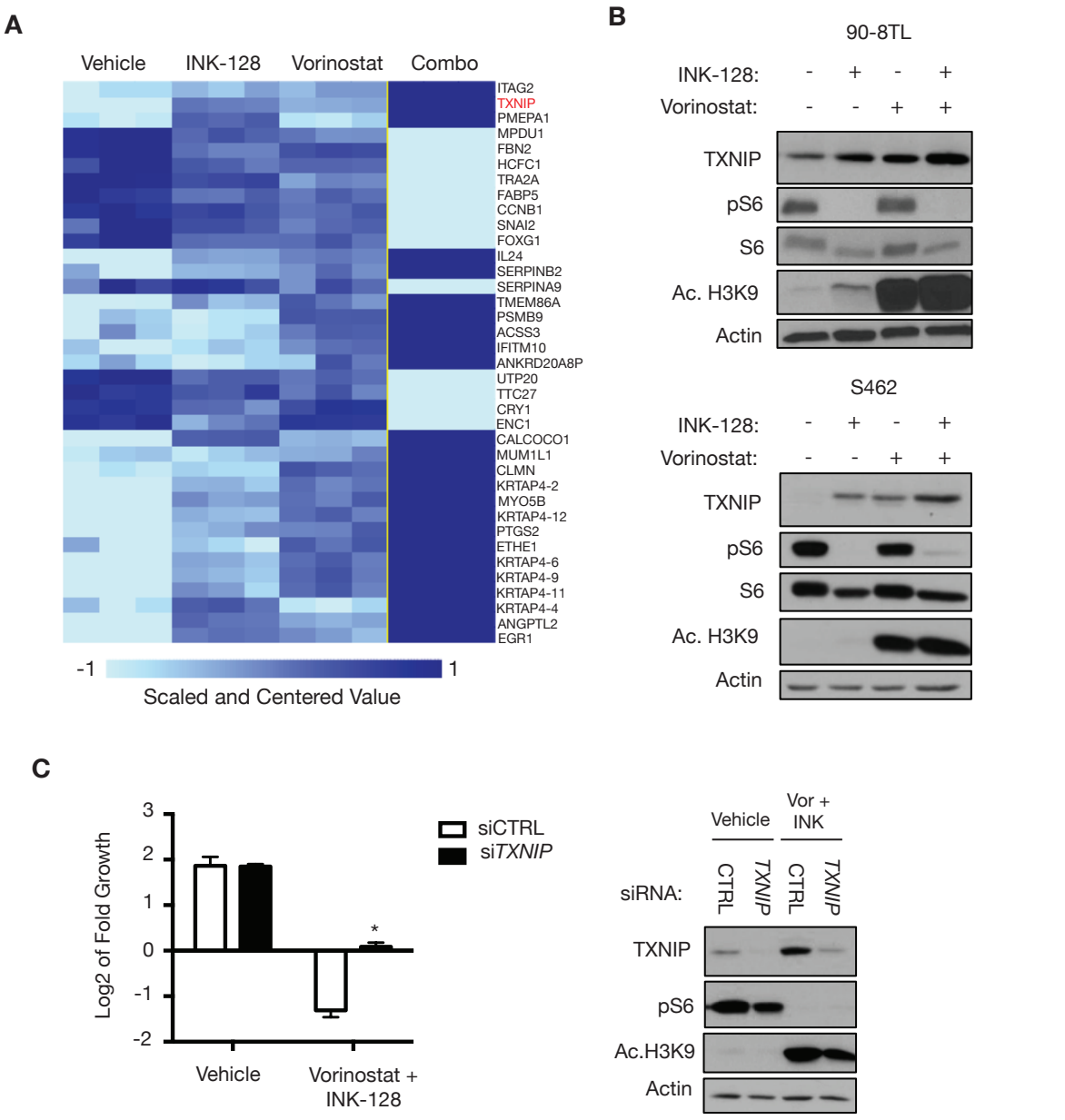

Figure 3–7 TXNIP is Upregulated after Combination Treatment and Contributes to Cell Death. **A,** Heat map showing genes whose expression was altered more than 1.5-fold and reached a significance of at least p<0.001 in the combination treated cells relative to single treatment and untreated cells. Dark blue indicates highest expression while pale blue indicates lowest expression. In red, *TXNIP* is highlighted. **B,** Immunoblot showing TXNIP, phosphorylated S6 and histone 3 lysine 9 (H3K9) acetylation levels after 24 hours of treatment with vehicle, INK-128 (100nM 90-8TLs, 200nM S462s), vorinostat (2μM) or both. Actin and S6 serve as controls. **C,** S462s were transfected with siRNAs targeting *TXNIP* (black) or control siRNA (white) and treated with vehicle or INK-128 (200nM) and vorinostat (2μM). Data points indicate triplicate averages ± SD of log2 fold growth after 72 hours. Immunoblot at right shows TXNIP, phosphorylated S6, and acetylated H3K9 72 hours after transfection with indicated siRNA, and 24 hours after treatment with vehicle or INK-128 (200nM) and vorinostat (2μM). Actin serves as a control.

either INK-128 or vorinostat in both MPNST cell lines, but TXNIP levels were even further elevated after combined treatment, confirming that this transcriptional change leads to increased protein levels (Figure 3–7B). TXNIP is a negative regulator of the cellular ROS scavenger thioredoxin (TRX), and has been previously reported to be upregulated by HDAC inhibition (Butler et al., 2002). In addition to increasing ROS, TXNIP binding to TRX can drive apoptosis by blocking the interaction between TRX and ASK1 (Lu and Holmgren, 2012; Saitoh et al., 1998). Interestingly, TXNIP is also transcriptionally induced by proteotoxic stress in a PERK-dependent but ATF4-independent manner, and is in fact key for the switch from a protective UPR to a terminal UPR (Anthony and Wek, 2012; Lerner et al., 2012; Oslowski et al., 2012). Thus TXNIP provides a potential mechanistic link between oxidative and proteotoxic stress and cell death.

Because TXNIP can be a driver of apoptosis in the context of unresolved ER stress and oxidative stress, we wanted to determine whether the increased TXNIP expression observed after combination treatment was contributing to the therapeutic effect. To that end, we ablated TXNIP expression using pooled siRNAs targeting *TXNIP*. We were able to decrease basal TXNIP expression as well as block the increase in expression induced by the combination of vorinostat and INK-128 (Figure 3–7C). We found that siRNA-mediated inhibition of TXNIP completely blocked the cytotoxic effect of combined vorinostat and INK-128 treatment, suggesting that TXNIP could in fact be a key driver of the therapeutic response. Additional studies that are currently underway to better understand this mechanism will be discussed later.

DISCUSSION

The combination of HSP90 inhibitors and mTOR inhibitors recently entered clinical trials for MPNSTs, based on promising pre-clinical data. However, it remains unclear whether an acceptable therapeutic window can be determined for this combination Even if an appropriate

dose can be identified, some patients may not be able to tolerate this particular combination. Thus, alternative therapeutic options that target the same cancer vulnerabilities could provide significant clinical benefit. In the present study, we have identified the successful therapeutic combination of rapamycin and vorinostat, which are both FDA-approved agents. This combination could be rapidly translated to the clinic where there are currently no effective therapies for MPNSTs. Phase I clinical trails are currently underway to determine the dosing of this combination in other cancers (NCT01087554, NCT01174199) so the tolerable dose will be determined soon, at which point this dosing strategy could be tested for efficacy in patients with MPNSTs. We have previously found that effective therapies in this model of *NF1*-mutant cancer can be successfully translated to other NF1-deficient models and *KRAS* mutant lung cancer (De Raedt et al., 2011; Maertens et al., 2013; Malone et al., 2014). Therefore, this combination should also be tested in pre-clinical models for other cancer types to determine the full scope of efficacy.

One of the key considerations for any combination therapy is whether a tolerable but effective combined dose can be identified, which is why we selected a relatively low dose of vorinostat for these studies. However, vorinostat is a pan-HDAC inhibitor, and thus is likely to have more side effects than more selective HDAC inhibitors now in development (Balasubramanian et al., 2009). Therefore, it will be important to identify which specific HDACs are mediating this effect. Notably, we found that HDAC6 inhibition alone is not sufficient to synergize with rapamycin, suggesting that HDAC6 specific inhibitors are unlikely to be effective in this setting. Further study is warranted to determine whether a specific HDAC or HDACs are mediating this effect, which could inform future clinical drug selection and development.

Moreover, our studies demonstrate the mechanism of action of this combination. Interestingly, we identified the UPR mediator PERK as necessary for a full therapeutic response to the combined therapy, suggesting that UPR activation is driving cell death in this context.

This is an important mechanistic difference between HSP90 inhibition and HDAC inhibition, as UPR destabilization is a critical mediator of HSP90 efficacy (De Raedt et al., 2011). This further underscores the double-edged sword of the UPR, and demonstrates that both the adaptive and terminal roles of the UPR can be therapeutically exploited. Unexpectedly, we found that PERK is not driving apoptosis through ATF4, and in fact ATF4 is promoting cellular survival in this context. In addition to regulation of the pro-apoptotic transcription factor CHOP, ATF4 has a large number of transcriptional targets that could be promoting cellular survival. It is interesting to note that ATF4 upregulates a number of genes involved in protein synthesis including genes encoding proteins that are essential for GSH synthesis (Han et al., 2013; Harding et al., 2003). As a result, ATF4 -/- cells have been reported to have decreased levels of GSH and are hyper sensitive to oxidative stress (Dickhout et al., 2012). Given the critical role for oxidative stress identified here, this could explain why ATF4 loss sensitizes MPNSTs to combination treatment. It will be important to determine which specific targets of ATF4 are sensitizing MPNSTs to this combination, as this could provide further mechanistic insight and might reveal therapeutic opportunities.

Transcriptional profiling identified the thioredoxin inhibitor *TXNIP* as one of the most significantly upregulated genes in combination treated cells. Interestingly, both mTOR and HDAC inhibition have been reported to upregulate *TXNIP* transcription in other contexts. mTOR directly interacts with MondoA-Mxl, a transcription factor complex that regulates *TXNIP* expression (Kaadige et al., 2015). When mTOR is inhibited, MondoA-Mxl is released, driving *TXNIP* expression. HDAC inhibition on the other hand has been shown to increase histone H3 and histone H4 acetylation of the *TXNIP* gene, promoting transcription, but activation of the UPR may also be driving *TXNIP* expression (Cha-Molstad et al., 2009; Oslowski et al., 2012). Here we found that PERK ablation contributes to cell death, but ATF4 ablation does not. However, PERK has been shown to increase TXNIP expression through ATF5 and chREBP

(Oslowski et al., 2012). Therefore, we are currently interested in determining whether UPR activation is directly affecting TXNIP expression, and whether ATF5 or chREBP are contributing to the therapeutic effect of HDAC and mTOR inhibition (Figure 3–8).

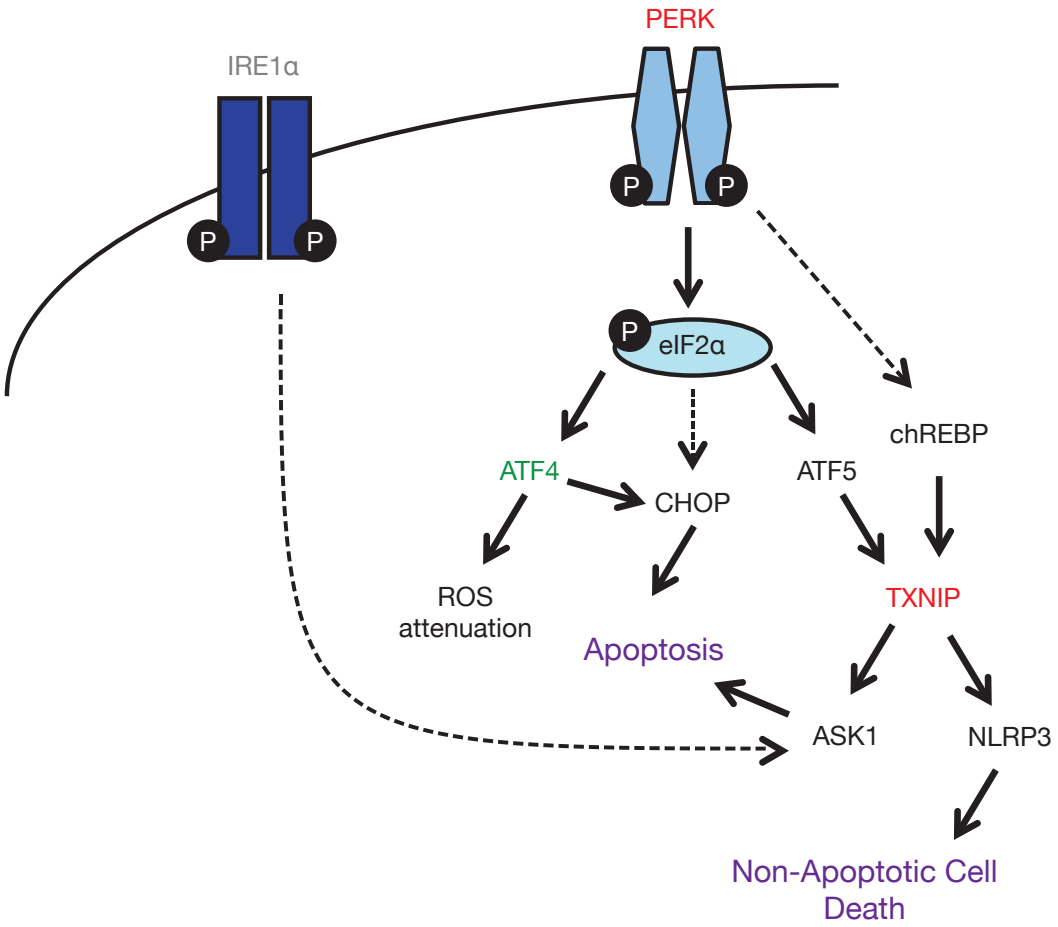

Figure 3–8. Model of UPR Activation Contributing to TXNIP-Mediated Cell Death. IRE1α and PERK are key arms of the unfolded protein response that can drive a terminal UPR. IRE1α canonically activates cell death through ASK1, while PERK drives cell death through ATF4 and CHOP. Loss of IRE1α (grey) does not affect therapeutic efficacy. Loss of PERK or TXNIP (red) has a protective effect, suggesting that they are driving cell death after combined treatment. Loss of ATF4 (green) exacerbates cell death, indicating that ATF4 has a protective role in this context, possibly due to its regulation of ROS attenuating genes. We are now looking at the contribution of CHOP, ATF5, and chREBP (black) to the therapeutic response, as well as to TXNIP upregulation. Additionally, we are interested in determining whether TXNIP is driving cell death through ASK1 or the NLRP3 inflammasome.

It appears that TXNIP expression is essential for the therapeutic effect of combined mTOR and HDAC inhibition in this context. TXNIP binds the reduced form of thioredoxin, a major cellular ROS scavenger, and impairs the thiol-reducing activity of TRX (Lu and Holmgren, 2014). Thus TXNIP expression increases ROS, and could at least partially be driving oxidative stress in this context. Importantly, TXNIP is directly connected with apoptotic pathways in the context of both ER stress and oxidative stress. TXNIP drives apoptosis through ASK1 in conditions of oxidative stress, and can activate the NLRP3 inflammasome to promote cell death during either oxidative or proteotoxic stress (Lerner et al., 2012; Oslowski et al., 2012; Zhou et al., 2010). We are currently exploring whether activation of either ASK1 or the NLRP3 inflammasome is promoting cell death in this context (Figure 3–8).

It remains unclear whether TXNIP upregulation drives oxidative stress, which induces proteotoxic stress and the unfolded protein response, or whether activation of the unfolded protein response is in part driving TXNIP expression, contributing to oxidative stress because these processes are all intimately connected (Figure 3–9). While the exact details of this mechanism are still being explored, our data demonstrate that the UPR, ROS, and TXNIP expression are all mediating the therapeutic response, suggesting that a vicious cycle of oxidative and proteotoxic stress is induced by HDAC and mTOR inhibition and that TXNIP is a key point of convergence between these stress pathways. Our studies provide further support for the concept that oxidative stress and proteotoxic stress represent vulnerabilities for cancer cells that can be therapeutically exploited and we have identified key regulators of this process.

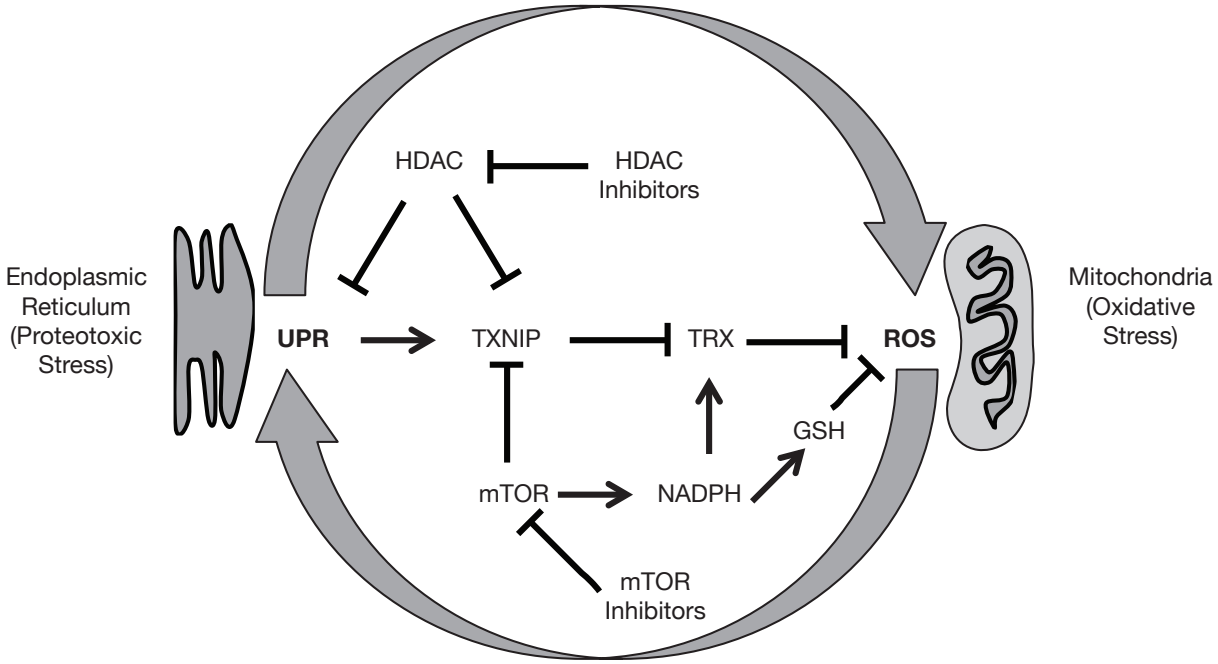

Figure 3–9. Combined HDAC and mTOR Inhibition Drives a Vicious Cycle of Proteotoxic and Oxidative Stress Converging on TXNIP. HDAC inhibition may directly upregulate TXNIP through histone acetylation; in addition HDAC inhibition induces ER stress and activates the UPR, which can further drive TXNIP expression. mTOR inhibition also upregulates *TXNIP* transcription, possibly through activation of the transcription factor MondoA-Mxl, in addition to lowering levels of reduced GSH and TRX, impairing the cellular attenuation of ROS. Increased ER Stress promotes increased ROS, and increased ROS causes further ER stress, producing a vicious cycle of stress.

METHODS

Cell Lines and Reagents

S462s were purchased from the ATCC. 90-8TLs were kindly provided by Dr. Eric Legius (KU Leuven, Belgium). All cell lines were cultured in Dulbecco's Modified Eagle Medium (DMEM) supplemented with 10% FBS and L-glutamine. Antibodies were purchased as follows: Cell Signaling Technologies: HDAC6, pS6, Vinculin, pEIF2α, XBP1-(s), ATF4, CHOP, Histone H3, PERK, IRE1α; Millipore: HSP90; Sigma Aldrich: Tubulin, Actin; Acetylated Tubulin. Nexturastat A, Vorinostat, and INK-128 were all purchased from Selleck Chemicals. Rapamycin was

purchased from LC Laboratories. For all *in vitro* studies, inhibitors were dissolved in DMSO. DCFDA was purchased from Life Technologies.

RNAi

ON-TARGETplus siRNA pools were purchased from Dharmacon. siRNAs were transfected overnight in antibiotic free medium using RNAiMax lipofectamine from Invitrogen.

Cellular Death Studies

Approximately 250,000 cells per well were seeded into 6-well plates. For siRNA experiments, cells were seeded 12-26 hours after transfection. Twenty-four hours after plating, day 0 counts were taken using a hemocytometer. For drug treatment experiments, inhibitors were added at this time. Final cell counts were taken 72 hours after day 0 counts.

In Vivo Drug Treatments

Animal procedures were approved by the Center for Animal and Comparative Medicine at Harvard Medical School in accordance with the NIH Guide for the Care and Use of Laboratory Animals and the Animal Welfare Act. C56/BL6 NPcis mice have been previously described (Cichowski et al., 1999). Mice were treated daily with 50mg/kg vorinostat, 100 mg/kg vorinostat, 5mg/kg rapamycin, or a combination of rapamycin and vorinostat via i.p. injections. Compounds given in combination were administered sequentially. Rapamycin was prepared as previously described (Johannessen et al., 2008). Vorinostat was dissolved directly into cyclodextrin as described (Hockly et al., 2003).

Tumor Volume Measurements

Tumors were measured every 2–3 days using a Vernier caliper. Tumor volume was calculated using the standard calculation L X W^2 X0.52.

Microarray

RNA was isolated using a Trizol extraction, and RNA was purified using an RNeasy kit (Qiagen) according to manufacturers instructions. RNA was hybridized to the Affymetrix Human 1.0 STS

array chip by the Molecular Biology Core Facilities at Dana-Farber Cancer Institute. To determine genes and gene sets differentially expressed amongst treatment groups a class comparison analysis was performed using BRB-Array tools developed by Dr. Richard Simon (National Cancer Institute, NIH, Rockville, MD) and the BRB-ArrayTools Development team. Thresholds were set at $P < 0.001$.

Flow Cytometry

Cells were stained with 10μM DFCDA for 15 minutes and then analyzed Accuri C6 Analyzer. Counts were gated on live cells, and 10,000 counts per condition were collected. Data was analyzed using FlowJo. All flow cytometry was performed at the Brigham and Women's Flow Cytometry Core facility.

Immunoprecipitation

Cells were treated as indicated and then lysed in a 1% Triton buffer supplemented with PhosSTOP tablets and sodium orthovanadate. Lysates were pre-cleared with protein G beads. IP was performed over night at 4˚C with an antibody against acetylated lysine, and then pulled down using agarose conjugated protein G beads.

Electron Microscopy

Mice were treated with rapamycin and vorinostat and then euthanized and tumor tissue was collected after the indicated amount of time. Tumor tissues were fixed in 2% glutaraldehyde and 4% paraformaldehyde in 0.1M sodium cacodylate buffer and processed for EM using standard methods.

Chapter 4: Conclusion and Future Directions

CONCLUSION

The goal of my thesis work was to identify novel combination therapies for *NF1*-mutant tumors, and MPNSTs in particular. We successfully discovered two new combination therapies for MPNSTs through two distinct approaches. First, by taking the approach of targeting signaling pathways that are hyper-activated when NF1 is lost, we developed an effective strategy by combining mTORC1 and MEK inhibitors. Second, by exploiting cellular stress pathways we found that the combination of HDAC and mTOR inhibitors is also effective in these tumors. Both combinations can be readily translated into patients.

When NF1 is lost, RAS and downstream effector pathways become aberrantly activated. There is a plethora of drugs targeting these effector pathways available, but the specific signaling nodes that represent the best therapeutic targets were unknown, making drug selection difficult. In Chapter 2, using genetic and biochemical techniques, I identified p110α as the key PI3K catalytic isoform downstream of NF1. When p110α was ablated, downstream mTORC1 activity was blocked, and proliferation of NF1-deficient cells was impaired. However, loss of either p110β or p110δ did not affect mTORC1 signaling or cellular proliferation. Together, this suggests that p110α represents a potential therapeutic target in NF1-deficient cancers. Conversely, inhibition of AKT did not affect mTORC1 signaling or MPNST cell proliferation, demonstrating that AKT was not necessary for NF1-deficient growth. Furthermore, we discovered that blocking mTORC1 activity slowed cell proliferation, but mTORC2 ablation had no effect. Together, these findings support an essential role for p110α and mTORC1, but suggest that mTORC2, AKT, and the other p110 catalytic isoforms are not likely to be effective therapeutic targets in NF1-deficient cancers.

Armed with the knowledge that mTORC1 was a key signaling node, I then wanted to use this information to develop an effective combination therapy. We had previously shown that inhibition of mTORC1 exerted a cytostatic effect on our mouse MPNST model. In Chapter

2, I demonstrated that when combined with a MEK inhibitor, mTORC1 inhibitors promote dramatic tumor regression *in vivo.* Importantly, we found that only sustained inhibition of both pathways was sufficient for this therapeutic effect. Because the major hurdle in developing combination therapies is identifying a dose that is both safe and effective, I wanted to identify a biomarker of combined mTORC1 and MEK inhibition, which could be used in clinical trials to determine whether these targets are inhibited at tolerable doses. I found that the glucose transporter *GLUT1* was substantially downregulated by the combination treatment, and showed that protein levels of GLUT1 also decreased after combination treatment. Because GLUT1 is a key glucose transporter and can be the rate-limiting step in glucose uptake, this lead me to look at ^{18}F-FDG PET imaging, a non-invasive measure of glucose uptake. I found that ^{18}F-FDG uptake is significantly impaired in combination treated tumors, and that early change in ^{18}F-FDG uptake was correlated with ultimate change in tumor size.

Together, these data support the conclusion that mTORC1 and p110α are key signaling nodes in *NF1*-mutant cancers. Furthermore, these findings support the clinical development of the combination of mTORC1 and MEK inhibitors in MPNSTs, and possibly other *NF1*- or *RAS*-mutant cancers, with ^{18}F-FDG PET imaging as a biomarker of successful target inhibition. Often when efficacy is not seen in clinical trials, it is not known if that is because the tolerable dose was not high enough to inhibit the intended target, or because inhibition of that target was achieved but was not as efficacious as anticipated. Our studies suggest that ^{18}F-FDG uptake can be used to verify effective target inhibition non-invasively. This finding is now being incorporated into a clinical trial using mTOR and MEK inhibitors in combination.

In Chapter 3 we took an alternative approach to developing therapies, specifically by targeting cellular stress. We have previously shown that underlying proteotoxic and oxidative stress also represent a therapeutic opportunity for MPNSTs. I decided to look for an FDA-approved drug that was also known to inhibit ER stress, so that any effective combination

could rapidly enter the clinic. In the work described in Chapter 3, I demonstrated that the pan-HDAC inhibitor vorinostat induces ER stress in MPNSTs, and that the combination of vorinostat and an mTOR inhibitor had a potent cytotoxic effect *in vitro* and *in vivo* in a genetically engineered mouse model of MPNSTs. I found that combined treatment with HDAC and mTOR inhibitors leads to swollen ER and mitochondria. I further demonstrated that this effect is dependent on both the unfolded protein response and oxidative stress, as genetic ablation of the UPR effector PERK and treatment with the ROS scavenger NAC attenuated the therapeutic effect. Further supporting a role for ER stress and oxidative stress in the therapeutic response, we found that transcriptional signatures of both proteotoxic and oxidative stress were significantly altered by the combination therapy. Together, these data suggest that combined HDAC and mTOR inhibition exploits both proteotoxic and oxidative stress to promote cell death.

I next wanted to identify specific genes that were involved in mediating the response. Using transcriptional profiling, I discovered that expression of thioredoxin interacting protein *TXNIP* is significantly upregulated after combination treatment, and we verified that protein levels of TXNIP are also elevated. TXNIP expression is intimately connected with both the conversion to UPR-driven and oxidative-stress-induced cell death. I found that ablation of TXNIP protected cells from combined HDAC and mTOR inhibition, suggesting that TXNIP may be driving the cytotoxic effect of this therapy.

While the details of this model are being finalized, these studies have provided important mechanistic insight into how these agents cooperate. There are currently three different Phase I clinical trials underway in solid tumor settings to determine tolerable dosing of HDAC inhibitors and mTOR inhibitors (NCT01087554, NCT01174199, NCT01582009).

As soon as a tolerable dose for this combination has been identified, trials in MPNSTs can move forward using this dosing strategy.

Together, these data support the clinical development of two different combination therapies for MPNSTs, and possibly other *NF1*-mutant tumors. Importantly, this work provides support for two distinct approaches to therapeutic development for cancer. We showed that hyperactivated signaling downstream of NF1-loss can be therapeutically targeted, and provided further support for the concept that cellular stress represents a vulnerability that can also be therapeutically exploited.

FUTURE DIRECTIONS

PI3K-Dependent, AKT-Independent Activation of mTORC1

It has been established PI3K typically activates mTORC1 through AKT. However, in Chapter 2 of this dissertation, I found that downstream of NF1-loss PI3K inhibition is sufficient to block mTORC1 activation but AKT inhibition is not. Similarly, mTORC2 inhibition, which reduces AKT activity, has no effect on mTORC1 activity. From a therapeutic perspective, this finding suggests that AKT inhibitors will not be very effective in this cancer type. However, mechanistically, this result raises several questions about how mTORC1 is regulated in *NF1*-deficient MPNSTs (Figure 4–1). First, why is AKT inhibition not sufficient to inhibit mTORC1 in this setting? The lack of efficacy of AKT inhibitors suggests that there are other pathways that are feeding into mTORC1 activation, and can compensate for the loss of AKT signaling. One possibility is that the ERK pathway is promoting sustained mTORC1 activity in the context of AKT inhibition.

TSC2 has several ERK phosphorylation sites and its activity can be regulated by ERK as well (Mendoza et al., 2011). As demonstrated in Chapter 2 of this dissertation, ERK inhibition is similarly not sufficient to block mTORC1 activity. In the context of activating RAS mutations

or NF1 loss, both the PI3K and ERK pathways are hyperactivated. Thus, we hypothesize that these there may be a shift in dependency when AKT is inhibited, allowing active ERK to drive mTORC1 signaling. It will be interesting to determine whether combined inhibition of AKT and the ERK pathway would be sufficient to inhibit mTORC1 signaling in this setting.

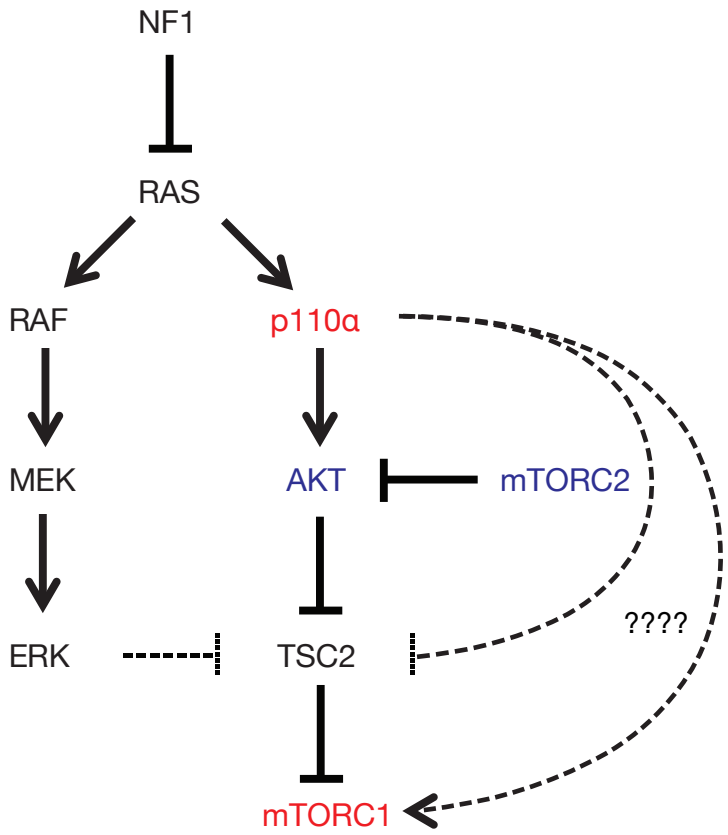

Figure 4–1. mTORC1 Regulation Downstream of NF1. When NF1 is lost, both the PI3K and ERK pathways are hyperactivated. In the present study we show that p110α and mTORC1 (red) are critical for MPNST proliferation, while AKT and mTORC2 (blue) are dispensable. Further, we find that AKT or mTORC2 inhibition does not affect mTORC1 signaling. The canonical signaling pathways are shown with solid lines. Our findings suggest that mTORC1 activity can be sustained even in the absence of AKT signaling, which could be explained by ERK inhibition of TSC2 (dotted inhibition arrow). However, these findings suggest that mTORC1 activity is p110α-dependent, even though it is AKT-independent. Thus, p110α could regulate either TSC2 activity or mTORC1 activity directly, through unknown mechanisms (dotted lines). This represents an intriguing area for further study.

A second, perhaps more interesting question arising from these findings is why PI3K and specifically p110α inhibition is sufficient to inhibit mTORC1 activation, if not through AKT? Our lab has previously shown that hyper-activation of PI3K occurs downstream of NF1 loss, and this seems to be the primary positive signal driving mTORC1 activation (Johannessen et al., 2005). This positive signal seems to be mediated by AKT. Moreover, we know that AKT inhibition is not sufficient to block mTORC1 activity. Therefore, PI3K inhibition must provide additional inhibitory signals to mTORC1, other than through loss of the positive signal from AKT. A better understanding of this signaling network will not only improve our mechanistic understanding of the pathway, but could also lead to alternative therapeutic approaches, as this may reveal additional ways to target mTORC1 activity.

Of primary interest is determining whether this effect is TSC2 dependent. TSC2 can be regulated by AKT, ERK, and RSK, so it is possible that PI3K inhibition is modulating TSC2 through something other than AKT. It will be important to determine whether PI3K inhibition can ablate mTORC1 activity in NF1-deficient cells when TSC2 is ablated. If so, this would suggest that PI3K is having an effect downstream of TSC2, possibly affecting raptor or mTOR phosphorylation. Alternatively, PI3K inhibition could be affecting localization of the mTORC1 complex to the lysosome, preventing its activation by RHEB. mTOR localization to the lysosome is thought to be primarily regulated by amino acid availability mediated by AMPK and the Ragulator Complex. PI3K inhibition could be causing a more generalized stress response that affects this signaling pathway, blocking mTORC1 activation. Regardless of the mechanism, this AKT-independent regulation of mTORC1 by PI3K is an unexpected and interesting finding, and warrants further study.

Selecting PI3K/mTOR Inhibitors for Clinical Trials

As described in Chapter 2, I found that mTORC1 is the minimal, key signaling node in the PI3K pathway that must be inhibited for therapeutic benefit in *NF1*-mutant cancers. In our

mouse model, I found that rapamycin has superior pharmacodynamics relative to the PI3K inhibitor GDC-0941. However, these data suggest that a PI3K inhibitor with a better pharmacodynamics profile could be just as effective as a direct mTORC1 inhibitor. Thus, in selecting agents for human trials, it will be important to identify the inhibitors that display sustained target inhibition in humans, while still minimizing toxicity. Importantly, I found that AKT and mTORC2 inhibition are not important, and that AKT inhibition does not improve the response to rapamycin, alleviating any concerns about feedback activation on AKT in this context. Therefore, mTOR kinase inhibitors do not need to be favored over rapalogs unless they show superior pharmacodynamics. Another potential therapeutic approach to inhibiting mTOR is through the use of p110α-specific inhibitors or β-sparing inhibitors, which are expected to have less toxicity than pan-PI3K inhibitors (Liu et al., 2009). The specific pharmacodynamic and toxicity profiles of various mTOR and PI3K inhibitors can only be addressed in human clinical trials, but this work suggests that duration of mTORC1 inhibition should be a primary factor in selecting agents for clinical trials in this tumor type.

Mechanistic Role of Reduced Glucose Uptake

In the present study, we explore the impaired glucose uptake in mTOR/MEK inhibitor treated tumors primarily as a biomarker for combined target inhibition. However, it is possible that suppression of *GLUT1* expression has a mechanistic role as well. As Otto Warburg first described in the early 1900s, cancer cells typically preferentially use glycolysis instead of oxidative phosphorylation for ATP production, even in aerobic conditions. Cancer cells have an increased need for glucose relative to normal cells at least in part because this process is much less efficient. The observation that cancer cells take up more glucose than surrounding tissue lead to the development of ^{18}F-FDG PET imaging as a prognostic and diagnostic tool, but more recently it has been appreciated that this might also represent a vulnerability in cancer cells.

Glucose uptake and altered cancer metabolism are now being studies as potential therapeutic targets in cancer. Inhibition of GLUT1 has been shown to have an apoptotic effect in many cancer settings, so it would be interesting to determine whether the decreased GLUT1 expression observed in the present study is contributing to the therapeutic effect (Adekola et al., 2012). If this is the case, then that would suggest that GLUT1 inhibitors, which have recently been discovered, might be effective in this model (Wang et al., 2012). The altered metabolism observed in cancer offers many intriguing therapeutic opportunities, so it will be important to better understand the potential mechanistic role of GLUT1 suppression and reduced glucose uptake in this therapy.

^{18}F-FDG PET Uptake as a Biomarker in other Tumor Types

The combination of mTOR or PI3K inhibitors with MEK inhibitors has been successful in a number of preclinical settings, most notably in RAS mutant cancers (Engelman et al., 2008; Posch et al., 2013). However, the challenge will be to identify a combined dosing strategy that is both tolerated and effective. I demonstrated in Chapter 2 of this dissertation that ^{18}F-FDG uptake can serve as a non-invasive biomarker of combined target inhibition in NF1-deficient MPNSTs, and this will be a powerful tool for determining dosing in the clinic. It will be important to determine whether FDG-PET imaging can be similarly applied to other cancers where combined mTOR and MEK inhibition is effective. In *VHL* and *LKB1* mutant cancers, mTOR inhibition alone is sufficient to reduce *GLUT1* expression and ^{18}F-FDG uptake (Shackelford et al., 2009; Thomas et al., 2006). In the present study we resolved a previous question in the field as to why mTOR inhibition was not sufficient to reduce *GLUT1* in NF1-deficient contexts, as we found that both the ERK and mTORC1 pathways must be inhibited to reduce *GLUT1* expression. Thus we would hypothesize that this biomarker should be useful in other contexts where both pathways are hyper-activated, such as cancers with activating *RAS* mutations or other *NF1*-mutant cancers. Importantly, our lab has shown that the combination

of mTORC1 and MEK inhibition is also effective in a xenograft mouse model of *NF1*-mutant melanoma (Maertens and Cichowski, 2014). It will be interesting to determine whether these tumors also show a reduction in *GLUT1* after combined treatment, and if FDG-PET imaging is an effective biomarker in this context. *RAS* mutant cancers are also sensitive to combined PI3K and ERK pathway inhibition in pre-clinical models (Engelman et al., 2008). As *KRAS* activating mutations, similar to *NF1* loss, will lead to activation of both the PI3K and ERK pathway, we would expect that reduction in *GLUT1* might similarly require inhibition of both pathways, in which case FDG-PET will also be an effective biomarker in this setting.

Targeting Effectors Downstream of mTORC1

In Chapter 2 of this dissertation we provide proof of concept that combined inhibition of mTORC1 and MEK leads to tumor regression in *NF1*-mutant cancers. However, it remains to be determined whether an effective but tolerable dose can be identified in clinical trials. Given the differences in toxicity between humans and mice, this can only be addressed in human trials. The mTORC1 and ERK pathways are both master regulators of a number of cellular processes, and inhibition of all of these downstream targets may not be necessary for therapeutic efficacy. Identifying the minimal necessary components for therapeutic efficacy could allow for a better therapeutic window.

mTORC1 directly regulates two distinct primary pathways, through phosphorylation of S6 kinase and 4E-BP1. S6 kinase directly phosphorylates a number of target proteins including ribosomal protein S6, eIF4B, eEF2K, CREM, Pdcd4, BAD1, and MDM2. Through the phosphorylation of these target proteins, S6 kinase regulates a number of downstream processes including protein synthesis, cytoskeletal rearrangement, proliferation, splicing, and cell survival (Fenton and Gout, 2011). On the other hand, when hypo-phosphorylated, 4E-BP1 directly binds to eIF4E, the rate-limiting factor in cap-dependent translation. Phosphorylation of 4E-BP1 by mTOR prevents the association with eIF4E, allowing cap-dependent translation to

occur (Morita et al., 2015). Given their divergent roles, it may be possible that directly targeting S6 kinase or cap-dependent translation would be sufficient to promote tumor regression in combination with ERK pathway inhibitors.

Several pre-clinical S6 Kinase specific inhibitors have been developed, and could be easily tested in this model (Couty et al., 2013). Targeting 4E-BP1 is not as straightforward because it is not a kinase, but several approaches have been taken to inhibit cap-dependent translation by targeting eIF4E, including anti-sense RNAs and inhibitors of eIF4E assembly with eIF4G (Pettersson et al., 2014). eIF4E is also phosphorylated by the MNK kinases, and this phosphorylation event appears to be important for eIF4E activity in cancer, so MNK kinase inhibitors represent another potential therapeutic approach (Konicek et al., 2011). It will be important to determine if any of these therapeutic approaches, when combined with MEK inhibition can promote tumor regression. Recent studies in our lab suggest that eIF4E is indeed a critical component of therapeutic efficacy, and MNK inhibitors, which block eIF4E phosphorylation, can shrink MPNSTs when combined with MEK inhibitors.

Mechanism of TXNIP Activation (Work in Progress)

In Chapter 3 of this dissertation, I identified TXNIP upregulation as a critical mediator of cell death in response to combined HDAC and mTOR inhibition. Interestingly, TXNIP upregulation appears to be a key factor in the switch from an adaptive UPR to a terminal UPR (Lerner et al., 2012; Oslowski et al., 2012). I also found that knockdown of the UPR-mediator PERK partially protects cells from combined treatment, suggesting that the UPR activation is contributing to the cell death phenotype. Given recent studies that have identified PERK activation as regulating TXNIP transcription through the transcription factors ATF5 and chREBP, I hypothesize that UPR activation may be contributing to the increased expression of TXNIP observed here. Therefore, it will be important to determine whether increased

expression of TXNIP induced by combined HDAC and mTOR inhibition is impaired in the context of PERK or ATF5 knockdown (Figure 3–8).

We hypothesize that TXNIP is being at least partially induced due to the activation of the UPR and irresolvable ER stress. However, it is also possible that *TXNIP* transcription is being more directly activated by HDAC inhibition through epigenetic regulation of the *TXNIP* gene. Therefore, it will also be important to determine whether acetylation marks on histones in the *TXNIP* gene are altered by vorinostat treatment in this context.

Increased *TXNIP* expression after mTOR inhibition has been described to be regulated by the transcription factor complex MondoA-Mxl. mTOR appears to inhibit MondoA-Mxl transcription of *TXNIP*, so when mTOR is inhibited this releases MondoA-Mxl to drive *TXNIP* expression (Kaadige et al., 2015). Here, we find that mTOR inhibition can modestly increase *TXNIP* expression, but it remains to be determined if this is dependent on MondoA-Mxl. The combined effect of HDAC and mTOR inhibition on *TXNIP* expression seems to be critical for the efficacy of this therapy, so further study on their relative control of *TXNIP* transcription is warranted.

TXNIP-Driven Cell Death

The experiments outlined above will answer how TXNIP is upregulated. However, another question is how TXNIP activation contributes to cell death. Interestingly, TXNIP is known to mediate cell death through two distinct mechanisms. TXNIP can mediate apoptosis through ASK1, and can induce cell death through activation of the NLRP3 inflammasome, a process referred to as pyroptosis (Lu and Holmgren, 2012; Zhou et al., 2010). Activation of ASK1 and the NLRP3 inflammasome have been demonstrated in the context of oxidative and proteotoxic stress (Sano and Reed, 2013; Zhou et al., 2010). Therefore, it will be important to determine whether the TXNIP-mediated cell death observed here is either ASK1 or NLRP3-dependent.

The NLRP3 inflammasome is thought to play a critical role in mediating stress responses and cellular death in a number of contexts as a result of oxidative or proteotoxic stress. This complex has been well studied in the context of atherosclerosis, gout, diabetes, and other sterile inflammatory diseases (Ozaki et al., 2015). However, it remains relatively under-studied in cancer. Interestingly, unlike other inflammasome complexes, which seem to have very specific pathogenic-triggers, the NLRP3 complex can be formed in response to a broad number of stimuli, so it is though that rather than direct binding of activators, NLRP3 is activated through a more proximal signal. Of note, ROS are currently thought to be one of the proximal signals that can lead to NLRP3 formation (Abderrazak et al., 2015). Given the high level of ROS observed in cancers, and the further induction of ROS observed here upon treatment with HDAC inhibitors, it will be very interesting to determine whether the NLRP3 complex is indeed activated in this context. More recently, direct binding of TXNIP to NLRP3 has been reported to activate NLRP3 in response to high cellular ROS and drive a terminal cell fate (Zhou et al., 2010). If TXNIP-driven cell death is independent of ASK1 in the context of combined HDAC/mTOR inhibition this would provide a very interesting avenue of study.

ASK1 drives canonical apoptosis and can also be directly regulated by the thioredoxin system. Reduced TRX is a negative regulator of ASK1, but in conditions of high cellular ROS TRX is oxidized and releases ASK1, allowing ASK1 to drive an apoptotic cell fate. Importantly, TXNIP is also a direct binding partner and inhibitor of reduced TRX, preventing the interaction with ASK1, so high levels of TXNIP can also result in activation of the ASK1 cascade (Saxena et al., 2010). Ultimately, understanding the mechanism of TXNIP-driven cell death in the context of combined HDAC and mTOR inhibition will be critical to our understanding of the therapy described in Chapter 3, and could possibly further our knowledge of the terminal stress response in cancer as well.

Identifying Specific HDACs Contributing to Therapeutic Efficacy

In Chapter 3 of this dissertation we report the therapeutic efficacy of vorinostat, a pan-HDAC inhibitor, when combined with mTOR inhibition. Vorinostat has activity against all Zn^{2+}-dependent HDACs, which includes Class I (HDAC 1, 2, 3, and 8), Class IIa (HDAC 4,5, 7, and 9), Class IIb (HDAC6 and 10) and Class IV (HDAC 11). Vorinostat inhibits HDACs 1-3 and HDAC6 at low nanomolar concentrations, but is less potent against the other Zn^{2+}-dependent HDACs. Vorinostat is one of two currently FDA-approved HDAC inhibitors, but more selective inhibitors are being developed in the hope that this will reduce toxicity. Therefore it is important to identify which HDAC(s) must be effectively inhibited to promote a therapeutic response. In Chapter 3 we find that neither HDAC6 knockdown nor HDAC6-specific inhibitors have a cytotoxic effect when combined with mTOR inhibition, demonstrating that HDAC6 inhibition alone is not sufficient. However, it remains possible that inhibition of select HDACs is driving the therapeutic response, and if this is the case, identifying the responsible HDACs could inform therapeutic development in the future as more HDAC-specific inhibitors are available because it is anticipated that these inhibitors will have better toxicity profiles.

HDAC and mTOR Inhibitors in other Therapeutic Contexts

In addition to the combination of mTOR and MEK inhibitors described in Chapter 2, we found that mTOR inhibitors and HDAC inhibitors also combine to promote tumor regression, as detailed in Chapter 3. Our lab has previously found that the combination of HSP90 inhibitors and mTOR inhibitors, which was effective in this model, was also effective in an aggressive model of *KRAS*-mutant lung cancer. Because the HDAC/mTOR inhibitor combination seems to be targeting similar cellular vulnerabilities, it is likely that *KRAS* mutant lung cancer will also respond to this combination (De Raedt et al., 2011). Unlike the combination described in Chapter 2, which targets activation of specific signaling pathways, this combination targets a more generalized phenotype and thus might be effective in any number of cancer types.

Therefore it will be important to understand the specific biological characteristics that make cancers sensitive to this therapy.

Predictive Biomarkers of Response to Combined HDAC and mTOR Inhibition

In Chapter 3 of this dissertation, we describe the effective combination of HDAC and mTOR inhibitors in MPNSTs, but as discussed above, a broad number of tumor types could be responsive to this therapy. Additionally, we saw a variable response in our mouse model, which recapitulates what is typically seen in patients and is expected because each of these tumors arises from an independent genetic event and the tumors are heterogeneous. In order to identify the cancer types most likely to be vulnerable to this combination, as well as identify specific patients who could benefit from this therapy, it will be important to understand the factors governing sensitivity and identify tractable biomarkers.

One possible factor that contributes to sensitivity is aneuploidy. Aneuploidy is known to contribute to proteotoxic stress due to imbalanced stoichiometry (Oromendia and Amon, 2014). Alternatively, basal activation of the UPR could be a predictor of sensitivity, as these tumors already have a high level of ER stress (De Raedt et al., 2011). Given the critical role of ROS and ROS scavengers for therapeutic efficacy, high basal ROS may also be a predictor of sensitivity. Regardless, it will be important to determine if there are any biomarkers that are predictive of sensitivity as this will aid in the translation of this combination to other cancer types, as well as patient selection in the clinic.

Other Therapeutic Approaches Targeting Oxidative and Proteotoxic Stress

We have now identified two combination therapies that exploit cancer cell stress—the combination of HDAC and mTOR inhibitors described in Chapter 3 of this thesis, as well as the combination of HSP90 and mTOR inhibitors that we have previously published (De Raedt et al,. 2011, reprinted in Appendix B). Together, this provides compelling support for the concept that proteotoxic and oxidative stress represent serious vulnerabilities in cancer cells that can be

exploited successfully. While these data are compelling and we are optimistic that one or both of these combinations will yield clinical benefit, these data also suggest that a large number of agents that perturb these stress responses could be effective.

For example, ER associated degradation (ERAD) is a critical process that prevents accumulation of misfolded proteins and inhibiting this process induces ER stress (Kim et al., 2008). One critical component of ERAD is p97, for which inhibitors are now available (Chapman et al., 2015). Thus p97 inhibitors may be able to synergize with mTOR inhibition to promote cancer cell death. Alternatively, they may be able to synergize with either HSP90 inhibitors or HDAC inhibitors as well, because while all three drugs converge on ER stress and the UPR, they appear to do so through distinct mechanisms. Conversely, instead of driving activation of the terminal UPR by inducing ER stress, we might be able to use agents that inhibit the UPR. Several inhibitors targeting IRE1 endonuclease activity and PERK kinase activity have been developed. These agents might be effective in combination with mTOR inhibitors, or in combination with a second inducer of ER stress.

In addition to the role of proteotoxic stress, these findings further underscore the importance of oxidative stress. The efficacy of the HDAC/mTOR combination and the HSP90/mTOR combination can be blocked by the addition of ROS scavengers, demonstrating that ROS induction is critical. Thus we might be able to directly induce reactive oxygen species, and promote a similar therapeutic effect. Several drugs are known to induce ROS including arsenic trioxide, elesclomol, and buthionine sulfoximine. To date we have not been able to identify a combination of ROS inducers with mTOR inhibitors that is both effective and tolerated in our mouse model (data not included in this dissertation), but this remains an interesting avenue for exploration.

Sequential or Alternate Dosing of Combination Therapies

We have now identified a number of different combination therapies that are effective in this mouse model of MPNSTs, in addition to the two described in this dissertation (De Raedt et al., 2011; 2014). We are optimistic that these combinations will show significant clinical benefit and that responses will be durable. However, for therapies currently in the clinic, the reality is that most responders will eventually relapse. Therefore, it will be interesting to determine whether animals that are no longer responding to one combination therapy remain sensitive to another. The two therapeutic approaches presented in this dissertation target different underlying vulnerabilities: the combination of mTOR and MEK inhibitors described in Chapter 2 targets specific signaling pathways, while the combination described in Chapter 3 exploits underlying stress in the cancer cell. Thus, a tumor that has become resistant to one therapeutic approach could remain sensitive to the other. Therefore, it will be interesting to determine whether sequential dosing of the combination therapies results in an improved and more durable response. The population of tumor cells that is sensitive to one combination therapy versus another may also differ, in which case superior efficacy could be seen by alternating therapeutic strategies. For example, sustained treatment with an mTOR inhibitor and alternating treatment with a MEK inhibitor and an HDAC inhibitor might improve efficacy over either combination therapy alone if the population of sensitive tumor cells is not entirely overlapping. In any case, a better understanding of how these combination therapies can be sequentially or alternately dosed could provide insight into the factors governing sensitivity and resistance as well as inform future clinical strategies. These questions can be readily addressed in our mouse model.

The findings presented here, as well as the future directions, aim to provide a better understanding of *NF1*-mutant cancers. Specifically, the studies presented in this dissertation

expand our understanding of signaling and stress vulnerabilities in *NF1*-mutant cancers, and provide promising pre-clinical data for two combination therapies. We sincerely hope that these findings, in conjunction with the future directions they inspire, will ultimately improve patient outcome for these devastating tumors.

References

Abderrazak, A., Syrovets, T., Couchie, D., Hadri, El, K., Friguet, B., Simmet, T., and Rouis, M. (2015). NLRP3 inflammasome: From a danger signal sensor to a regulatory node of oxidative stress and inflammatory diseases. Redox Biol *4C*, 296–307.

Abramowicz, A., and Gos, M. (2014). Neurofibromin in neurofibromatosis type 1 - mutations in NF1gene as a cause of disease. Dev Period Med *18*, 297–306.

Adekola, K., Rosen, S.T., and Shanmugam, M. (2012). Glucose transporters in cancer metabolism. Curr Opin Oncol *24*, 650–654.

Aloj, L., Caracó, C., Jagoda, E., Eckelman, W.C., and Neumann, R.D. (1999). Glut-1 and hexokinase expression: relationship with 2-fluoro-2-deoxy-D-glucose uptake in A431 and T47D cells in culture. Cancer Res. *59*, 4709–4714.

Amann, T., Maegdefrau, U., Hartmann, A., Agaimy, A., Marienhagen, J., Weiss, T.S., Stoeltzing, O., Warnecke, C., Schölmerich, J., Oefner, P.J., et al. (2009). GLUT1 expression is increased in hepatocellular carcinoma and promotes tumorigenesis. Am. J. Pathol. *174*, 1544–1552.

Ando, K., Kurihara, M., Kataoka, H., Ueyama, M., Togo, S., Sato, T., Doi, T., Iwakami, S.-I., Takahashi, K., Seyama, K., et al. (2013). The efficacy and safety of low-dose sirolimus for treatment of lymphangioleiomyomatosis. Respir Investig *51*, 175–183.

Anthony, T.G., and Wek, R.C. (2012). TXNIP switches tracks toward a terminal UPR. Cell Metab. *16*, 135–137.

Avril, N. (2004). GLUT1 expression in tissue and (18)F-FDG uptake. J. Nucl. Med. *45*, 930–932.

Bader, A.G., Kang, S., and Vogt, P.K. (2006). Cancer-specific mutations in PIK3CA are oncogenic in vivo. Proc. Natl. Acad. Sci. U.S.a. *103*, 1475–1479.

Baehring, J.M., Betensky, R.A., and Batchelor, T.T. (2003). Malignant peripheral nerve sheath tumor: the clinical spectrum and outcome of treatment. Neurology *61*, 696–698.

Balasubramanian, S., Verner, E., and Buggy, J.J. (2009). Isoform-specific histone deacetylase inhibitors: the next step? Cancer Lett. *280*, 211–221.

Balcer, L.J., Liu, G.T., Heller, G., Bilaniuk, L., Volpe, N.J., Galetta, S.L., Molloy, P.T., Phillips, P.C., Janss, A.J., Vaughn, S., et al. (2001). Visual loss in children with neurofibromatosis type 1 and optic pathway gliomas: relation to tumor location by magnetic resonance imaging. Am. J. Ophthalmol. *131*, 442–445.

Benz, M.R., Czernin, J., Dry, S.M., Tap, W.D., Allen-Auerbach, M.S., Elashoff, D., Phelps, M.E., Weber, W.A., and Eilber, F.C. (2010). Quantitative F18-fluorodeoxyglucose positron emission tomography accurately characterizes peripheral nerve sheath tumors as malignant or benign. Cancer *116*, 451–458.

Bernards, A. (2003). GAPs galore! A survey of putative Ras superfamily GTPase activating proteins in man and Drosophila. Biochim. Biophys. Acta *1603*, 47–82.

Berner, J.M., Sørlie, T., Mertens, F., Henriksen, J., Saeter, G., Mandahl, N., Brøgger, A., Myklebost, O., and Lothe, R.A. (1999). Chromosome band 9p21 is frequently altered in malignant peripheral nerve sheath tumors: studies of CDKN2A and other genes of the pRB pathway. Genes Chromosomes Cancer *26*, 151–160.

Bi, L., Okabe, I., Bernard, D.J., Wynshaw-Boris, A., and Nussbaum, R.L. (1999). Proliferative defect and embryonic lethality in mice homozygous for a deletion in the p110alpha subunit of phosphoinositide 3-kinase. J. Biol. Chem. *274*, 10963–10968.

Bi, L., Okabe, I., Bernard, D.J., and Nussbaum, R.L. (2002). Early embryonic lethality in mice deficient in the p110beta catalytic subunit of PI 3-kinase. Mamm. Genome *13*, 169–172.

Birindelli, S., Perrone, F., Oggionni, M., Lavarino, C., Pasini, B., Vergani, B., Ranzani, G.N., Pierotti, M.A., and Pilotti, S. (2001). Rb and TP53 pathway alterations in sporadic and NF1-related malignant peripheral nerve sheath tumors. Lab. Invest. *81*, 833–844.

Bolden, J.E., Shi, W., Jankowski, K., Kan, C.-Y., Cluse, L., Martin, B.P., MacKenzie, K.L., Smyth, G.K., and Johnstone, R.W. (2013). HDAC inhibitors induce tumor-cell-selective pro-apoptotic transcriptional responses. Cell Death Dis *4*, e519.

Boudry-Labis, E., Roche-Lestienne, C., Nibourel, O., Boissel, N., Terre, C., Perot, C., Eclache, V., Gachard, N., Tigaud, I., Plessis, G., et al. (2013). Neurofibromatosis-1 gene deletions and mutations in de novo adult acute myeloid leukemia. Am. J. Hematol. *88*, 306–311.

Boyault, C., Zhang, Y., Fritah, S., Caron, C., Gilquin, B., Kwon, S.H., Garrido, C., Yao, T.-P., Vourc'h, C., Matthias, P., et al. (2007). HDAC6 controls major cell response pathways to cytotoxic accumulation of protein aggregates. Genes Dev. *21*, 2172–2181.

Brannan, C.I., Perkins, A.S., Vogel, K.S., Ratner, N., Nordlund, M.L., Reid, S.W., Buchberg, A.M., Jenkins, N.A., Parada, L.F., and Copeland, N.G. (1994). Targeted disruption of the neurofibromatosis type-1 gene leads to developmental abnormalities in heart and various neural crest-derived tissues. Genes Dev. *8*, 1019–1029.

Bridge, R.S., Bridge, J.A., Neff, J.R., Naumann, S., Althof, P., and Bruch, L.A. (2004). Recurrent chromosomal imbalances and structurally abnormal breakpoints within complex karyotypes of malignant peripheral nerve sheath tumour and malignant triton tumour: a cytogenetic and molecular cytogenetic study. J. Clin. Pathol. *57*, 1172–1178.

Britten, C.D. (2013). PI3K and MEK inhibitor combinations: examining the evidence in selected tumor types. Cancer Chemother. Pharmacol. *71*, 1395–1409.

Brown, A.P., Carlson, T.C.G., Loi, C.-M., and Graziano, M.J. (2007). Pharmacodynamic and toxicokinetic evaluation of the novel MEK inhibitor, PD0325901, in the rat following oral and intravenous administration. Cancer Chemother. Pharmacol. *59*, 671–679.

Butler, L.M., Zhou, X., Xu, W.-S., Scher, H.I., Rifkind, R.A., Marks, P.A., and Richon, V.M. (2002). The histone deacetylase inhibitor SAHA arrests cancer cell growth, up-regulates

thioredoxin-binding protein-2, and down-regulates thioredoxin. Proc. Natl. Acad. Sci. U.S.a. *99*, 11700–11705.

Cawthon, R.M., Weiss, R., Xu, G.F., Viskochil, D., Culver, M., Stevens, J., Robertson, M., Dunn, D., Gesteland, R., and O'Connell, P. (1990). A major segment of the neurofibromatosis type 1 gene: cDNA sequence, genomic structure, and point mutations. Cell *62*, 193–201.

Cha-Molstad, H., Saxena, G., Chen, J., and Shalev, A. (2009). Glucose-stimulated expression of Txnip is mediated by carbohydrate response element-binding protein, p300, and histone H4 acetylation in pancreatic beta cells. J. Biol. Chem. *284*, 16898–16905.

Chang, T., Krisman, K., Theobald, E.H., Xu, J., Akutagawa, J., Lauchle, J.O., Kogan, S., Braun, B.S., and Shannon, K. (2013). Sustained MEK inhibition abrogates myeloproliferative disease in Nf1 mutant mice. J. Clin. Invest. *123*, 335–339.

Chantry, D., Vojtek, A., Kashishian, A., Holtzman, D.A., Wood, C., Gray, P.W., Cooper, J.A., and Hoekstra, M.F. (1997). p110delta, a novel phosphatidylinositol 3-kinase catalytic subunit that associates with p85 and is expressed predominantly in leukocytes. J. Biol. Chem. *272*, 19236–19241.

Chapman, E., Maksim, N., la Cruz, de, F., and La Clair, J.J. (2015). Inhibitors of the AAA+ chaperone p97. Molecules *20*, 3027–3049.

Chen, X., Shen, J., and Prywes, R. (2002). The luminal domain of ATF6 senses endoplasmic reticulum (ER) stress and causes translocation of ATF6 from the ER to the Golgi. J. Biol. Chem. *277*, 13045–13052.

Chen, Z., Liu, C., Patel, A.J., Liao, C.-P., Wang, Y., and Le, L.Q. (2014). Cells of origin in the embryonic nerve roots for NF1-associated plexiform neurofibroma. Cancer Cell *26*, 695–706.

Chin, L., Tam, A., Pomerantz, J., Wong, M., Holash, J., Bardeesy, N., Shen, Q., O'Hagan, R., Pantginis, J., Zhou, H., et al. (1999). Essential role for oncogenic Ras in tumour maintenance. Nature *400*, 468–472.

Choudhary, C., Kumar, C., Gnad, F., Nielsen, M.L., Rehman, M., Walther, T.C., Olsen, J.V., and Mann, M. (2009). Lysine acetylation targets protein complexes and co-regulates major cellular functions. Science *325*, 834–840.

Cichowski, K., Shih, T.S., Schmitt, E., Santiago, S., Reilly, K., McLaughlin, M.E., Bronson, R.T., and Jacks, T. (1999). Mouse models of tumor development in neurofibromatosis type 1. Science *286*, 2172–2176.

Couty, S., Westwood, I.M., Kalusa, A., Cano, C., Travers, J., Boxall, K., Chow, C.L., Burns, S., Schmitt, J., Pickard, L., et al. (2013). The discovery of potent ribosomal S6 kinase inhibitors by high-throughput screening and structure-guided drug design. Oncotarget *4*, 1647–1661.

De Raedt, T., Beert, E., Pasmant, E., Luscan, A., Brems, H., Ortonne, N., Helin, K., Hornick, J.L., Mautner, V., Kehrer-Sawatzki, H., et al. (2014). PRC2 loss amplifies Ras-driven transcription and confers sensitivity to BRD4-based therapies. Nature *514*, 247–251.

De Raedt, T., Walton, Z., Yecies, J.L., Li, D., Chen, Y., Malone, C.F., Maertens, O., Jeong, S.M., Bronson, R.T., Lebleu, V., et al. (2011). Exploiting cancer cell vulnerabilities to develop a combination therapy for ras-driven tumors. Cancer Cell *20*, 400–413.

DeClue, J.E., Papageorge, A.G., Fletcher, J.A., Diehl, S.R., Ratner, N., Vass, W.C., and Lowy, D.R. (1992). Abnormal regulation of mammalian p21ras contributes to malignant tumor growth in von Recklinghausen (type 1) neurofibromatosis. Cell *69*, 265–273.

Dickhout, J.G., Carlisle, R.E., Jerome, D.E., Mohammed-Ali, Z., Jiang, H., Yang, G., Mani, S., Garg, S.K., Banerjee, R., Kaufman, R.J., et al. (2012). Integrated stress response modulates cellular redox state via induction of cystathionine γ-lyase: cross-talk between integrated stress response and thiol metabolism. J. Biol. Chem. *287*, 7603–7614.

Ding, L., Getz, G., Wheeler, D.A., Mardis, E.R., McLellan, M.D., Cibulskis, K., Sougnez, C., Greulich, H., Muzny, D.M., Morgan, M.B., et al. (2008). Somatic mutations affect key pathways in lung adenocarcinoma. Nature *455*, 1069–1075.

Donovan, S., See, W., Bonifas, J., Stokoe, D., and Shannon, K.M. (2002). Hyperactivation of protein kinase B and ERK have discrete effects on survival, proliferation, and cytokine expression in Nf1-deficient myeloid cells. Cancer Cell *2*, 507–514.

Doorn, P.F., Molenaar, W.M., Buter, J., and Hoekstra, H.J. (1995). Malignant peripheral nerve sheath tumors in patients with and without neurofibromatosis. Eur J Surg Oncol *21*, 78–82.

Ducatman, B.S., Scheithauer, B.W., Piepgras, D.G., Reiman, H.M., and Ilstrup, D.M. (1986). Malignant peripheral nerve sheath tumors. A clinicopathologic study of 120 cases. Cancer *57*, 2006–2021.

Düvel, K., Yecies, J.L., Menon, S., Raman, P., Lipovsky, A.I., Souza, A.L., Triantafellow, E., Ma, Q., Gorski, R., Cleaver, S., et al. (2010). Activation of a metabolic gene regulatory network downstream of mTOR complex 1. Mol. Cell *39*, 171–183.

Eickholt, B.J., Ahmed, A.I., Davies, M., Papakonstanti, E.A., Pearce, W., Starkey, M.L., Bilancio, A., Need, A.C., Smith, A.J.H., Hall, S.M., et al. (2007). Control of axonal growth and regeneration of sensory neurons by the p110delta PI 3-kinase. PLoS ONE *2*, e869.

Eletto, D., Chevet, E., Argon, Y., and Appenzeller-Herzog, C. (2014). Redox controls UPR to control redox. J. Cell. Sci. *127*, 3649–3658.

Endo, M., Yamamoto, H., Setsu, N., Kohashi, K., Takahashi, Y., Ishii, T., Iida, K.-I., Matsumoto, Y., Hakozaki, M., Aoki, M., et al. (2013). Prognostic significance of AKT/mTOR and MAPK pathways and antitumor effect of mTOR inhibitor in NF1-related and sporadic malignant peripheral nerve sheath tumors. Clin. Cancer Res. *19*, 450–461.

Engelman, J.A., Chen, L., Tan, X., Crosby, K., Guimaraes, A.R., Upadhyay, R., Maira, M., McNamara, K., Perera, S.A., Song, Y., et al. (2008). Effective use of PI3K and MEK inhibitors to treat mutant Kras G12D and PIK3CA H1047R murine lung cancers. Nat. Med. *14*, 1351–1356.

Erem, C., Onder Ersöz, H., Ukinç, K., Hacihasanoglu, A., Alhan, E., Cobanoğlu, U., Koçak, M., and Erdöl, H. (2007). Neurofibromatosis type 1 associated with pheochromocytoma: a case

report and a review of the literature. J. Endocrinol. Invest. *30*, 59–64.

Evans, D.G.R., Baser, M.E., McGaughran, J., Sharif, S., Howard, E., and Moran, A. (2002). Malignant peripheral nerve sheath tumours in neurofibromatosis 1. J. Med. Genet. *39*, 311–314.

Farid, M., Demicco, E.G., Garcia, R., Ahn, L., Merola, P.R., Cioffi, A., and Maki, R.G. (2014). Malignant peripheral nerve sheath tumors. Oncologist *19*, 193–201.

Fenton, T.R., and Gout, I.T. (2011). Functions and regulation of the 70kDa ribosomal S6 kinases. Int. J. Biochem. Cell Biol. *43*, 47–59.

Ferner, R.E., Huson, S.M., Thomas, N., Moss, C., Willshaw, H., Evans, D.G., Upadhyaya, M., Towers, R., Gleeson, M., Steiger, C., et al. (2007). Guidelines for the diagnosis and management of individuals with neurofibromatosis 1. J. Med. Genet. *44*, 81–88.

Fingar, D.C., and Blenis, J. (2004). Target of rapamycin (TOR): an integrator of nutrient and growth factor signals and coordinator of cell growth and cell cycle progression. Oncogene *23*, 3151–3171.

Fingar, D.C., Richardson, C.J., Tee, A.R., Cheatham, L., Tsou, C., and Blenis, J. (2004). mTOR controls cell cycle progression through its cell growth effectors S6K1 and 4E-BP1/eukaryotic translation initiation factor 4E. Mol. Cell. Biol. *24*, 200–216.

Finkel, T. (2012). Signal transduction by mitochondrial oxidants. J. Biol. Chem. *287*, 4434–4440.

Fisher, G.H., Wellen, S.L., Klimstra, D., Lenczowski, J.M., Tichelaar, J.W., Lizak, M.J., Whitsett, J.A., Koretsky, A., and Varmus, H.E. (2001). Induction and apoptotic regression of lung adenocarcinomas by regulation of a K-Ras transgene in the presence and absence of tumor suppressor genes. Genes Dev. *15*, 3249–3262.

Folkes, A.J., Ahmadi, K., Alderton, W.K., Alix, S., Baker, S.J., Box, G., Chuckowree, I.S., Clarke, P.A., Depledge, P., Eccles, S.A., et al. (2008). The identification of 2-(1H-indazol-4-yl)-6-(4-methanesulfonyl-piperazin-1-ylmethyl)-4-morpholin-4-yl-thieno[3,2-d]pyrimidine (GDC-0941) as a potent, selective, orally bioavailable inhibitor of class I PI3 kinase for the treatment of cancer . J. Med. Chem. *51*, 5522–5532.

Frahm, S., Mautner, V.-F., Brems, H., Legius, E., Debiec-Rychter, M., Friedrich, R.E., Knöfel, W.T., Peiper, M., and Kluwe, L. (2004). Genetic and phenotypic characterization of tumor cells derived from malignant peripheral nerve sheath tumors of neurofibromatosis type 1 patients. Neurobiol. Dis. *16*, 85–91.

Franz, D.N., Belousova, E., Sparagana, S., Bebin, E.M., Frost, M., Kuperman, R., Witt, O., Kohrman, M.H., Flamini, J.R., Wu, J.Y., et al. (2013). Efficacy and safety of everolimus for subependymal giant cell astrocytomas associated with tuberous sclerosis complex (EXIST-1): a multicentre, randomised, placebo-controlled phase 3 trial. Lancet *381*, 125–132.

Geering, B., Cutillas, P.R., Nock, G., Gharbi, S.I., and Vanhaesebroeck, B. (2007). Class IA phosphoinositide 3-kinases are obligate p85-p110 heterodimers. Proc. Natl. Acad. Sci. U.S.a.

104, 7809–7814.

Gorrini, C., Harris, I.S., and Mak, T.W. (2013). Modulation of oxidative stress as an anticancer strategy. Nat Rev Drug Discov *12*, 931–947.

Gregorian, C., Nakashima, J., Dry, S.M., Nghiemphu, P.L., Smith, K.B., Ao, Y., Dang, J., Lawson, G., Mellinghoff, I.K., Mischel, P.S., et al. (2009). PTEN dosage is essential for neurofibroma development and malignant transformation. Proc. Natl. Acad. Sci. U.S.a. *106*, 19479–19484.

Grover-McKay, M., Walsh, S.A., Seftor, E.A., Thomas, P.A., and Hendrix, M.J. (1998). Role for glucose transporter 1 protein in human breast cancer. Pathol. Oncol. Res. *4*, 115–120.

Gupta, G., and Maniker, A. (2007). Malignant peripheral nerve sheath tumors. Neurosurg Focus *22*, E12.

Han, J., Back, S.H., Hur, J., Lin, Y.-H., Gildersleeve, R., Shan, J., Yuan, C.L., Krokowski, D., Wang, S., Hatzoglou, M., et al. (2013). ER-stress-induced transcriptional regulation increases protein synthesis leading to cell death. Nat. Cell Biol. *15*, 481–490.

Hanahan, D., and Weinberg, R.A. (2000). The hallmarks of cancer. Cell *100*, 57–70.

Hara, K., Yonezawa, K., Kozlowski, M.T., Sugimoto, T., Andrabi, K., Weng, Q.P., Kasuga, M., Nishimoto, I., and Avruch, J. (1997). Regulation of eIF-4E BP1 phosphorylation by mTOR. J. Biol. Chem. *272*, 26457–26463.

Harding, H.P., Novoa, I., Zhang, Y., Zeng, H., Wek, R., Schapira, M., and Ron, D. (2000). Regulated translation initiation controls stress-induced gene expression in mammalian cells. Mol. Cell *6*, 1099–1108.

Harding, H.P., Zhang, Y., and Ron, D. (1999). Protein translation and folding are coupled by an endoplasmic-reticulum-resident kinase. Nature *397*, 271–274.

Harding, H.P., Zhang, Y., Zeng, H., Novoa, I., Lu, P.D., Calfon, M., Sadri, N., Yun, C., Popko, B., Paules, R., et al. (2003). An integrated stress response regulates amino acid metabolism and resistance to oxidative stress. Mol. Cell *11*, 619–633.

Hay, N., and Sonenberg, N. (2004). Upstream and downstream of mTOR. Genes Dev. *18*, 1926–1945.

Herman, S.E.M., Gordon, A.L., Wagner, A.J., Heerema, N.A., Zhao, W., Flynn, J.M., Jones, J., Andritsos, L., Puri, K.D., Lannutti, B.J., et al. (2010). Phosphatidylinositol 3-kinase-δ inhibitor CAL-101 shows promising preclinical activity in chronic lymphocytic leukemia by antagonizing intrinsic and extrinsic cellular survival signals. Blood *116*, 2078–2088.

Hiatt, K.K., Ingram, D.A., Zhang, Y., Bollag, G., and Clapp, D.W. (2001). Neurofibromin GTPase-activating protein-related domains restore normal growth in Nf1-/- cells. J. Biol. Chem. *276*, 7240–7245.

Hirai, H., Sootome, H., Nakatsuru, Y., Miyama, K., Taguchi, S., Tsujioka, K., Ueno, Y., Hatch,

H., Majumder, P.K., Pan, B.-S., et al. (2010). MK-2206, an allosteric Akt inhibitor, enhances antitumor efficacy by standard chemotherapeutic agents or molecular targeted drugs in vitro and in vivo. Mol. Cancer Ther. *9*, 1956–1967.

Hockly, E., Richon, V.M., Woodman, B., Smith, D.L., Zhou, X., Rosa, E., Sathasivam, K., Ghazi-Noori, S., Mahal, A., Lowden, P.A.S., et al. (2003). Suberoylanilide hydroxamic acid, a histone deacetylase inhibitor, ameliorates motor deficits in a mouse model of Huntington's disease. Proc. Natl. Acad. Sci. U.S.a. *100*, 2041–2046.

Hoellenriegel, J., Meadows, S.A., Sivina, M., Wierda, W.G., Kantarjian, H., Keating, M.J., Giese, N., O'Brien, S., Yu, A., Miller, L.L., et al. (2011). The phosphoinositide 3'-kinase delta inhibitor, CAL-101, inhibits B-cell receptor signaling and chemokine networks in chronic lymphocytic leukemia. Blood *118*, 3603–3612.

Holland, A.J., and Cleveland, D.W. (2009). Boveri revisited: chromosomal instability, aneuploidy and tumorigenesis. Nat. Rev. Mol. Cell Biol. *10*, 478–487.

Hollien, J., and Weissman, J.S. (2006). Decay of endoplasmic reticulum-localized mRNAs during the unfolded protein response. Science *313*, 104–107.

Hollien, J., Lin, J.H., Li, H., Stevens, N., Walter, P., and Weissman, J.S. (2009). Regulated Ire1-dependent decay of messenger RNAs in mammalian cells. J. Cell Biol. *186*, 323–331.

Hölzel, M., Huang, S., Koster, J., Ora, I., Lakeman, A., Caron, H., Nijkamp, W., Xie, J., Callens, T., Asgharzadeh, S., et al. (2010). NF1 is a tumor suppressor in neuroblastoma that determines retinoic acid response and disease outcome. Cell *142*, 218–229.

Hu, P., Mondino, A., Skolnik, E.Y., and Schlessinger, J. (1993). Cloning of a novel, ubiquitously expressed human phosphatidylinositol 3-kinase and identification of its binding site on p85. Mol. Cell. Biol. *13*, 7677–7688.

Huang, J., and Manning, B.D. (2009). A complex interplay between Akt, TSC2 and the two mTOR complexes. Biochem. Soc. Trans. *37*, 217–222.

Huson, S.M., Compston, D.A., Clark, P., and Harper, P.S. (1989). A genetic study of von Recklinghausen neurofibromatosis in south east Wales. I. Prevalence, fitness, mutation rate, and effect of parental transmission on severity. J. Med. Genet. *26*, 704–711.

Ikeda, H., Hideshima, T., Fulciniti, M., Perrone, G., Miura, N., Yasui, H., Okawa, Y., Kiziltepe, T., Santo, L., Vallet, S., et al. (2010). PI3K/p110{delta} is a novel therapeutic target in multiple myeloma. Blood *116*, 1460–1468.

Ikenoue, T., Kanai, F., Hikiba, Y., Obata, T., Tanaka, Y., Imamura, J., Ohta, M., Jazag, A., Guleng, B., Tateishi, K., et al. (2005). Functional analysis of PIK3CA gene mutations in human colorectal cancer. Cancer Res. *65*, 4562–4567.

Ingram, D.A., Yang, F.C., Travers, J.B., Wenning, M.J., Hiatt, K., New, S., Hood, A., Shannon, K., Williams, D.A., and Clapp, D.W. (2000). Genetic and biochemical evidence that haploinsufficiency of the Nf1 tumor suppressor gene modulates melanocyte and mast cell fates in vivo. J. Exp. Med. *191*, 181–188.

Inoki, K., Li, Y., Zhu, T., Wu, J., and Guan, K.-L. (2002). TSC2 is phosphorylated and inhibited by Akt and suppresses mTOR signalling. Nat. Cell Biol. *4*, 648–657.

Isakoff, S.J., Engelman, J.A., Irie, H.Y., Luo, J., Brachmann, S.M., Pearline, R.V., Cantley, L.C., and Brugge, J.S. (2005). Breast cancer-associated PIK3CA mutations are oncogenic in mammary epithelial cells. Cancer Res. *65*, 10992–11000.

Ito, T., Noguchi, Y., Satoh, S., Hayashi, H., Inayama, Y., and Kitamura, H. (1998). Expression of facilitative glucose transporter isoforms in lung carcinomas: its relation to histologic type, differentiation grade, and tumor stage. Mod. Pathol. *11*, 437–443.

Jacinto, E., Loewith, R., Schmidt, A., Lin, S., Rüegg, M.A., Hall, A., and Hall, M.N. (2004). Mammalian TOR complex 2 controls the actin cytoskeleton and is rapamycin insensitive. Nat. Cell Biol. *6*, 1122–1128.

Jacks, T., Shih, T.S., Schmitt, E.M., Bronson, R.T., Bernards, A., and Weinberg, R.A. (1994). Tumour predisposition in mice heterozygous for a targeted mutation in Nf1. Nat. Genet. *7*, 353–361.

Jamieson, S., Flanagan, J.U., Kolekar, S., Buchanan, C., Kendall, J.D., Lee, W.-J., Rewcastle, G.W., Denny, W.A., Singh, R., Dickson, J., et al. (2011). A drug targeting only p110α can block phosphoinositide 3-kinase signalling and tumour growth in certain cell types. Biochem. J. *438*, 53–62.

Janssen-Heininger, Y.M.W., Mossman, B.T., Heintz, N.H., Forman, H.J., Kalyanaraman, B., Finkel, T., Stamler, J.S., Rhee, S.G., and van der Vliet, A. (2008). Redox-based regulation of signal transduction: principles, pitfalls, and promises. Free Radic. Biol. Med. *45*, 1–17.

Jeong, S.-Y., Park, S.-J., and Kim, H.J. (2006). The spectrum of NF1 mutations in Korean patients with neurofibromatosis type 1. J. Korean Med. Sci. *21*, 107–112.

Jessen, W.J., Miller, S.J., Jousma, E., Wu, J., Rizvi, T.A., Brundage, M.E., Eaves, D., Widemann, B., Kim, M.-O., Dombi, E., et al. (2013). MEK inhibition exhibits efficacy in human and mouse neurofibromatosis tumors. J. Clin. Invest. *123*, 340–347.

Jhanwar, S.C., Chen, Q., Li, F.P., Brennan, M.F., and Woodruff, J.M. (1994). Cytogenetic analysis of soft tissue sarcomas. Recurrent chromosome abnormalities in malignant peripheral nerve sheath tumors (MPNST). Cancer Genet. Cytogenet. *78*, 138–144.

Jia, S., Liu, Z., Zhang, S., Liu, P., Zhang, L., Lee, S.H., Zhang, J., Signoretti, S., Loda, M., Roberts, T.M., et al. (2008). Essential roles of PI(3)K-p110beta in cell growth, metabolism and tumorigenesis. Nature *454*, 776–779.

Johannessen, C.M., Johnson, B.W., Williams, S.M.G., Chan, A.W., Reczek, E.E., Lynch, R.C., Rioth, M.J., McClatchey, A., Ryeom, S., and Cichowski, K. (2008). TORC1 is essential for NF1-associated malignancies. Curr. Biol. *18*, 56–62.

Johannessen, C.M., Reczek, E.E., James, M.F., Brems, H., Legius, E., and Cichowski, K. (2005). The NF1 tumor suppressor critically regulates TSC2 and mTOR. Proc. Natl. Acad. Sci. U.S.a. *102*, 8573–8578.

John, J., Sohmen, R., Feuerstein, J., Linke, R., Wittinghofer, A., and Goody, R.S. (1990). Kinetics of interaction of nucleotides with nucleotide-free H-ras p21. Biochemistry *29*, 6058–6065.

Joseph, N.M., Mosher, J.T., Buchstaller, J., Snider, P., McKeever, P.E., Lim, M., Conway, S.J., Parada, L.F., Zhu, Y., and Morrison, S.J. (2008). The loss of Nf1 transiently promotes self-renewal but not tumorigenesis by neural crest stem cells. Cancer Cell *13*, 129–140.

Kaadige, M.R., Yang, J., Wilde, B.R., and Ayer, D.E. (2015). MondoA-Mlx transcriptional activity is limited by mTOR-MondoA interaction. Mol. Cell. Biol. *35*, 101–110.

Kahali, S., Sarcar, B., and Chinnaiyan, P. (2011). The emerging role of histone deacetylases (HDACs) in UPR regulation. Meth. Enzymol. *490*, 159–174.

Kahali, S., Sarcar, B., Fang, B., Williams, E.S., Koomen, J.M., Tofilon, P.J., and Chinnaiyan, P. (2010). Activation of the unfolded protein response contributes toward the antitumor activity of vorinostat. Neoplasia *12*, 80–86.

Kahali, S., Sarcar, B., Prabhu, A., Seto, E., and Chinnaiyan, P. (2012). Class I histone deacetylases localize to the endoplasmic reticulum and modulate the unfolded protein response. Faseb J. *26*, 2437–2445.

Kang, S., Bader, A.G., and Vogt, P.K. (2005). Phosphatidylinositol 3-kinase mutations identified in human cancer are oncogenic. Proc. Natl. Acad. Sci. U.S.a. *102*, 802–807.

Kang, S., Denley, A., Vanhaesebroeck, B., and Vogt, P.K. (2006). Oncogenic transformation induced by the p110beta, -gamma, and -delta isoforms of class I phosphoinositide 3-kinase. Proc. Natl. Acad. Sci. U.S.a. *103*, 1289–1294.

Karakas, B., Bachman, K.E., and Park, B.H. (2006). Mutation of the PIK3CA oncogene in human cancers. Br. J. Cancer *94*, 455–459.

Kekatpure, V.D., Dannenberg, A.J., and Subbaramaiah, K. (2009). HDAC6 modulates Hsp90 chaperone activity and regulates activation of aryl hydrocarbon receptor signaling. J. Biol. Chem. *284*, 7436–7445.

Kim, I., Xu, W., and Reed, J.C. (2008). Cell death and endoplasmic reticulum stress: disease relevance and therapeutic opportunities. Nat Rev Drug Discov *7*, 1013–1030.

Kim, J., Kundu, M., Viollet, B., and Guan, K.-L. (2011). AMPK and mTOR regulate autophagy through direct phosphorylation of Ulk1. Nat. Cell Biol. *13*, 132–141.

Klaunig, J.E., Kamendulis, L.M., and Hocevar, B.A. (2010). Oxidative stress and oxidative damage in carcinogenesis. Toxicol Pathol *38*, 96–109.

Klose, A., Ahmadian, M.R., Schuelke, M., Scheffzek, K., Hoffmeyer, S., Gewies, A., Schmitz, F., Kaufmann, D., Peters, H., Wittinghofer, A., et al. (1998). Selective disactivation of neurofibromin GAP activity in neurofibromatosis type 1. Hum. Mol. Genet. *7*, 1261–1268.

Ko, J.M., Sohn, Y.B., Jeong, S.-Y., Kim, H.-J., and Messiaen, L.M. (2013). Mutation spectrum

of NF1 and clinical characteristics in 78 Korean patients with neurofibromatosis type 1. Pediatr. Neurol. *48*, 447–453.

Koga, T., Iwasaki, H., Ishiguro, M., Matsuzaki, A., and Kikuchi, M. (2002). Losses in chromosomes 17, 19, and 22q in neurofibromatosis type 1 and sporadic neurofibromas: a comparative genomic hybridization analysis. Cancer Genet. Cytogenet. *136*, 113–120.

Kokame, K., Kato, H., and Miyata, T. (2001). Identification of ERSE-II, a new cis-acting element responsible for the ATF6-dependent mammalian unfolded protein response. J. Biol. Chem. *276*, 9199–9205.

Kolch, W. (2005). Coordinating ERK/MAPK signalling through scaffolds and inhibitors. Nat. Rev. Mol. Cell Biol. *6*, 827–837.

Konicek, B.W., Stephens, J.R., McNulty, A.M., Robichaud, N., Peery, R.B., Dumstorf, C.A., Dowless, M.S., Iversen, P.W., Parsons, S., Ellis, K.E., et al. (2011). Therapeutic inhibition of MAP kinase interacting kinase blocks eukaryotic initiation factor 4E phosphorylation and suppresses outgrowth of experimental lung metastases. Cancer Res. *71*, 1849–1857.

Korf, B.R. (1999). Plexiform neurofibromas. Am. J. Med. Genet. *89*, 31–37.

Kourea, H.P., Orlow, I., Scheithauer, B.W., Cordon-Cardo, C., and Woodruff, J.M. (1999). Deletions of the INK4A gene occur in malignant peripheral nerve sheath tumors but not in neurofibromas. Am. J. Pathol. *155*, 1855–1860.

Krueger, D.A., Wilfong, A.A., Holland-Bouley, K., Anderson, A.E., Agricola, K., Tudor, C., Mays, M., Lopez, C.M., Kim, M.-O., and Franz, D.N. (2013). Everolimus treatment of refractory epilepsy in tuberous sclerosis complex. Ann. Neurol. *74*, 679–687.

Kumar, V., Abbas, A.K., Fausto, N., and Aster, J.C. (2009). Robbins and Cotran Pathologic Basis of Disease, Professional Edition (Elsevier Health Sciences).

Lannutti, B.J., Meadows, S.A., Herman, S.E.M., Kashishian, A., Steiner, B., Johnson, A.J., Byrd, J.C., Tyner, J.W., Loriaux, M.M., Deininger, M., et al. (2011). CAL-101, a p110delta selective phosphatidylinositol-3-kinase inhibitor for the treatment of B-cell malignancies, inhibits PI3K signaling and cellular viability. Blood *117*, 591–594.

Laplante, M., and Sabatini, D.M. (2009). An emerging role of mTOR in lipid biosynthesis. Curr. Biol. *19*, R1046–R1052.

Lau, N., Feldkamp, M.M., Roncari, L., Loehr, A.H., Shannon, P., Gutmann, D.H., and Guha, A. (2000). Loss of neurofibromin is associated with activation of RAS/MAPK and PI3-K/AKT signaling in a neurofibromatosis 1 astrocytoma. J. Neuropathol. Exp. Neurol. *59*, 759–767.

Lauchle, J.O., Braun, B.S., Loh, M.L., and Shannon, K. (2006). Inherited predispositions and hyperactive Ras in myeloid leukemogenesis. Pediatr Blood Cancer *46*, 579–585.

Legius, E., Dierick, H., Wu, R., Hall, B.K., Marynen, P., Cassiman, J.J., and Glover, T.W. (1994). TP53 mutations are frequent in malignant NF1 tumors. Genes Chromosomes Cancer *10*, 250–255.

Lerner, A.G., Upton, J.-P., Praveen, P.V.K., Ghosh, R., Nakagawa, Y., Igbaria, A., Shen, S., Nguyen, V., Backes, B.J., Heiman, M., et al. (2012). IRE1α induces thioredoxin-interacting protein to activate the NLRP3 inflammasome and promote programmed cell death under irremediable ER stress. Cell Metab. *16*, 250–264.

Leroy, K., Dumas, V., Martin-Garcia, N., Falzone, M.C., Voisin, M.C., Wechsler, J., Revuz, J., Créange, A., Levy, E., Lantieri, L., et al. (2001). Malignant peripheral nerve sheath tumors associated with neurofibromatosis type 1: a clinicopathologic and molecular study of 17 patients. Arch Dermatol *137*, 908–913.

Liapis, H., Marley, E.F., Lin, Y., and Dehner, L.P. (1999). p53 and Ki-67 proliferating cell nuclear antigen in benign and malignant peripheral nerve sheath tumors in children. Pediatr. Dev. Pathol. *2*, 377–384.

Lim, S.M., Westover, K.D., Ficarro, S.B., Harrison, R.A., Choi, H.G., Pacold, M.E., Carrasco, M., Hunter, J., Kim, N.D., Xie, T., et al. (2014). Therapeutic targeting of oncogenic K-Ras by a covalent catalytic site inhibitor. Angew. Chem. Int. Ed. Engl. *53*, 199–204.

Liu, P., Cheng, H., Roberts, T.M., and Zhao, J.J. (2009). Targeting the phosphoinositide 3-kinase pathway in cancer. Nat Rev Drug Discov *8*, 627–644.

Loewith, R., Jacinto, E., Wullschleger, S., Lorberg, A., Crespo, J.L., Bonenfant, D., Oppliger, W., Jenoe, P., and Hall, M.N. (2002). Two TOR complexes, only one of which is rapamycin sensitive, have distinct roles in cell growth control. Mol. Cell *10*, 457–468.

Lopez, G., Torres, K., Liu, J., Hernandez, B., Young, E., Belousov, R., Bolshakov, S., Lazar, A.J., Slopis, J.M., McCutcheon, I.E., et al. (2011). Autophagic survival in resistance to histone deacetylase inhibitors: novel strategies to treat malignant peripheral nerve sheath tumors. Cancer Res. *71*, 185–196.

LoRusso, P.M., Krishnamurthi, S.S., Rinehart, J.J., Nabell, L.M., Malburg, L., Chapman, P.B., DePrimo, S.E., Bentivegna, S., Wilner, K.D., Tan, W., et al. (2010). Phase I pharmacokinetic and pharmacodynamic study of the oral MAPK/ERK kinase inhibitor PD-0325901 in patients with advanced cancers. Clin. Cancer Res. *16*, 1924–1937.

Lu, J., and Holmgren, A. (2012). Thioredoxin system in cell death progression. Antioxid. Redox Signal. *17*, 1738–1747.

Lu, J., and Holmgren, A. (2014). The thioredoxin antioxidant system. Free Radic. Biol. Med. *66*, 75–87.

Luo, J., Solimini, N.L., and Elledge, S.J. (2009). Principles of cancer therapy: oncogene and non-oncogene addiction. Cell *136*, 823–837.

Ma, X.M., and Blenis, J. (2009). Molecular mechanisms of mTOR-mediated translational control. Nat. Rev. Mol. Cell Biol. *10*, 307–318.

Maertens, O., and Cichowski, K. (2014). An expanding role for RAS GTPase activating proteins (RAS GAPs) in cancer. Adv Biol Regul *55*, 1–14.

Maertens, O., Johnson, B., Hollstein, P., Frederick, D.T., Cooper, Z.A., Messiaen, L., Bronson, R.T., McMahon, M., Granter, S., Flaherty, K., et al. (2013). Elucidating distinct roles for NF1 in melanomagenesis. Cancer Discov *3*, 338–349.

Maertens, O., Prenen, H., Debiec-Rychter, M., Wozniak, A., Sciot, R., Pauwels, P., De Wever, I., Vermeesch, J.R., De Raedt, T., De Paepe, A., et al. (2006). Molecular pathogenesis of multiple gastrointestinal stromal tumors in NF1 patients. Hum. Mol. Genet. *15*, 1015–1023.

Malhotra, J.D., and Kaufman, R.J. (2007). Endoplasmic reticulum stress and oxidative stress: a vicious cycle or a double-edged sword? Antioxid. Redox Signal. *9*, 2277–2293.

Malone, C.F., Fromm, J.A., Maertens, O., DeRaedt, T., Ingraham, R., and Cichowski, K. (2014). Defining Key Signaling Nodes and Therapeutic Biomarkers in NF1-Mutant Cancers. Cancer Discov *4*, 1062–1073.

Mann, B.S., Johnson, J.R., Cohen, M.H., Justice, R., and Pazdur, R. (2007). FDA approval summary: vorinostat for treatment of advanced primary cutaneous T-cell lymphoma. Oncologist *12*, 1247–1252.

Manning, B.D., Tee, A.R., Logsdon, M.N., Blenis, J., and Cantley, L.C. (2002). Identification of the tuberous sclerosis complex-2 tumor suppressor gene product tuberin as a target of the phosphoinositide 3-kinase/akt pathway. Mol. Cell *10*, 151–162.

Martin, G.A., Viskochil, D., Bollag, G., McCabe, P.C., Crosier, W.J., Haubruck, H., Conroy, L., Clark, R., O'Connell, P., and Cawthon, R.M. (1990). The GAP-related domain of the neurofibromatosis type 1 gene product interacts with ras p21. Cell *63*, 843–849.

Mayes, D.A., Rizvi, T.A., Cancelas, J.A., Kolasinski, N.T., Ciraolo, G.M., Stemmer-Rachamimov, A.O., and Ratner, N. (2011). Perinatal or adult Nf1 inactivation using tamoxifen-inducible PlpCre each cause neurofibroma formation. Cancer Res. *71*, 4675–4685.

McGillicuddy, L.T., Fromm, J.A., Hollstein, P.E., Kubek, S., Beroukhim, R., De Raedt, T., Johnson, B.W., Williams, S.M.G., Nghiemphu, P., Liau, L.M., et al. (2009). Proteasomal and genetic inactivation of the NF1 tumor suppressor in gliomagenesis. Cancer Cell *16*, 44–54.

McLaughlin, S.K., Olsen, S.N., Dake, B., De Raedt, T., Lim, E., Bronson, R.T., Beroukhim, R., Polyak, K., Brown, M., Kuperwasser, C., et al. (2013). The RasGAP Gene, RASAL2, Is a Tumor and Metastasis Suppressor. Cancer Cell *24*, 365–378.

Meadows, S.A., Vega, F., Kashishian, A., Johnson, D., Diehl, V., Miller, L.L., Younes, A., and Lannutti, B.J. (2012). PI3Kδ inhibitor, GS-1101 (CAL-101), attenuates pathway signaling, induces apoptosis, and overcomes signals from the microenvironment in cellular models of Hodgkin lymphoma. Blood *119*, 1897–1900.

Meikle, L., Pollizzi, K., Egnor, A., Kramvis, I., Lane, H., Sahin, M., and Kwiatkowski, D.J. (2008). Response of a neuronal model of tuberous sclerosis to mammalian target of rapamycin (mTOR) inhibitors: effects on mTORC1 and Akt signaling lead to improved survival and function. J. Neurosci. *28*, 5422–5432.

Mendoza, M.C., Er, E.E., and Blenis, J. (2011). The Ras-ERK and PI3K-mTOR pathways: cross-

talk and compensation. Trends Biochem. Sci. *36*, 320–328.

Menon, A.G., Anderson, K.M., Riccardi, V.M., Chung, R.Y., Whaley, J.M., Yandell, D.W., Farmer, G.E., Freiman, R.N., Lee, J.K., and Li, F.P. (1990). Chromosome 17p deletions and p53 gene mutations associated with the formation of malignant neurofibrosarcomas in von Recklinghausen neurofibromatosis. Proc. Natl. Acad. Sci. U.S.a. *87*, 5435–5439.

Menon, S., Dibble, C.C., Talbott, G., Hoxhaj, G., Valvezan, A.J., Takahashi, H., Cantley, L.C., and Manning, B.D. (2014). Spatial Control of the TSC Complex Integrates Insulin and Nutrient Regulation of mTORC1 at the Lysosome. Cell *156*, 771–785.

Min, J., Zaslavsky, A., Fedele, G., McLaughlin, S.K., Reczek, E.E., De Raedt, T., Guney, I., Strochlic, D.E., Macconaill, L.E., Beroukhim, R., et al. (2010). An oncogene-tumor suppressor cascade drives metastatic prostate cancer by coordinately activating Ras and nuclear factor-kappaB. Nat. Med. *16*, 286–294.

Moodie, S.A., Willumsen, B.M., Weber, M.J., and Wolfman, A. (1993). Complexes of Ras.GTP with Raf-1 and mitogen-activated protein kinase kinase. Science *260*, 1658–1661.

Morita, M., Gravel, S.-P., Hulea, L., Larsson, O., Pollak, M., St-Pierre, J., and Topisirovic, I. (2015). mTOR coordinates protein synthesis, mitochondrial activity and proliferation. Cell Cycle *14*, 473–480.

Nishioka, C., Ikezoe, T., Yang, J., Takeuchi, S., Koeffler, H.P., and Yokoyama, A. (2008). MS-275, a novel histone deacetylase inhibitor with selectivity against HDAC1, induces degradation of FLT3 via inhibition of chaperone function of heat shock protein 90 in AML cells. Leuk. Res. *32*, 1382–1392.

Nylander, S., Kull, B., Björkman, J.A., Ulvinge, J.C., Oakes, N., Emanuelsson, B.M., Andersson, M., Skärby, T., Inghardt, T., Fjellström, O., et al. (2012). Human target validation of phosphoinositide 3-kinase (PI3K)β: effects on platelets and insulin sensitivity, using AZD6482 a novel PI3Kβ inhibitor. J. Thromb. Haemost. *10*, 2127–2136.

Oh, W.J., and Jacinto, E. (2011). mTOR complex 2 signaling and functions. Cell Cycle *10*, 2305–2316.

Oh, W.J., Wu, C.-C., Kim, S.J., Facchinetti, V., Julien, L.-A., Finlan, M., Roux, P.P., Su, B., and Jacinto, E. (2010). mTORC2 can associate with ribosomes to promote cotranslational phosphorylation and stability of nascent Akt polypeptide. Embo J. *29*, 3939–3951.

Oromendia, A.B., and Amon, A. (2014). Aneuploidy: implications for protein homeostasis and disease. Dis Model Mech *7*, 15–20.

Oslowski, C.M., Hara, T., O'Sullivan-Murphy, B., Kanekura, K., Lu, S., Hara, M., Ishigaki, S., Zhu, L.J., Hayashi, E., Hui, S.T., et al. (2012). Thioredoxin-interacting protein mediates ER stress-induced β cell death through initiation of the inflammasome. Cell Metab. *16*, 265–273.

Ostrem, J.M., Peters, U., Sos, M.L., Wells, J.A., and Shokat, K.M. (2013). K-Ras(G12C) inhibitors allosterically control GTP affinity and effector interactions. Nature *503*, 548–551.

Oyadomari, S., and Mori, M. (2004). Roles of CHOP/GADD153 in endoplasmic reticulum stress. Cell Death Differ. *11*, 381–389.

Ozaki, E., Campbell, M., and Doyle, S.L. (2015). Targeting the NLRP3 inflammasome in chronic inflammatory diseases: current perspectives. J Inflamm Res *8*, 15–27.

Pacold, M.E., Suire, S., Perisic, O., Lara-Gonzalez, S., Davis, C.T., Walker, E.H., Hawkins, P.T., Stephens, L., Eccleston, J.F., and Williams, R.L. (2000). Crystal structure and functional analysis of Ras binding to its effector phosphoinositide 3-kinase gamma. Cell *103*, 931–943.

Park, I.-H., Bachmann, R., Shirazi, H., and Chen, J. (2002). Regulation of ribosomal S6 kinase 2 by mammalian target of rapamycin. J. Biol. Chem. *277*, 31423–31429.

Parkin, B., Ouillette, P., Wang, Y., Liu, Y., Wright, W., Roulston, D., Purkayastha, A., Dressel, A., Karp, J., Bockenstedt, P., et al. (2010). NF1 inactivation in adult acute myelogenous leukemia. Clin. Cancer Res. *16*, 4135–4147.

Parsons, D.W., Jones, S., Zhang, X., Lin, J.C.-H., Leary, R.J., Angenendt, P., Mankoo, P., Carter, H., Siu, I.-M., Gallia, G.L., et al. (2008). An integrated genomic analysis of human glioblastoma multiforme. Science *321*, 1807–1812.

Pearce, L.R., Huang, X., Boudeau, J., Pawłowski, R., Wullschleger, S., Deak, M., Ibrahim, A.F.M., Gourlay, R., Magnuson, M.A., and Alessi, D.R. (2007). Identification of Protor as a novel Rictor-binding component of mTOR complex-2. Biochem. J. *405*, 513–522.

Peterson, T.R., Laplante, M., Thoreen, C.C., Sancak, Y., Kang, S.A., Kuehl, W.M., Gray, N.S., and Sabatini, D.M. (2009). DEPTOR is an mTOR inhibitor frequently overexpressed in multiple myeloma cells and required for their survival. Cell *137*, 873–886.

Petruccelli, L.A., Dupéré-Richer, D., Pettersson, F., Retrouvey, H., Skoulikas, S., and Miller, W.H. (2011). Vorinostat induces reactive oxygen species and DNA damage in acute myeloid leukemia cells. PLoS ONE *6*, e20987.

Pettersson, F., Del Rincon, S.V., and Miller, W.H. (2014). Eukaryotic translation initiation factor 4E as a novel therapeutic target in hematological malignancies and beyond. Expert Opin. Ther. Targets *18*, 1035–1048.

Porter, D.E., Prasad, V., Foster, L., Dall, G.F., Birch, R., and Grimer, R.J. (2009). Survival in Malignant Peripheral Nerve Sheath Tumours: A Comparison between Sporadic and Neurofibromatosis Type 1-Associated Tumours. Sarcoma *2009*, 756395.

Posch, C., Moslehi, H., Feeney, L., Green, G.A., Ebaee, A., Feichtenschlager, V., Chong, K., Peng, L., Dimon, M.T., Phillips, T., et al. (2013). Combined targeting of MEK and PI3K/mTOR effector pathways is necessary to effectively inhibit NRAS mutant melanoma in vitro and in vivo. Proc. Natl. Acad. Sci. U.S.a. *110*, 4015–4020.

Potter, C.J., Pedraza, L.G., and Xu, T. (2002). Akt regulates growth by directly phosphorylating Tsc2. Nat. Cell Biol. *4*, 658–665.

Price, D.J., Grove, J.R., Calvo, V., Avruch, J., and Bierer, B.E. (1992). Rapamycin-induced

inhibition of the 70-kilodalton S6 protein kinase. Science *257*, 973–977.

Rao, R., Lee, P., Fiskus, W., Yang, Y., Joshi, R., Wang, Y., Buckley, K., Balusu, R., Chen, J., Koul, S., et al. (2009). Co-treatment with heat shock protein 90 inhibitor 17-dimethylaminoethylamino-17-demethoxygeldanamycin (DMAG) and vorinostat: a highly active combination against human mantle cell lymphoma (MCL) cells. Cancer Biol. Ther. *8*, 1273–1280.

Rao, R., Nalluri, S., Kolhe, R., Yang, Y., Fiskus, W., Chen, J., Ha, K., Buckley, K.M., Balusu, R., Coothankandaswamy, V., et al. (2010). Treatment with panobinostat induces glucose-regulated protein 78 acetylation and endoplasmic reticulum stress in breast cancer cells. Mol. Cancer Ther. *9*, 942–952.

Rasmussen, S.A., Overman, J., Thomson, S.A., Colman, S.D., Abernathy, C.R., Trimpert, R.E., Moose, R., Virdi, G., Roux, K., Bauer, M., et al. (2000). Chromosome 17 loss-of-heterozygosity studies in benign and malignant tumors in neurofibromatosis type 1. Genes Chromosomes Cancer *28*, 425–431.

Raught, B., Gingras, A.C., Gygi, S.P., Imataka, H., Morino, S., Gradi, A., Aebersold, R., and Sonenberg, N. (2000). Serum-stimulated, rapamycin-sensitive phosphorylation sites in the eukaryotic translation initiation factor 4GI. Embo J. *19*, 434–444.

Reagan-Shaw, S., Nihal, M., and Ahmad, N. (2008). Dose translation from animal to human studies revisited. Faseb J. *22*, 659–661.

Renouf, D.J., Velazquez-Martin, J.P., Simpson, R., Siu, L.L., and Bedard, P.L. (2012). Ocular toxicity of targeted therapies. J. Clin. Oncol. *30*, 3277–3286.

Rodriguez-Viciana, P., Warne, P.H., Dhand, R., Vanhaesebroeck, B., Gout, I., Fry, M.J., Waterfield, M.D., and Downward, J. (1994). Phosphatidylinositol-3-OH kinase as a direct target of Ras. Nature *370*, 527–532.

Ron, D., and Walter, P. (2007). Signal integration in the endoplasmic reticulum unfolded protein response. Nat. Rev. Mol. Cell Biol. *8*, 519–529.

Saelen, M.G., Ree, A.H., Kristian, A., Fleten, K.G., Furre, T., Hektoen, H.H., and Flatmark, K. (2012). Radiosensitization by the histone deacetylase inhibitor vorinostat under hypoxia and with capecitabine in experimental colorectal carcinoma. Radiat Oncol *7*, 165.

Saitoh, M., Nishitoh, H., Fujii, M., Takeda, K., Tobiume, K., Sawada, Y., Kawabata, M., Miyazono, K., and Ichijo, H. (1998). Mammalian thioredoxin is a direct inhibitor of apoptosis signal-regulating kinase (ASK) 1. Embo J. *17*, 2596–2606.

Sakashita, M., Aoyama, N., Minami, R., Maekawa, S., Kuroda, K., Shirasaka, D., Ichihara, T., Kuroda, Y., Maeda, S., and Kasuga, M. (2001). Glut1 expression in T1 and T2 stage colorectal carcinomas: its relationship to clinicopathological features. Eur. J. Cancer *37*, 204–209.

Samuels, Y., Diaz, L.A., Schmidt-Kittler, O., Cummins, J.M., Delong, L., Cheong, I., Rago, C., Huso, D.L., Lengauer, C., Kinzler, K.W., et al. (2005). Mutant PIK3CA promotes cell growth and invasion of human cancer cells. Cancer Cell *7*, 561–573.

Samuels, Y., Wang, Z., Bardelli, A., Silliman, N., Ptak, J., Szabo, S., Yan, H., Gazdar, A., Powell, S.M., Riggins, G.J., et al. (2004). High frequency of mutations of the PIK3CA gene in human cancers. Science *304*, 554.

Sano, R., and Reed, J.C. (2013). ER stress-induced cell death mechanisms. Biochim. Biophys. Acta *1833*, 3460–3470.

Sarbassov, D.D., Ali, S.M., Kim, D.-H., Guertin, D.A., Latek, R.R., Erdjument-Bromage, H., Tempst, P., and Sabatini, D.M. (2004). Rictor, a novel binding partner of mTOR, defines a rapamycin-insensitive and raptor-independent pathway that regulates the cytoskeleton. Curr. Biol. *14*, 1296–1302.

Sarbassov, D.D., Guertin, D.A., Ali, S.M., and Sabatini, D.M. (2005). Phosphorylation and regulation of Akt/PKB by the rictor-mTOR complex. Science *307*, 1098–1101.

Saxena, G., Chen, J., and Shalev, A. (2010). Intracellular shuttling and mitochondrial function of thioredoxin-interacting protein. J. Biol. Chem. *285*, 3997–4005.

Scheuner, D., Song, B., McEwen, E., Liu, C., Laybutt, R., Gillespie, P., Saunders, T., Bonner-Weir, S., and Kaufman, R.J. (2001). Translational control is required for the unfolded protein response and in vivo glucose homeostasis. Mol. Cell *7*, 1165–1176.

Scroggins, B.T., Robzyk, K., Wang, D., Marcu, M.G., Tsutsumi, S., Beebe, K., Cotter, R.J., Felts, S., Toft, D., Karnitz, L., et al. (2007). An acetylation site in the middle domain of Hsp90 regulates chaperone function. Mol. Cell *25*, 151–159.

See, W.L., Tan, I.-L., Mukherjee, J., Nicolaides, T., and Pieper, R.O. (2012). Sensitivity of glioblastomas to clinically available MEK inhibitors is defined by neurofibromin 1 deficiency. Cancer Res. *72*, 3350–3359.

Shackelford, D.B., Vasquez, D.S., Corbeil, J., Wu, S., Leblanc, M., Wu, C.-L., Vera, D.R., and Shaw, R.J. (2009). mTOR and HIF-1alpha-mediated tumor metabolism in an LKB1 mouse model of Peutz-Jeghers syndrome. Proc. Natl. Acad. Sci. U.S.a. *106*, 11137–11142.

Sheltzer, J.M., Torres, E.M., Dunham, M.J., and Amon, A. (2012). Transcriptional consequences of aneuploidy. Proc. Natl. Acad. Sci. U.S.a. *109*, 12644–12649.

Shi, Y., Vattem, K.M., Sood, R., An, J., Liang, J., Stramm, L., and Wek, R.C. (1998). Identification and characterization of pancreatic eukaryotic initiation factor 2 alpha-subunit kinase, PEK, involved in translational control. Mol. Cell. Biol. *18*, 7499–7509.

Sidrauski, C., and Walter, P. (1997). The transmembrane kinase Ire1p is a site-specific endonuclease that initiates mRNA splicing in the unfolded protein response. Cell *90*, 1031–1039.

Singh, A., Greninger, P., Rhodes, D., Koopman, L., Violette, S., Bardeesy, N., and Settleman, J. (2009). A gene expression signature associated with “K-Ras addiction” reveals regulators of EMT and tumor cell survival. Cancer Cell *15*, 489–500.

Smith, T.A. (2001). The rate-limiting step for tumor [18F]fluoro-2-deoxy-D-glucose (FDG)

incorporation. Nucl. Med. Biol. *28*, 1–4.

Solimini, N.L., Luo, J., and Elledge, S.J. (2007). Non-oncogene addiction and the stress phenotype of cancer cells. Cell *130*, 986–988.

Som, P., Atkins, H.L., Bandoypadhyay, D., Fowler, J.S., MacGregor, R.R., Matsui, K., Oster, Z.H., Sacker, D.F., Shiue, C.Y., Turner, H., et al. (1980). A fluorinated glucose analog, 2-fluoro-2-deoxy-D-glucose (F-18): nontoxic tracer for rapid tumor detection. J. Nucl. Med. *21*, 670–675.

Tee, A.R., Fingar, D.C., Manning, B.D., Kwiatkowski, D.J., Cantley, L.C., and Blenis, J. (2002). Tuberous sclerosis complex-1 and -2 gene products function together to inhibit mammalian target of rapamycin (mTOR)-mediated downstream signaling. Proc. Natl. Acad. Sci. U.S.a. *99*, 13571–13576.

Teske, B.F., Wek, S.A., Bunpo, P., Cundiff, J.K., McClintick, J.N., Anthony, T.G., and Wek, R.C. (2011). The eIF2 kinase PERK and the integrated stress response facilitate activation of ATF6 during endoplasmic reticulum stress. Mol. Biol. Cell *22*, 4390–4405.

The, I., Murthy, A.E., Hannigan, G.E., Jacoby, L.B., Menon, A.G., Gusella, J.F., and Bernards, A. (1993). Neurofibromatosis type 1 gene mutations in neuroblastoma. Nat. Genet. *3*, 62–66.

Thedieck, K., Polak, P., Kim, M.L., Molle, K.D., Cohen, A., Jenö, P., Arrieumerlou, C., and Hall, M.N. (2007). PRAS40 and PRR5-like protein are new mTOR interactors that regulate apoptosis. PLoS ONE *2*, e1217.

Thomas, G.V., Tran, C., Mellinghoff, I.K., Welsbie, D.S., Chan, E., Fueger, B., Czernin, J., and Sawyers, C.L. (2006). Hypoxia-inducible factor determines sensitivity to inhibitors of mTOR in kidney cancer. Nat. Med. *12*, 122–127.

Thorpe, L.M., Yuzugullu, H., and Zhao, J.J. (2015). PI3K in cancer: divergent roles of isoforms, modes of activation and therapeutic targeting. Nat. Rev. Cancer *15*, 7–24.

Torres, E.M., Dephoure, N., Panneerselvam, A., Tucker, C.M., Whittaker, C.A., Gygi, S.P., Dunham, M.J., and Amon, A. (2010). Identification of aneuploidy-tolerating mutations. Cell *143*, 71–83.

Ungerstedt, J.S., Sowa, Y., Xu, W.-S., Shao, Y., Dokmanovic, M., Perez, G., Ngo, L., Holmgren, A., Jiang, X., and Marks, P.A. (2005). Role of thioredoxin in the response of normal and transformed cells to histone deacetylase inhibitors. Proc. Natl. Acad. Sci. U.S.a. *102*, 673–678.

Ungerstedt, J., Du, Y., Zhang, H., Nair, D., and Holmgren, A. (2012). In vivo redox state of human thioredoxin and redox shift by the histone deacetylase inhibitor suberoylanilide hydroxamic acid (SAHA). Free Radic. Biol. Med. *53*, 2002–2007.

Vanhaesebroeck, B., Welham, M.J., Kotani, K., Stein, R., Warne, P.H., Zvelebil, M.J., Higashi, K., Volinia, S., Downward, J., and Waterfield, M.D. (1997). P110delta, a novel phosphoinositide 3-kinase in leukocytes. Proc. Natl. Acad. Sci. U.S.a. *94*, 4330–4335.

Veskoukis, A.S., Tsatsakis, A.M., and Kouretas, D. (2012). Dietary oxidative stress and

antioxidant defense with an emphasis on plant extract administration. Cell Stress Chaperones *17*, 11–21.

Vojtek, A.B., Hollenberg, S.M., and Cooper, J.A. (1993). Mammalian Ras interacts directly with the serine/threonine kinase Raf. Cell *74*, 205–214.

Wallin, J.J., Guan, J., Prior, W.W., Lee, L.B., Berry, L., Belmont, L.D., Koeppen, H., Belvin, M., Friedman, L.S., and Sampath, D. (2012). GDC-0941, a novel class I selective PI3K inhibitor, enhances the efficacy of docetaxel in human breast cancer models by increasing cell death in vitro and in vivo. Clin. Cancer Res. *18*, 3901–3911.

Wang, D., Chu, P.-C., Yang, C.-N., Yan, R., Chuang, Y.-C., Kulp, S.K., and Chen, C.-S. (2012). Development of a novel class of glucose transporter inhibitors. J. Med. Chem. *55*, 3827–3836.

Warne, P.H., Viciana, P.R., and Downward, J. (1993). Direct interaction of Ras and the amino-terminal region of Raf-1 in vitro. Nature *364*, 352–355.

Widemann, B.C. (2009). Current status of sporadic and neurofibromatosis type 1-associated malignant peripheral nerve sheath tumors. Curr Oncol Rep *11*, 322–328.

Widemann, B.C., Dombi, E., Gillespie, A., Wolters, P.L., Belasco, J., Goldman, S., Korf, B.R., Solomon, J., Martin, S., Salzer, W., et al. (2014). Phase 2 randomized, flexible crossover, double-blinded, placebo-controlled trial of the farnesyltransferase inhibitor tipifarnib in children and young adults with neurofibromatosis type 1 and progressive plexiform neurofibromas. Neuro-Oncology *16*, 707–718.

Williams, B.R., Prabhu, V.R., Hunter, K.E., Glazier, C.M., Whittaker, C.A., Housman, D.E., and Amon, A. (2008). Aneuploidy affects proliferation and spontaneous immortalization in mammalian cells. Science *322*, 703–709.

Willumsen, B.M., Christensen, A., Hubbert, N.L., Papageorge, A.G., and Lowy, D.R. (1984). The p21 ras C-terminus is required for transformation and membrane association. Nature *310*, 583–586.

Woo, S.-Y., Kim, D.-H., Jun, C.-B., Kim, Y.-M., Haar, E.V., Lee, S.-I., Hegg, J.W., Bandhakavi, S., Griffin, T.J., and Kim, D.-H. (2007). PRR5, a novel component of mTOR complex 2, regulates platelet-derived growth factor receptor beta expression and signaling. J. Biol. Chem. *282*, 25604–25612.

Wu, J., Williams, J.P., Rizvi, T.A., Kordich, J.J., Witte, D., Meijer, D., Stemmer-Rachamimov, A.O., Cancelas, J.A., and Ratner, N. (2008). Plexiform and dermal neurofibromas and pigmentation are caused by Nf1 loss in desert hedgehog-expressing cells. Cancer Cell *13*, 105–116.

Xu, S., De Veirman, K., Evans, H., Santini, G.C., Vande Broek, I., Leleu, X., De Becker, A., Van Camp, B., Croucher, P., Vanderkerken, K., et al. (2013). Effect of the HDAC inhibitor vorinostat on the osteogenic differentiation of mesenchymal stem cells in vitro and bone formation in vivo. Acta Pharmacol. Sin. *34*, 699–709.

Ying, H., Kimmelman, A.C., Lyssiotis, C.A., Hua, S., Chu, G.C., Fletcher-Sananikone, E.,

Locasale, J.W., Son, J., Zhang, H., Coloff, J.L., et al. (2012). Oncogenic Kras maintains pancreatic tumors through regulation of anabolic glucose metabolism. Cell *149*, 656–670.

Yoshida, H., Haze, K., Yanagi, H., Yura, T., and Mori, K. (1998). Identification of the cis-acting endoplasmic reticulum stress response element responsible for transcriptional induction of mammalian glucose-regulated proteins. Involvement of basic leucine zipper transcription factors. J. Biol. Chem. *273*, 33741–33749.

Yoshida, H., Okada, T., Haze, K., Yanagi, H., Yura, T., Negishi, M., and Mori, K. (2001). Endoplasmic reticulum stress-induced formation of transcription factor complex ERSF including NF-Y (CBF) and activating transcription factors 6alpha and 6beta that activates the mammalian unfolded protein response. Mol. Cell. Biol. *21*, 1239–1248.

Younes, M., Brown, R.W., Stephenson, M., Gondo, M., and Cagle, P.T. (1997a). Overexpression of Glut1 and Glut3 in stage I nonsmall cell lung carcinoma is associated with poor survival. Cancer *80*, 1046–1051.

Younes, M., Ertan, A., Lechago, L.V., Somoano, J., and Lechago, J. (1997b). Human erythrocyte glucose transporter (Glut1) is immunohistochemically detected as a late event during malignant progression in Barrett's metaplasia. Cancer Epidemiol. Biomarkers Prev. *6*, 303–305.

Zehou, O., Fabre, E., Zelek, L., Sbidian, E., Ortonne, N., Banu, E., Wolkenstein, P., and Valeyrie-Allanore, L. (2013). Chemotherapy for the treatment of malignant peripheral nerve sheath tumors in neurofibromatosis 1: a 10-year institutional review. Orphanet J Rare Dis *8*, 127.

Zhang, X.F., Settleman, J., Kyriakis, J.M., Takeuchi-Suzuki, E., Elledge, S.J., Marshall, M.S., Bruder, J.T., Rapp, U.R., and Avruch, J. (1993). Normal and oncogenic p21ras proteins bind to the amino-terminal regulatory domain of c-Raf-1. Nature *364*, 308–313.

Zhao, L., and Vogt, P.K. (2008). Class I PI3K in oncogenic cellular transformation. Oncogene *27*, 5486–5496.

Zhou, R., Tardivel, A., Thorens, B., Choi, I., and Tschopp, J. (2010). Thioredoxin-interacting protein links oxidative stress to inflammasome activation. Nat. Immunol. *11*, 136–140.

Zhu, Y., Ghosh, P., Charnay, P., Burns, D.K., and Parada, L.F. (2002). Neurofibromas in NF1: Schwann cell origin and role of tumor environment. Science *296*, 920–922.

Appendix A: Effective Combination of a Next-Generation HSP90 Inhibitor and an mTOR Inhibitor in Malignant Peripheral Nerve Sheath Tumors

INTRODUCTION

Previous work has demonstrated efficacy of IPI-504, an HSP90 inhibitor, and mTOR inhibition in a genetically engineered mouse model of NF1-deficient MPNSTs as well as KRAS mutant lung cancer (De Raedt et. al 2011, reprinted in Appendix B). This work inspired a clinical trial of IPI-504 and everolimus in *KRAS* mutant non-small cell lung cancer (NCT01427946). This trial was recently completed, with results still pending. However, in any combination therapy there is a concern about combined toxicity in the clinic. Therefore a major goal of this thesis is to develop novel therapies using a variety of different agents that exploit this mechanism (as discussed in Chapter 3).

IPI-504 is a first-generation HSP90 inhibitor derived from the natural compound geldanamycin (Hanson and Vesole, 2009). Rationally designed second-generation inhibitors, which are structurally distinct from first generation 17-AAG derivatives, are now entering clinical trials. Ganetespib (STA-9090) a second-generation inhibitor binds HSP90 in more of its confirmations, in more multi-protein complexes, and has a 50-fold increased affinity for HSP90 relative to 17-AAG. Importantly, while other second-generation inhibitors have shown high ocular toxicity in the clinic, ganetespib does not appear to have this side effect. Here we report that STA-1474, a pro-drug of ganetespib, is effective in combination with rapamycin *in vitro*, and *in vivo*, supporting the clinical development of second-generation HSP90 inhibitors in combination with mTOR inhibitors.

RESULTS

Similar to other ER stress inducing agents, STA-1474 was cytotoxic as a monotherapy in MPNST cells *in vitro* (Figure A–1A). However, the addition of rapamycin leads to cell death at sub-lethal concentrations of STA-1474 (Figure A–1B).

To verify the potential clinical efficacy of this combination, a genetically engineered mouse model of MPNSTs was used. These mice are *Nf1* and *p53* heterozygous and develop

spontaneous MPNSTs. Tumor bearing mice were treated with STA-1474 or STA-1474 in combination with rapamycin. Similar to what was observed with IPI-504, STA-1474 had little effect on tumor growth as a monotherapy. However, when combined with rapamycin, this lead to potent tumor regression, suggesting that ganetespib is a promising agent to combine with mTOR inhibitors in clinical trials (Figure A–1C).

A

Drug	LD50 (nM)
IPI-504	339nM
STA-1474	75nM

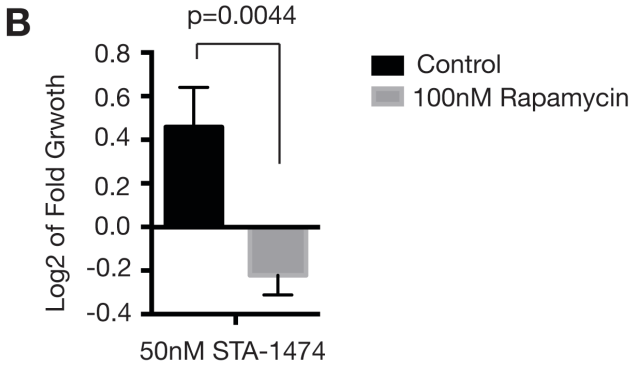

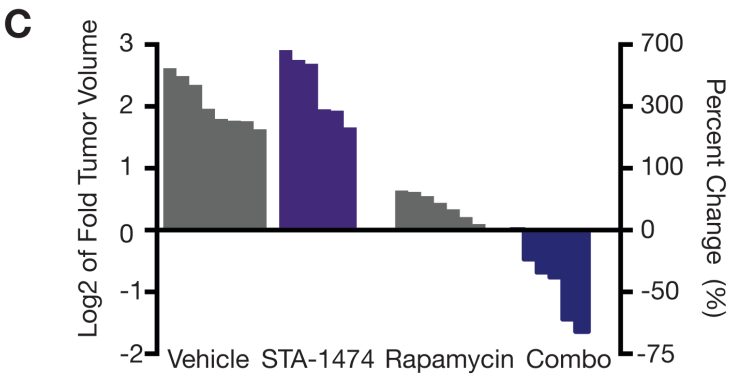

Figure A–1. Second-generation HSP90 Inhibitor STA-1474 Synergizes with mTORC1 Inhibition *in vitro* and *in vivo.* (A) Experimentally determined LD50 for human MPNST cell line S462 for first-generation inhibitor IPI-504 and second-generation inhibitor STA-1474. (B) S462 cells treated were treated with 50nM of STA-1474 +/- 100nM rapamycin for 72 hours. Shown is the log2 of fold change relative to day 0 counts,. (C) Tumor bearing NPCis mice were treated with 50mg/kg STA-1474 once a week (purple) or STA-1474 plus 5mg/kg Rapamycin daily (Combo—blue). Shown is the change in tumor size after 10 days. Left y-axis indicates the log2 of fold change after 10 days, right y-axis indicates percent change in tumor volume. Vehicle and rapamycin (grey) are historical data shown for comparison. Historical data previously published in De Raedt et al, 2011.

DISCUSSION

Here we show that the second-generation HSP90 inhibitor induces a cytotoxic effect on MPNSTs *in vitro* and *in vivo* when combined with the mTORC1 inhibitor rapamycin. We have

previously shown that the geldanamycin derivative IPI-504 is similarly effective, but this work further supports that this is on-target efficacy. IPI-504, like other geldanamycin-derivatives, contains a quinone group which is oxidized by NAD(P)H: quinone oxidoreductase 1 (NQO1). This quinone activity has been reported to induce reactive oxygen species independent of HSP90 inhibition (Dikalov et al., 2002). The efficacy observed with STA-1474, which does not contain a quinone group, demonstrates that HSP90 inhibition is sufficient to induce the therapeutic effect observed, and that the quinone group is not necessary although it may be contributing to IPI-504's efficacy.

Importantly, this quinone activity is also associated with hepatotoxicity. These findings suggest that inhibitors that do not contain the quinone group can be used with similar efficacy, so that hepatotoxicity can be avoided without sacrificing therapeutic benefit.

Together, these findings further support the clinical development of HSP90 inhibitors in combination with mTORC1 inhibitors, and specifically demonstrate that STA-1474, the pro-drug of ganetespib, is effective in the pre-clinical setting. These results lay the groundwork for a Phase I/II clinical trial (NCT02008877) of ganetespib and sirolimus, which is now enrolling.

MATERIALS AND METHODS

Cell Lines and Reagents

S462s were purchased from ATCC. Cells were cultured in Dulbecco's Modified Eagle Medium (DMEM) supplemented with 10% fetal bovine serum and L-glutamine. STA-1474 was generously provided by Synta Pharmaceuticals. Rapamycin was purchased from LC Labs.

Cellular Death Assays

Cells were seeded into 6-well plates at approximately 250,000 cells per-well. 24-hours after plating, cells were counted using a hemocytometer and drug was added as indicated. Final counts were taken after 72 hours.

Drug Treatments and Dosing Schedule

Animal procedures were approved by the Center for Animal and Comparative Medicine in Harvard Medical School in accordance with the NIH Guide for the Care and Use of Laboratory Animals and the Animal Welfare Act. C56/BL6 NPcis mice have been previously described (Cichowski et al., 1999). Mice were treated daily with rapamycin via IP injections at 5 mg/kg prepared as previously described (Johannessen et al 2008). STA-1474 was prepared in PBS and administered via tail vein injection once per week, starting on day 1, at a dose of 50mg/kg. Compounds given in combination were administered sequentially.

Tumor Volume Measurements

Mice were enrolled in the study when tumor size was measured at 300-800 mm3. Tumor size was monitored every 2-3 days via measurement with a Vernier caliper. Tumor volume was then calculated using the standard formula $L \times W^2 \times 0.52$.

Appendix B: *Reprint:* Exploiting Cancer Cell Vulnerabilities to Develop a Combination Therapy for Ras-Driven Tumors

This Appendix contains a reprint of the following publication, in which I performed the experiments shown in Figure 3F, and 4E and F. This publication also provides the basis for the work presented in Chapter 3 of this thesis.

Exploiting Cancer Cell Vulnerabilities to Develop a Combination Therapy for Ras-Driven Tumors. Thomas De Raedt, Zandra Walton, Jessica Yecies, Dana Li, Yimei Chen, Clare F. Malone, Ophélia Maertens, Seung Min Jeong, Roderick T Bronson, Valerie Lebleu, Raghu Kalluri, Emmanuel Normant, Marcia C Haigis, Brendan D. Manning, Kwok-Kin Wong, and Karen Cichowski (2011). *Cancer Cell* 20, 400-413.

Cancer Cell
Article

Exploiting Cancer Cell Vulnerabilities to Develop a Combination Therapy for Ras-Driven Tumors

Thomas De Raedt,[1,2,3] Zandra Walton,[2,4] Jessica L. Yecies,[2,5] Danan Li,[2,4] Yimei Chen,[6] Clare F. Malone,[1,2] Ophélia Maertens,[1,2] Seung Min Jeong,[7] Roderick T. Bronson,[2] Valerie Lebleu,[2,8] Raghu Kalluri,[2,8] Emmanuel Normant,[9] Marcia C. Haigis,[7] Brendan D. Manning,[2,5] Kwok-Kin Wong,[1,2,3] Kay F. Macleod,[6] and Karen Cichowski[1,2,3,*]
[1]Genetics Division, Department of Medicine, Brigham and Women's Hospital, Boston, MA, 02115, USA
[2]Harvard Medical School, Boston, MA, 02115, USA
[3]Ludwig Center at Dana-Farber/Harvard Cancer Center, Boston, MA 02115
[4]Department of Medical Oncology, Dana-Farber Cancer Institute, Boston, MA 02115
[5]Department of Genetics and Complex Diseases, Harvard School of Public Health, Boston, MA 02115
[6]The Ben May Institute for Cancer Research, The University of Chicago, Chicago, IL 60637
[7]Department of Pathology, Harvard Medical School, Boston, MA 02115
[8]Division of Matrix Biology, Beth Israel Deaconess Medical Center, Boston, MA 02115
[9]Infinity Pharmaceuticals, 780 Memorial Drive, Cambridge, MA 02139
*Correspondence: kcichowski@rics.bwh.harvard.edu
DOI 10.1016/j.ccr.2011.08.014

SUMMARY

Ras-driven tumors are often refractory to conventional therapies. Here we identify a promising targeted therapeutic strategy for two Ras-driven cancers: *Nf1*-deficient malignancies and *Kras/p53* mutant lung cancer. We show that agents that enhance proteotoxic stress, including the HSP90 inhibitor IPI-504, induce tumor regression in aggressive mouse models, but only when combined with rapamycin. These agents synergize by promoting irresolvable ER stress, resulting in catastrophic ER and mitochondrial damage. This process is fueled by oxidative stress, which is caused by IPI-504-dependent production of reactive oxygen species, and the rapamycin-dependent suppression of glutathione, an important endogenous antioxidant. Notably, the mechanism by which these agents cooperate reveals a therapeutic paradigm that can be expanded to develop additional combinations.

INTRODUCTION

Although significant advances have been made in developing targeted therapies, identifying treatments for tumors driven by mutations that do not affect a targetable protein represents a major challenge in cancer research. Ras-driven cancers are a classic example of this challenge and despite the fact that Ras signaling has been studied for over 25 years, there are still no effective targeted therapies (Young et al., 2009). Small-molecule inhibitors that target Ras effectors are being evaluated; however, studies suggest that the therapeutic efficacy of single targeted agents may be limited, underscoring the need to identify additional targets and/or more effective drug combinations (Engelman et al., 2008; Young et al., 2009).

To develop new therapies, we initially focused on a distinct subset of Ras-driven tumors: those that possess mutations in the *NF1* tumor suppressor. *NF1* encodes a Ras GTPase-activating protein (RasGAP), which negatively regulates Ras by catalyzing the hydrolysis of Ras-GTP (Martin et al., 1990; Cawthon et al., 1990). Accordingly, *NF1*-deficient tumors are driven by aberrant Ras activation (DeClue et al., 1992; Johannessen et al., 2005). *NF1* mutations underlie neurofibromatosis type 1 (NF1) (Martin et al., 1990; Cawthon et al., 1990) and *NF1* is mutated or suppressed in sporadic glioblastoma (TCGA

Significance

Ras-driven tumors are often refractory to conventional therapies and a clinically effective targeted therapy has not yet been developed. Moreover, in some cancers *KRAS* mutations are used to exclude patients from being treated with specific targeted agents. As such, developing an effective targeted therapy for Ras-driven tumors is an important endeavor. We have identified a promising therapy for two distinct Ras-driven cancers: *Nf1*-deficient nervous system malignancies and *Kras/p53* mutant non-small cell lung cancer (NSCLC). Importantly, these studies have defined a specific drug combination that can now be assessed in patients with these largely untreatable cancers. Moreover, these studies establish a therapeutic paradigm that can be expanded to develop additional drug combinations.

Consortium, 2008; Parsons et al., 2008; McGillicuddy et al., 2009), NSCLC (Ding et al., 2008), and neuroblastoma (Hölzel et al., 2010), demonstrating a broader role for *NF1*-loss in cancer. The most common malignancy associated with NF1 is malignant peripheral nerve sheath tumors (MPNSTs), which are highly aggressive and frequently metastasize. Despite radiation, and in some cases chemotherapy, inoperable tumors rapidly progress and can become lethal within months. As such, identifying an effective treatment for these tumors is critical.

We and others have reported that mTOR is hyperactivated in *NF1*-deficient tumors as a consequence of aberrant Ras signaling (Johannessen et al., 2005, Dasgupta et al., 2005). Using an *Nf1/p53*-mutant MPNST model, we further demonstrated that the mTOR inhibitor rapamycin suppressed tumor growth (Johannessen et al., 2008). However, although the response to rapamycin was potent, effects were cytostatic. Therefore, we have been using this model to develop more effective mTOR-inhibitor-based combination therapies, with the expectation that successful combinations might also be effective in other Ras and/or mTOR-driven tumors.

To identify additional therapeutic agents, we considered drugs that might exploit specific cellular vulnerabilities of cancer cells. In addition to the pro-tumorigenic hallmarks of cancer (Hanahan and Weinberg, 2000), tumor cells often exhibit specific stress-related phenotypes caused by insults such as excessive DNA damage, as well as replicative, metabolic, and proteotoxic stress (Luo et al., 2009). Accordingly, it has been suggested that agents that further enhance or sensitize cancer cells to these stresses could be developed as potential therapies (Luo et al., 2009; Taipale et al., 2010.). In this study we investigated agents that augment proteotoxic or ER (endoplasmic reticulum) stress. ER stress is induced when unfolded proteins accumulate in the ER (Ron and Walter, 2007). Cancer cells frequently exhibit high levels of ER stress caused by factors such as high mutational load, copy number variation, oxidative stress, hypoxia, and nutrient deprivation (Luo et al., 2009; Taipale et al., 2010). Aneuploidy in particular has recently been shown to induce proteotoxic stress in both normal and cancer cells (Tang et al., 2011). Oncogenic *RAS* also causes ER stress (Denoyelle et al., 2006). Once triggered, ER stress activates a signal transduction pathway known as the unfolded protein response (UPR) (Ron and Walter, 2007). The UPR is initially engaged as a protective mechanism to reduce protein accumulation; however, when ER stress levels become insurmountable, cell death ensues (Ron and Walter, 2007). This observation has led to the speculation that agents that further enhance ER stress in vulnerable cancer cells could be developed as anti-cancer therapies (Luo et al., 2009; Tang et al., 2011). In this study we evaluated the therapeutic effects of compounds that augment proteotoxic stress in cancer cells, alone and in combination with mTOR inhibitors, in two Ras-driven mouse tumor models.

RESULTS

MPNSTs Are Sensitive to Agents that Enhance ER Stress

To determine whether MPNSTs might be sensitive to agents that induce ER stress, we first evaluated basal stress levels. MPNSTs are highly aneuploid and are driven by constitutive activation of Ras and therefore might be subject to substantial ER stress. Indeed, ER stress levels were much higher in tumors compared with normal peripheral nerve, as confirmed by three independent markers of UPR activation: BiP upregulation, phosphorylation of eukaryotic translational initiation factor 2α (eIF2α), and accumulation of the spliced active form of XBP-1 (sXBP-1) (Figure 1A) (Ron and Walter, 2007). Next, we assessed the sensitivity of human and mouse MPNSTs to classic ER stress-inducing agents: thapsigargin (an ER calcium ATPase inhibitor) and tunicamycin (a glycosylation inhibitor). Both agents enhanced ER stress (Figure 1B) and triggered cell death at concentrations that did not affect the viability of normal cells (Figure 1C,D), indicating that MPNSTs are hypersensitive to these ER stress-inducing agents.

ER Stress-Inducing Agents Promote Tumor Regression In Vivo but Only When Combined with Rapamycin

Based on the hypersensitivity of MPNST cells to these agents in vitro, we hypothesized that they might promote tumor regression. In the *Nf1/p53* tumor model, animals develop MPNSTs in ~5 months (Cichowski et al., 1999) and survive an average of 10.7 days after tumor detection (Johannessen et al., 2008). Tumor-bearing animals were treated with vehicle, thapsigargin, or rapamycin (Figure 1E). Thapsigargin exhibited minimal efficacy (red bars) and was less potent than rapamycin (yellow bars). This finding was unexpected given the cytotoxic versus cytostatic effects of thapsigargin and rapamycin observed in vitro (Figure 1D) (Johannessen et al., 2008). However, combined rapamycin/thapsigargin treatment triggered rapid tumor regression (green bars; $p = 0.013$). On average tumors shrank 45%; however, some tumors regressed >75% (Figure 1F) and remaining masses were largely comprised of hemorrhage and cellular debris (Figure 1G). Maximal effects were observed within 10 days, although significant tumor regression was detected in 3 days (Figure 1F,G). Extensive long-term survival studies were not performed because mice often scratched or bit these rapidly shrinking lesions, resulting in ulceration that necessitated euthanasia. Nevertheless, when animals were successfully treated for a longer duration, tumors did not re-grow (Figure 1F). One animal survived 107 days after tumor development with no evidence of relapse, surviving more than 10 times as long as control animals (Figure 1F,G). Tunicamycin also induced tumor regression when co-administered with rapamycin, consistent with the conclusion that excessive ER stress was a critical driver of this response (Figure S1).

The HSP90 Inhibitor IPI-504 Cooperates with Rapamycin to Promote Tumor Regression

Although these observations were striking, thapsigargin and tunicamycin do not represent clinically viable agents. HSP90 inhibitors are another class of drugs known to induce ER stress and are currently being investigated in the clinic (www.clinicaltrials.gov). HSP90 maintains protein homeostasis by folding newly synthesized and misfolded proteins, assembling and dissembling protein complexes, and resolving protein aggregates (Whitesell and Lindquist, 2005). HSP90 also directly stabilizes two key stress-sensing components of the UPR: IRE1 and pPERK/PERK (Marcu et al., 2002). Therefore, HSP90 inhibitors would be expected to promote ER stress in cancer cells via two cooperating mechanisms: first, by directly

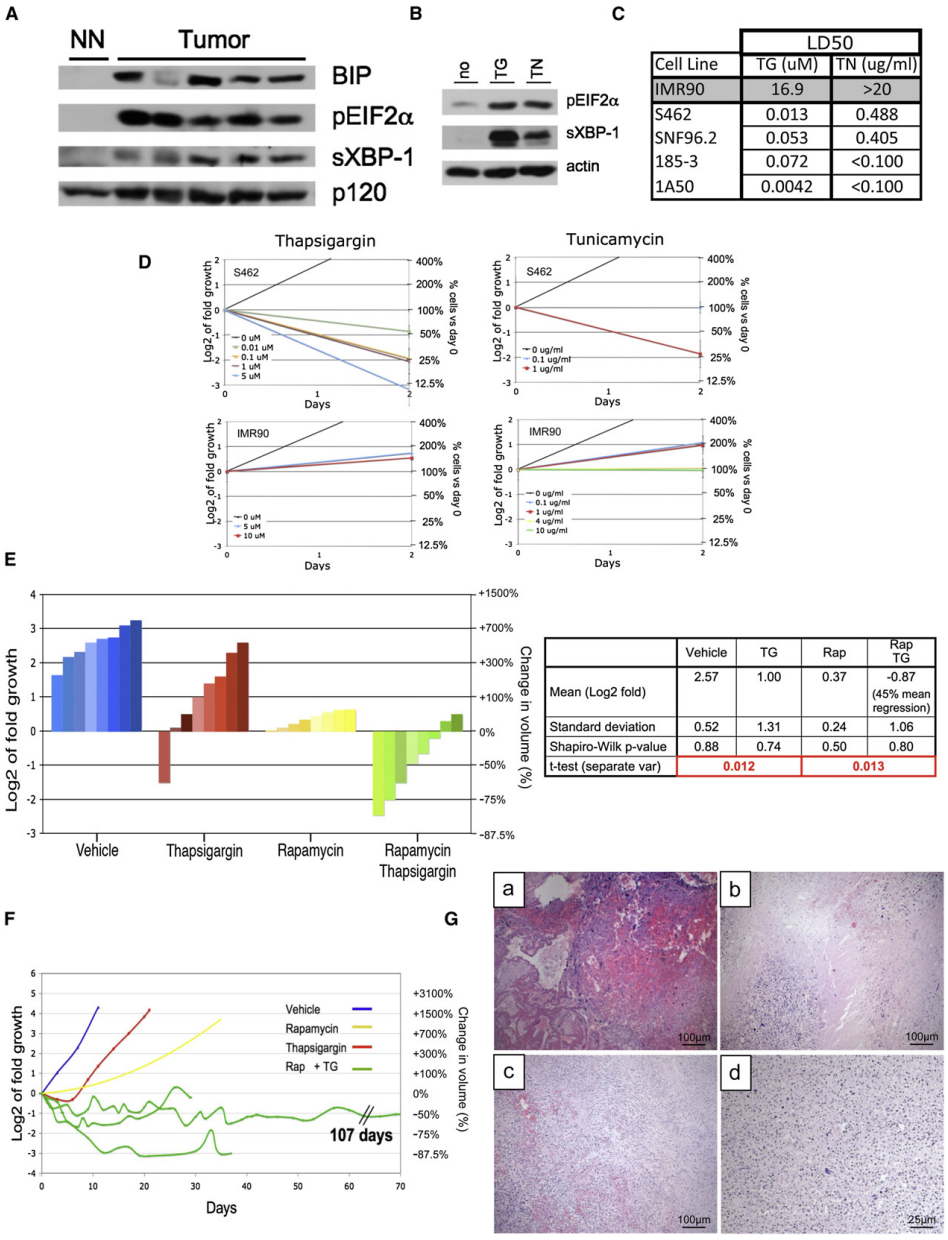

Figure 1. Therapeutic effects of rapamycin and ER stress-inducing agents on MPNSTs

(A) Immunoblots of tumor tissue derived from *Nf1/p53* mutant murine MPNSTs and normal peripheral nerve (NN). BIP, phospho-EIF2a (pEIF2α), and the spliced form of XBP-1 (sXBP-1) indicate UPR activation.

(B) Immunoblots of pEIF2α and sXBP-1 in MPNST cells after 4 hr of 100 nM thapsigargin (TG) or 0.5 μg/ml tunicamycin (TN). Actin is a loading control.

impairing global protein folding in these already compromised tumor cells, and second, by inactivating subsequent adaptive responses provided by two arms of the UPR. Accordingly, we assessed the therapeutic effects of IPI-504, a hydroquinone hydrochloride salt of the geldanamycin-derivative 17-AAG (Sydor et al., 2006).

As predicted, IPI-504 rapidly induced ER stress and activated the UPR, demonstrated by the upregulation of BiP, pEIF2α, sXBP-1, IRE1, and phosphorylated PERK within 2–4 hr (Figure 2A) (Healy et al., 2009). However, prolonged exposure to IPI-504 resulted in a destabilization of IRE1 and pPERK/PERK (Figure 2A). Consequently, downstream UPR signals including sXBP-1 and pEIF2α were inactivated by 8 hr, as expected (Marcu et al., 2002) (Figure 2A). Notably, BiP levels, which are not dependent on IRE1 and PERK, were elevated further by 16 hr, demonstrating that ER stress was enhanced in two phases in response to IPI-504 (Figure 2A) (Marcu et al., 2002). Similar to thapsigargin and tunicamycin, MPNST cells were sensitive to low doses of IPI-504 in vitro (Figure 2B,C).

Using a previously established dosing schedule of IPI-504 (Douglas et al., 2009), we assessed the effects of this agent alone and in combination with rapamycin in vivo. Like thapsigargin, IPI-504 was unable to promote tumor regression as a single agent but did so when combined with rapamycin (Figure 2D) ($p = 0.001$). On average, tumors shrank 49% (Figure 2D, green bars). Tumor regression was visually apparent (Figure 2E) and histological analysis revealed massive cell death and accumulating debris (Figure 2F).

The pharmacodynamic response to IPI-504 in clinical trials is assessed by measuring HSP70 levels, which increase when HSP90 is effectively inhibited (Ramanathan et al., 2007). Target inhibition was confirmed in vivo using this readout (Figure 2G). Rapamycin also effectively suppressed the mTOR pathway (Figure 2G). Maximal tumor regression in response to rapamycin/IPI-504 treatment occurred within 3–5 days and no toxicity was observed in the course of this study as determined by weight, grooming, or body score (Figure S2). TUNEL staining was apparent within 16 hr, which was not observed in tumors from animals exposed to rapamycin or IPI-504 alone (Figure 2H). To mimic the dose of IPI-504 used in clinical trials, IPI-504 was administered once rather than twice per week at 100 mg/kg. This treatment schedule also promoted tumor shrinkage and significantly prolonged survival (Figure 2I) ($p = 8.9 \times 10^{-5}$). This Kaplan-Meier curve likely underestimates survival, because most animals were euthanized because of self-inflicted damage at the site of residual lesions (denoted by Xs) (Figure 2I). No long-term toxicity was observed as determined after 50 days of treatment.

IPI-504 Mediates its Therapeutic Effects by Suppressing HSP90 and Promoting ER Stress

HSP90 is encoded by more than one gene, is extremely abundant, and interacts with more than 20 co-chaperones (Taipale et al., 2010). Therefore, it is not possible to completely inactivate HSP90 activity by genetically suppressing a single gene. However, two additional structurally distinct HSP90 inhibitors, BEP800 and AUY-922 (Massey et al., 2010), as well as 17-AAG itself, killed MPNSTs, induced ER stress, and impacted the UPR with the same kinetics as IPI-504 (Figure 3A, B, C and Figure S3A), confirming that these agents all function by suppressing HSP90.

The observation that HSP90 inhibitors enhance ER stress, and that three distinct ER stress-inducing agents (IPI-504, thapsigargin, tunicamycin) induce the same therapeutic response, supports the hypothesis that IPI-504 mediates its effects by triggering excessive ER stress. To formally address this possibility, we assessed whether ectopic expression of sXBP1, a downstream UPR component that can reduce ER stress (Ozcan et al., 2008), might attenuate the therapeutic effects of IPI-504. Notably, sXBP1 expression reduced and delayed cell death in response to IPI-504 (Figure 3D). Conversely, siRNAs that recognize PERK and IRE1 sensitized MPNSTs to sub-threshold doses of IPI-504 (Figure 3E). Together these data indicate that excessive ER stress plays a causal role in driving the therapeutic response.

Rapamycin sensitized MPNSTs to IPI-504 in vitro as it does in vivo (Figure 3F) and genetic ablation of raptor, a critical component of TORC1, did so as well (Figure 3F). Rapamycin also enhanced the suppressive effects of PERK and IRE1 siRNAs (Figure 3G). However, this combination was not as potent as rapamycin and IPI-504, consistent with the notion that PERK and IRE1 destabilization contribute to the therapeutic response but do not entirely mediate the effects of HSP90 suppression, which has a more global effect on protein homeostasis in these impaired cancer cells. Thus, both genetic and chemical studies demonstrate that IPI-504 and rapamycin function through their intended targets (HSP90 and TORC1) and that ER stress is an important mediator of the therapeutic response. Interestingly, although the proteasome inhibitor bortezomib can induce proteotoxic stress in professional secretory cells (e.g., multiple myeloma cells), bortezomib did not substantially induce ER stress in MPNSTs and did not promote tumor regression when combined with rapamycin (Figure S3B), further underscoring the importance of the ER stress response in mediating the observed therapeutic effects.

The limited clinical efficacy of mTOR inhibitors has been proposed to result from AKT activation that can occur via the

(C) LD50 values in response to TG or TN (48 hr) in normal cells (IMR90), human MPNST cell lines (S462, SNF96.2), and mouse MPNST cell lines (185-3, 1A50).
(D) Growth curves comparing the effects of different doses of thapsigargin and tunicamycin in S462 human MPNSTs and IMR90s.
(E) Waterfall plot depicting tumor growth after 10 days of treatment with vehicle (blue), thapsigargin (red), rapamycin (yellow) and rapamycin/thapsigargin (green). The left *y* axis indicates the log2 of tumor fold growth versus day 0 and the right *y* axis shows the change in fold volume. The table shown reports mean and standard deviation for each treatment arm (n = 8) and mean tumor shrinkage.
(F) Graph depicting the change in tumor size over time. Three animals on the rapamycin/thapsigargin combination are shown (green). For simplicity, the yellow line is an average volume of rapamycin-treated tumors (n = 8). Blue and red lines represent vehicle- and thapsigargin-treated animals, respectively.
(G) H&E-stained tumor remnants from animals treated with rapamycin/thapsigargin. Sections from tumors after (a) 107 days of treatment, (b) 35 days (c), 21 days, and (d) 4 days, showing pyknotic nuclei throughout the tumor. All images were taken using 10x objective, except (d), which has been magnified to 40x. (See also Figure S1.)

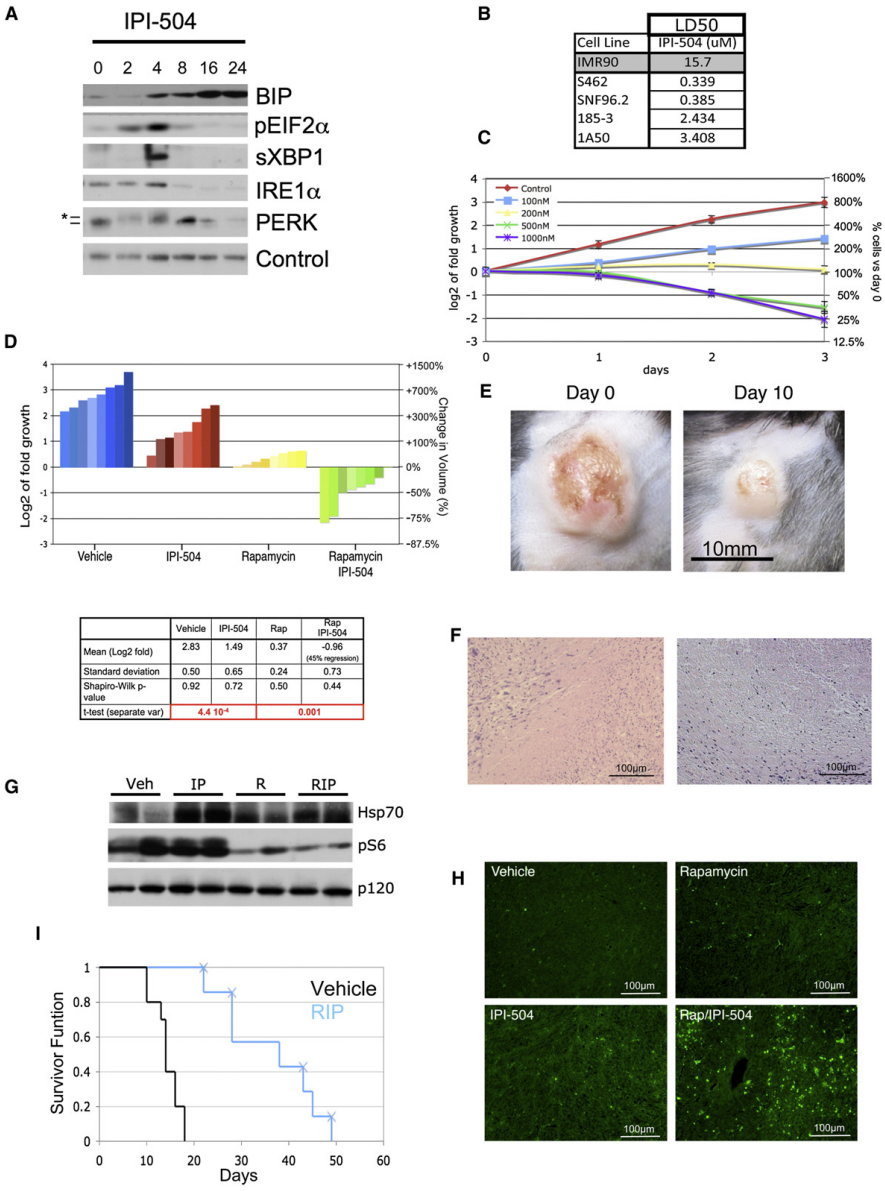

Figure 2. Rapamycin and IPI-504 promote MPNST regression

(A) Immunoblots of BIP, pEIF2α, sXBP-1, IRE1α, and PERK in human MPNSTs treated with IPI-504 over time (hours). Note that the activation of pEIF2α, sXBP1, IRE1, and PERK (*denotes activated phosphorylated PERK) and initial upregulation of BIP occurs within 2–4 hr. A second wave of BIP upregulation occurs between 8 and 16 hr, as pEIF2α, sXBP-1, IRE1α, and PERK become suppressed. Actin serves as a loading control.

(B) LD50 values in response to IPI-504 (72 hr) for normal cells (IMR90), human MPNST cell lines (S462, SNF96.2), and mouse MPNST cell lines (185-3, 1A50).

(C) Growth curves of the S462 cell line treated with different concentrations of IPI-504.

suppression of negative feedback pathways (Dancey et al., 2009). However, as we have previously reported, rapamycin did not induce AKT activation in MPNSTs in vivo (Figure 3H) (Johannessen et al., 2008). Moreover, combined rapamycin/IPI-504 treatment did not suppress AKT phosphorylation or expression levels, indicating that this combination is not more effective because it inhibits AKT (Figure 3H). However, it is still possible that an mTOR kinase inhibitor or dual PI3K/mTOR inhibitor may synergize even more potently with HSP90 inhibitors, by concomitantly suppressing this well-established survival pathway.

Rapamycin and IPI-504 Trigger a Catastrophic Destruction of the ER and Mitochondria in MPNSTs In Vivo

To elucidate the biological consequences of combined rapamycin/IPI-504 treatment, we performed transmission electron microscopy on MPNSTs in vivo. Within 7 hr, rapamycin/IPI-504 induced a massive accumulation of double-membraned vesicles (Figure 4A) (n = 5). These structures exhibited cellular hallmarks of autophagosomes and contained visible cargo (Figure 4B) (Klionsky et al., 2008). The ER and mitochondria can both act as a source of membranes for autophagosomes (Hayashi-Nishino et al., 2009; Ylä-Anttila et al., 2009; Hailey et al. 2010). We detected autophagosomes emerging from both organelles in response to rapamycin/IPI-504, the significance of which is discussed below (Figure 4C). The appearance of autophagic vesicles can be caused by autophagy induction or can occur when productive autophagy is blocked (Klionsky et al., 2008). However rapamycin/IPI-504 induced the degradation of p62/SQSTM1 in these tumors, which is degraded as a consequence of productive autophagy (Figure 4D) (Klionsky et al., 2008). In addition, rapamycin/IPI-504 triggered a rapid increase in LC3-expressing punctae in MPNSTs, which fused with lysozomes shortly thereafter, indicating that autophagy was induced rather than blocked (Figure 4E, F) (N'Diaye et al., 2009; Pankiv et al., 2007). Notably, excessive ER stress actively triggers autophagy, which is engaged as a protective mechanism to degrade unfolded protein aggregates (Hotamisligil, 2010). However, although IPI-504 and rapamycin can both induce signals that promote autophagy, individually each agent was unable to elicit a potent autophagic response in vivo (Figure 4A), suggesting that these agents were somehow synergizing.

To investigate this synergy we examined ER and mitochondria in MPNSTs. Notably, there is a complex interdependent relationship between the ER and mitochondria in response to ER stress (Malhotra and Kaufman, 2007) (Figure 4G). ER stress triggers intraluminal calcium release, which promotes mitochondrial membrane depolarization and ROS production (Malhotra and Kaufman, 2007;Kim et al., 2008). ROS further promotes protein misfolding, thereby enhancing ER stress. In response to low levels of ER stress, adaptive responses are engaged; however, when ER stress levels become insurmountable, a vicious cycle ensues, resulting in catastrophic damage to the ER and mitochondria, and in cell death (Malhotra and Kaufman, 2007). Consistent with the notion that rapamycin and IPI-504 synergize to induce irresolvable ER stress, we observed severe ER swelling within 7 hr (Figure 4H). In addition, we detected a dramatic accumulation of polyubiquitinated protein aggregates, which occur when unfolded proteins accumulate (Figure S4). Interestingly, after 16 hr ER membranes were nearly undetectable in rapamycin/IPI-504-treated tumors (Figure 4I), suggesting that ER membranes may have been depleted by excessive and continuous autophagy emanating from these membranes. Finally, because excessive ER stress ultimately triggers severe mitochondrial damage, after 16 hr mitochondria became swollen and highly vesicularized, and were engulfed by autophagosomes (mitophagy) (Figure 4J). The dramatic effects of combined rapamycin/IPI-504 treatment on autophagy, ER swelling and destruction, and mitochondrial damage were observed in all tumors examined ($\geq$5/5 for each condition) and were not detected in tumors from animals exposed to single agents.

Oxidative Stress Plays a Critical Role in Mediating the Therapeutic Response to Rapamycin and IPI-504

These observations suggest that rapamycin and IPI-504 promote tumor regression by inducing irresolvable ER stress, continuous autophagy, and progressive damage to ER and mitochondria (Figure 4G). Because ROS are thought to play a critical role in fueling this vicious cycle, we assessed the requirement for ROS in the therapeutic response in vitro and in vivo. Importantly, IPI-504 triggered ROS production (Figure 5A) and the antioxidant vitamin C suppressed MPNST cell death by 73% (Figure 5B). More strikingly, when mice were pre-treated with vitamin C, rapamycin/IPI-504 was no longer capable of inducing tumor regression (Figure 5C). Because geldanamycin derivatives may induce ROS via mechanisms in addition to effects on HSP90 (Sreedhar et al., 2003), we evaluated a structurally unrelated HSP90 inhibitor. Notably, BEP800 also induced an increase in ROS production (Figure S5A). Vitamin C also suppressed the therapeutic effects of this agent by 78% (Figure 5D), providing additional evidence that ROS is a general mediator of cell death in response to this class of drugs.

Given the demonstrated importance of ROS, we investigated whether IPI-504 and rapamycin might be synergizing in these tumors by enhancing oxidative stress. PML has been proposed to be an in vivo sensor of oxidative stress, because it becomes

(D) Waterfall plot depicting tumor growth after 10 days of treatment with vehicle (blue), IPI-504 (red), rapamycin (yellow), and rapamycin/IPI-504(green). The left *y* axis indicates the log2 of tumor fold growth versus day 0, and the right *y* axis shows the change in fold volume. The table reports mean and standard deviation for each treatment arm (n = 8) and mean tumor shrinkage. The Shapiro-Wilk test shows that all datasets have a normal distribution.
(E) A photograph of an MPNST is shown at day 0 and after 10 days of treatment with rapamycin/IPI-504.
(F) H&E-stained tumors from animals treated with rapamycin/IPI-504.
(G) Pharmacodynamic analysis of lung tissue after 16 hr of treatment as shown by an Hsp70 and phosphoS6 immunoblots. p120 serves as a loading control.
(H) TUNEL staining of tumors treated for 16 hr.
(I) Kaplan-Meier curve of tumor-bearing *Nf1/p53* mutant mice treated with vehicle (black) or rapamycin (blue) as described. Xs indicate an animal that was euthanized because of skin ulceration. All error bars show ± SD. (See also Figure S2.)

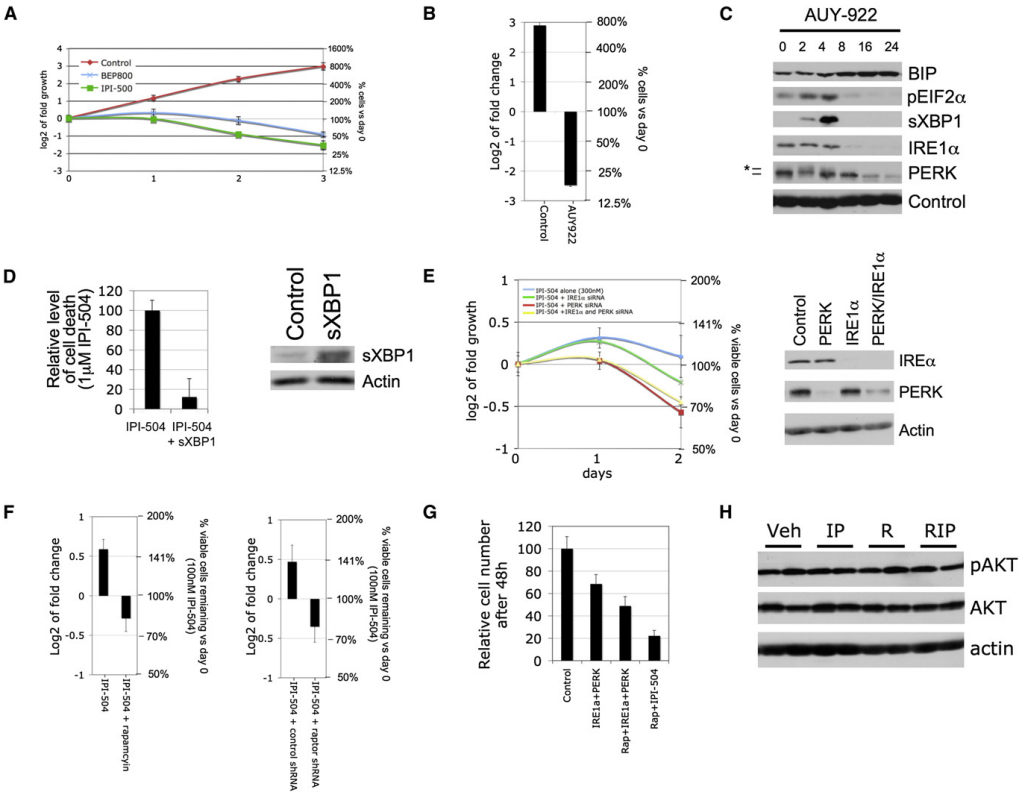

Figure 3. Cell death induced by IPI-504 is caused by inhibition of HSP90 and subsequent effects on the UPR and ER stress

(A) Growth curves of the MPNST cell line S462 treated with two different HSP90 inhibitors (500nM IPI-504 and 500nM BEP800).

(B) S462 cells were treated with the HSP90 inhibitor AUY-922 (100 nM) for 72 hr. The left *y* axis indicates the log2 of tumor fold change versus day 0 and the right *y* axis shows the relative change in cell number compared with day 0.

(C) Immunoblots showing the effects of AUY-922 on BIP, pEIF2α, sXBP-1, IRE1α, and PERK in human MPNST cells over time (hr). Actin serves as a loading control.

(D) Relative level of cell death in the presence of 1 μM IPI-504 with and without overexpression of sXBP1 (the activated spliced form of XBP1). The right hand panel confirms expression of sXBP1.

(E) Growth curves in response to low doses of IPI-504 in cells where IRE1α and/or PERK are knocked down by siRNA. The immunoblot confirms knock down.

(F) S462 cells were treated with 100nM IPI-504 for 72 hr, with and without rapamycin pretreatment (100 nM) (left) or Raptor shRNA (right). The left *y* axis indicates the log2 of tumor fold change versus day 0 and the right *y* axis shows the relative change in cell number compared with day 0.

(G) Relative number of S462 cells after combined knock down of IRE1α and PERK with or without rapamycin (100 nM) compared with rapamycin plus IPI-504 (300nM).

(H) pAKT/AKT immunoblots of tumor tissue from animals treated for 16 hr in mice exposed to vehicle (Veh), IPI-504 (IP), rapamycin (R), and rapamycin/IPI-504 (RIP). All error bars show ± SD. (See also Figure S3.)

associated with nuclear bodies in a ROS-dependent manner (Jeanne et al., 2010). Interestingly, only rapamycin/IPI-504 treatment induced the formation of PML-containing nuclear bodies in MPNSTs (Figure 5E), suggesting that rapamycin and IPI-504 together were required to achieve maximal levels of oxidative stress. These results were confirmed by measuring ROS levels in tumor tissue using dihydroethidium (DHE), where ROS was elevated within 7 hr of treatment (Figure 5E). Moreover, vitamin C suppressed the accumulation of polyubiquitin aggregates (Figure S5B), the formation of nuclear PML bodies (Figure S5C), the robust and sustained autophagic response (Figure S5D), ER swelling and destruction, and mitochondrial damage (Figure S5E). Collectively, these results demonstrate that oxidative stress is required for the therapeutic response in vivo. The finding that ER swelling, protein aggregation, and ROS production all occur within 7 hr of treatment (see Figures 4H, 5E, and 5F; Figure S4) and precede ATP depletion and mitochondrial destruction (Figures 5G and 4J), demonstrates that these effects are

triggered by ER stress and are not a secondary consequence of a mitochondrial metabolic collapse. This conclusion is further supported by the observation that sXBP1 expression suppresses cell death (Figure 3D).

Rapamycin and IPI-504 Promote Excessive Oxidative Stress by Inducing ROS and Simultaneously Suppressing the G6PD/Glutathione Antioxidant Pathway

Oxidative stress is caused by an imbalance between ROS production and ROS clearance pathways. Given that IPI-504 stimulates ROS production, we investigated whether rapamycin might be enhancing the effects of IPI-504 by suppressing endogenous antioxidants. Because of its high concentration and central role in maintaining redox state, the reduced form of glutathione (GSH) is one of the most important endogenous cellular antioxidants (Meister and Anderson, 1983). Glutathione reduction is dependent on NADPH, which is primarily produced by the pentose phosphate pathway (PPP). The first and rate-limiting enzyme of the PPP is Glucose 6-phosphate dehydrogenase (G6PD). Accordingly, G6PD plays a well-established role in protecting cells from oxidative stress via its effects on GSH production (Pandolfi et al., 1995; Xu et al., 2010; Efferth et al., 2006). The importance of G6PD in this pathway is highlighted by the observation that hypomorphic mutations in G6PD underlie favism, which causes acute hemolytic anemia in affected individuals exposed to fava beans and other oxidative stressors (Belsey, 1973). Interestingly, a direct connection between G6PD and the mTOR pathway has recently been established. Specifically, G6PD expression can be suppressed by mTOR inhibitors in vitro, through inhibitory effects on the transcription factor SREBP1 (Düvel et al., 2010). Therefore, we examined the components of this pathway (SREBP1, G6PD, GSH) in MPNSTs.

Consistent with cellular studies showing that SREBP1 is regulated by mTOR (Düvel et al., 2010; Porstmann et al., 2008), rapamycin significantly decreased the expression of known SREBP targets including *SREBP1* itself, *ACC*, and *FASN* in vivo within 7 hr (Figure 5H,I). IPI-504 exerted a slightly suppressive effect on *SREBP1*, but together both agents reduced *SREBP1* expression by 92% and effectively suppressed *ACC* and *FASN* (Figure 5H,I). Rapamycin also potently suppressed *G6PD* mRNA levels in MPNST tumor tissue (Figure 5J). However, rapamycin alone had inconsistent effects on G6PD protein levels (Figure 5I), perhaps reflecting a slower turnover of G6PD protein within this short time frame. Nevertheless, rapamycin and IPI-504 together dramatically suppressed both *G6PD* mRNA and protein expression in MPNSTs in vivo (Figure 5I, J). Accordingly, rapamycin/IPI-504 caused a 34% decrease in reduced glutathione levels in these tumors (Figure 5K, $p = 0.003$). The magnitude of this decrease in GSH is particularly significant given that individuals affected by favism similarly exhibit a 34% mean reduction of GSH in red blood cells, which sensitizes these cells to oxidative stressors, resulting in severe protein misfolding and protein aggregate formation (Szeinberg et al., 1958). Finally, to genetically confirm that G6PD can play a functional role in protecting tumor cells from IPI-504-induced oxidative stress, we ectopically expressed G6PD in MPNSTs. Importantly, G6PD suppressed IPI-504-induced MPNST cell death by 50% (Figure 5L). Taken together, these data suggest that rapamycin and IPI-504 synergize by promoting excessive oxidative stress, which is a consequence of both IPI-504-induced ROS production and rapamycin-dependent suppression of G6PD and GSH.

Rapamycin/IPI-504 Promotes Tumor Regression in a Model of *Kras/p53* Mutant NSCLC

To determine whether the efficacy of this combination might extend to *KRAS* mutant tumors, we performed a similar study in a mouse model of NSCLC (Jackson et al., 2005). Notably, NSCLCs are also highly aneuploid, illustrating an additional similarity between these two tumor types. In this model, lung adenocarcinomas are induced by intranasal administration of adenoviral Cre, which causes the concomitant expression of a single $Kras^{G12D}$ allele and loss of *p53* (termed LSL-$Kras^{G12D}$/+; $p53^{fl/fl}$). 8.5–9 weeks after infection, tumor burden was assessed by MRI. Animals were re-imaged 1 week later to assess the rate of tumor growth, and treatment commenced thereafter. In this mixed genetic background, 50%–80% of the tumors were confirmed to be adenocarcinomas within 10 weeks after Cre exposure (DuPage et al., 2009)(Figure S6). Neither rapamycin nor IPI-504 induced tumor regression alone; however, combined rapamycin/IPI-504 treatment resulted in dramatic tumor shrinkage (Figure 6A). 6/8 mice exhibited this potent response and individual responding masses shrunk up to 82% as determined by MRI analysis (Figure 6B). The overall reduction in total tumor volume, which is the sum of numerous independent tumors per mouse, is shown for each animal (Figure 6C). Histological analysis of tumors two weeks after treatment confirmed substantial tumor regression (Figure 6D). However, although tumor regression in response to rapamycin/IPI-504 was robust, three types of tumor remnants were detected. Minimal tumor remnants comprised of a few cells surrounding alveolar space were observed (Figure 6E, *a,b*). Slightly larger remnants surrounding alveoli were also detected (Figure 6E, *c,d*). Finally some lesions, albeit vastly smaller than vehicle, rapamycin, or IPI-504-treated tumors, were found (Figure 6E, *e,f*). However, even in these cases, significant gaps between tumor cells were observed, resulting in increased alveolar space (Figure 6E, *f*) in contrast to the dense, high-grade lesions observed in control animals. Moreover, there was a rapid and qualitatively obvious improvement in breathing in rapamycin/IPI-504-treated animals. The observation that not all tumors exhibit the identical therapeutic response is consistent with the fact that each individual lung tumor in this model represents an independent genetic event. Notably, although combined MEK and PI3K inhibitors have been shown to promote tumor regression in murine NSCLCs harboring the $Kras^{G12D}$ mutation alone (Engelman et al., 2008), no targeted therapy has been shown to promote the regression of the more aggressive $Kras^{G12D}$, *p53*-deficient tumors, underscoring the significance of this finding and its potential impact on therapeutic development in *KRAS* mutant NSCLC.

DISCUSSION

Currently, there are no effective targeted therapies for Ras-driven cancers. Moreover, in some cancers *KRAS* mutations are used to exclude patients from being treated with specific targeted agents (Karapetis et al., 2008). As such, identifying

a targeted therapy for Ras-driven tumors is an important endeavor. In this study we took an orthogonal therapeutic approach: combining an agent that targets an important downstream oncogenic pathway (mTOR) with agents that capitalize on a cancer-associated cellular vulnerability, specifically the enhanced sensitivity to proteotoxic stress (Luo et al., 2009). Importantly, we found that several agents that induce ER stress, including the HSP90 inhibitor IPI-504, cooperated with rapamycin to promote dramatic tumor regression in two distinct Ras driven-cancers. To date, no targeted agents have been shown to be capable of causing tumor regression in either of these highly aggressive genetically engineered models or, more importantly, in cognate human tumors. Given that these human cancers are generally refractory to standard therapies there is an urgent need to develop improved treatments. Thus, these studies have identified a promising therapeutic strategy for these two aggressive malignancies.

However, although we found that this combination was effective in two specific Ras-driven cancers, it will be important to determine whether its efficacy will extend to other Ras-driven tumors, other mTOR-driven tumors, and/or other tumors that exhibit high levels of ER stress. Our data suggest that a combination of these factors will be involved and that responsive tumors will require some dependence on mTOR and will also exhibit high levels of ER stress. On a molecular level, mutations in *RAS*, *NF1*, and possibly other genes that affect the mTOR pathway, may promote sensitivity to these combined agents. However, other variables, such as the extent of aneuploidy or copy number variation will likely impact the therapeutic response due to direct effects on basal ER stress levels. The recent observation that aneuploidy confers sensitivity to proteotoxic agents in normal cells, and cancer cells in some settings, supports this hypothesis (Tang et al., 2011).

Finally, although these studies provide compelling data to support the clinical investigation of rapamycin and IPI-504, they also serve as a foundation for developing combinations using other related agents. For example, mTOR kinase or dual mTOR/PI3K inhibitors may enhance the efficacy of this combination. Similarly, there are several structurally unrelated HSP90 inhibitors in clinical development, which should provide an array of compounds that may differ in efficacy and/or toxicity. Moreover, the mechanism by which IPI-504 and rapamycin cooperate reveals an even broader range of drug options. For example, other agents that enhance proteotoxic stress and/or alter the heat shock response could be combined with agents that either suppress antioxidant pathways or further stimulate ROS production. In this respect it is noteworthy that ROS production is thought to play a functional role in mediating the cytoxic effects of many conventional chemotherapies. However, targeted agents may prove to be more effective if they are better tolerated and consequently confer a greater therapeutic index. Regardless, the potential utility of these agents may be overlooked if they are assessed exclusively as monotherapies in genetically heterogeneous tumors, where individually they may exhibit minimal activity. Indeed, none of the single agents investigated in this study exerted a cytotoxic response when administered individually. Moreover, our studies suggest that potential drug combinations need to be tested empirically in rigorous models in vivo. For example, although the proteasome inhibitor bortezomib can induce proteotoxic stress in professional secretory cells (e.g., multiple myeloma cells), bortezomib did not substantially induce ER stress in MPNSTs and therefore did not promote tumor regression when combined with rapamycin. These observations highlight the challenge of developing effective combination therapies and underscore the utility of using robust animal to rapidly identify the most effective drug combinations among numerous possibilities.

EXPERIMENTAL PROCEDURES

Cell Lines and Reagents

S462, SNF96.2, and IMR90s (ATCC). 1A50 and 237-1 are mouse *Nf1/p53*-deficient MPNST cell lines (Johannessen et al., 2008). Antibodies were obtained from the following sources: Cell Signaling Technologies: pAKT (4060), AKT (9272), pEIF2α (3557), pS6 (2211), total S6 (2317), BIP (3183), FASN (3180), ACC (3676) and IREα (3294), PERK (3192); Anti-p120 (G12920) (Trans. Labs); Hsp70 (Sc24) and p62 (sc-10117) (Santa Cruz Biotechnology); actin (A2066) (Sigma); XBP-1 (619502) (Biolegend); poly-Ub (FK1)(Biolegend Int); PML (05-718)(Millipore); G6PD (A300-404A)(Bethyl Labs). IPI-504 and IPI-504 vehicle were supplied by Infinity Pharmaceuticals; Thapsigargin, tunicamycin 17-AAG and ascorbic acid (Vitamin C) (Sigma); BEP800 (Selleck Chemicals); AUY922 (Chemietek); Rapamycin (LC Labs).

Real-Time PCR

Tissues were crushed using an in-liquid-nitrogen-cooled Bessman Tissue Pulverizer and dissolved in Trizol reagent (Invitrogen). RNA was treated with DNaseI (Roche) and reverse-transcribed using the qScript Reverse transcriptase kit (Quanta). Real-time PCR analysis was performed using the PerfeCTa SYBR Green kit (Quanta) for the following genes: mouse *G6PDx* (5′-cctacc atctggtggctgtt-3′ 5′-tggctttaaagaagggctca-3′); human *G6PD* (5′-aagaacgtgaa gctccctga-3′ 5′-aatataggggatgggcttgg-3′); mouse *SREBP1* (5′-gatcaaagagga gccagtgc-3′ 5′-tagatggtggctgctgagtg-3′); human *SREBP1* (5′-tgcattttctgacac gcttc-3′ 5′- ccaagctgtacaggctctcc-3′).

RNAi

Non-targeting siRNAs and siRNAs against PERK were purchased from Dharmacon (D-001810-10-05 and L-004883-00 respectively); siRNA targeting IREα (QIAGEN, S100605248). siRNAs were transfected using lipofectamine RNAiMAX from Invitrogen. A lentiviral pLKO vector containing the following shRNA (5′-CGACTACTACATCTCCGTGTA-3′) was used to target Raptor.

(E) S462 cells were infected with mCherry-EGFP-LC3B and treated for 2 and 8 hr with 100nM rapamycin and 4 μM IPI-504. Yellow/green spots punctae represent autophagosomes. Red spots represent autophagolysosomes.
(F) Bar graph representing the average number of autophagosomes (yellow bar) and autophagolysosomes (red bar) after 0, 2, and 8 hr of treatment of rapamycin and IPI-504.
(G) Model illustrating cross-talk between ER stress, mitochondria, and ROS production.
(H) TEM depicting the relative size of the ER in tumors exposed to vehicle, IPI-504, rapamycin, or rapamycin/IPI-504.
(I) TEM showing numerous ER membranes in rapamycin-treated tumors (blue dots) in contrast to tumors exposed to rapamycin/IPI-504 for 16 hr, where they are not visible. Black arrows show a few autophagosomes in rapamycin-treated tumors and many in rapamycin/IPI-504-treated tumors.
(J) TEM showing normal mitochondria in vehicle-treated tumors (blue arrows, left) versus swollen vesicularized mitochondria in tumors treated with rapamycin/IPI-504 for 16 hr (blue arrows, right). The mitochondria on the left in this panel are being engulfed by an autophagosome. (See also Figure S4.)

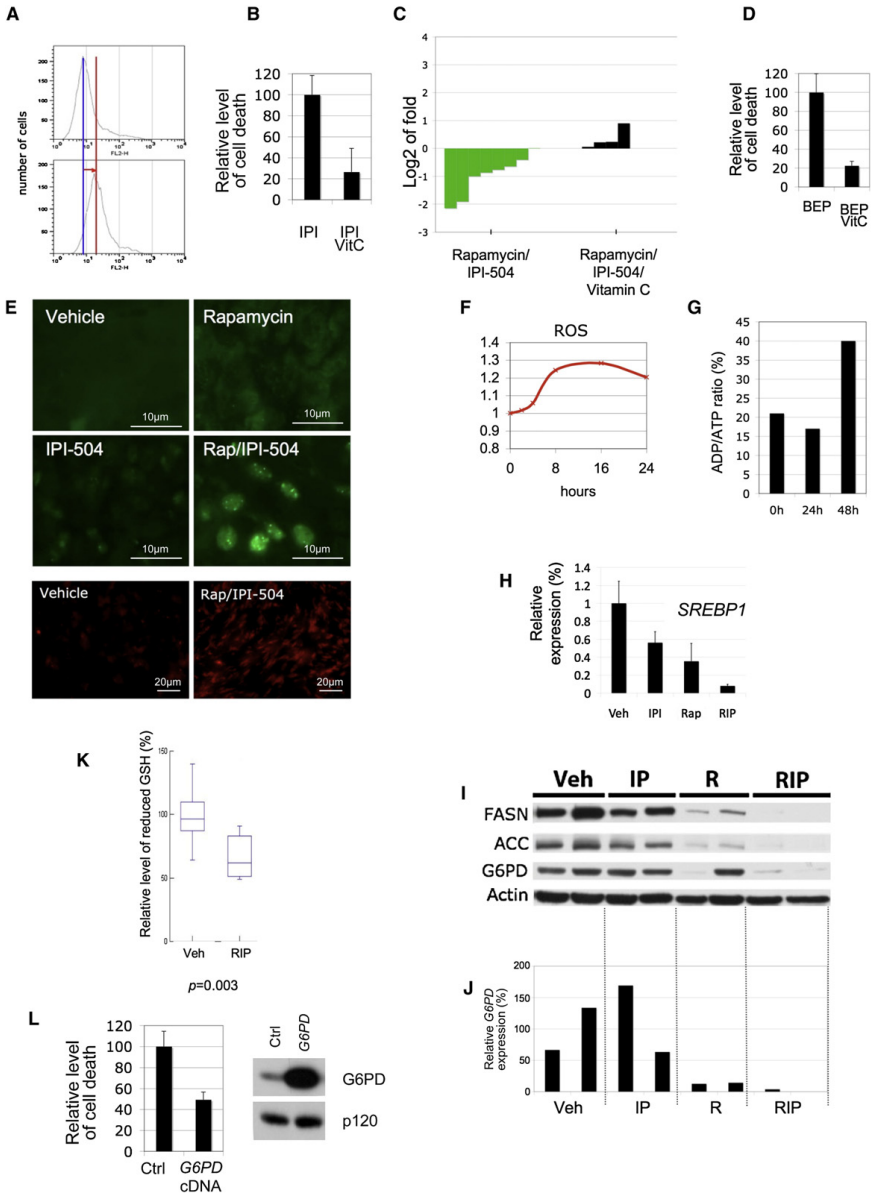

Figure 5. Oxidative stress plays a critical role in mediating the therapeutic response to IPI-504 and rapamycin

(A) Levels of ROS induced by IPI-504 in MPNST cell lines in vitro. The red line depicts the shift in fluorescence intensity, reflecting ROS production.

(B) Relative levels of cell death in the presence of 500nM IPI-504 ± 100 uM vitamin C.

(C) Waterfall plot depicting tumor growth after 10 days of treatment with rapamycin/IPI-504 as shown in Figure 2 (green) versus rapamycin/IPI-504 and vitamin C (black). The left *y* axis indicates the log2 of tumor fold growth versus day 0.

(D) Relative levels of cell death in response to 500nM BEP800 ± 100 uM vitamin C.

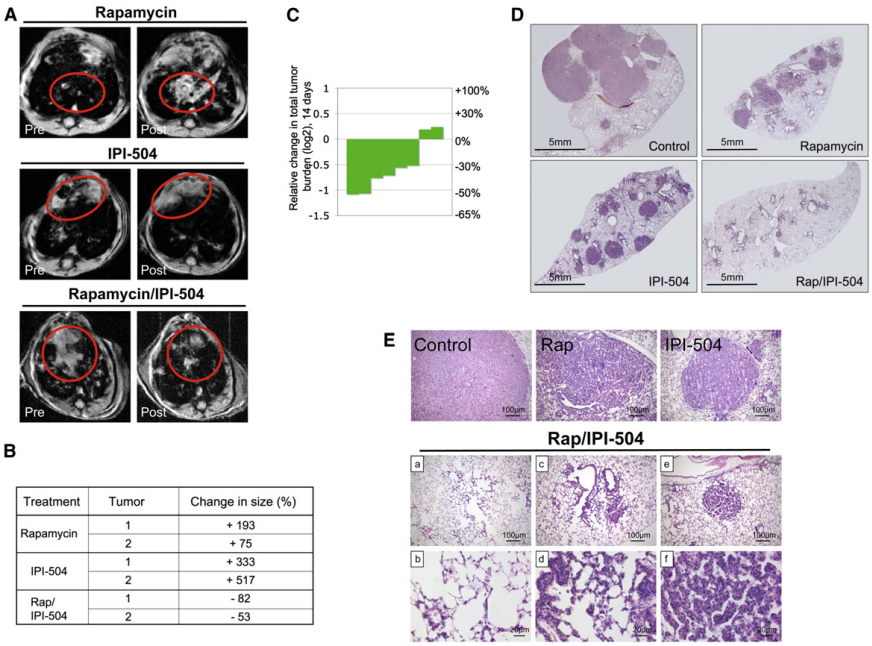

B

Treatment	Tumor	Change in size (%)
Rapamycin	1	+ 193
	2	+ 75
IPI-504	1	+ 333
	2	+ 517
Rap/ IPI-504	1	- 82
	2	- 53

Figure 6. Rapamycin/IPI-504 promotes regression of *Kras*^{G12D}, *p53*-deficient NSCLC

(A) MRI images of animals pre- and post-treatment as specified. The red circles highlight tumor masses.

(B) Table listing the volumetric change of individual tumor masses as determined by MRI.

(C) Waterfall plot depicting the reduction of total tumor volume in individual animals treated with rapamycin and IPI-504.

(D) H&E stain of histological sections of the lung after 14 days of treatment (2x).

(E) H&E stain of lesions from animals treated with vehicle, rapamycin, IPI-504, or rapamycin/IPI-504 for 2 weeks. Images b, d, and f are enlargements of images a, c, and e, respectively. (See also Figure S6.)

Immunofluorescence

Tissues were fixed in formalin and embedded in paraffin. A standard immunofluorescence protocol was followed. Antigen unmasking was performed by boiling the slides in 10mM citrate (pH 6) for 10 min followed by 30 min cooling. Blocking and hybridization were performed in 1x PBS with 5% serum and 0.3% Triton X-100. Antibodies were diluted 1:250.

TUNEL Staining, ROS detection, GSH assay, and ADP/ATP Ratio

TUNEL staining was performed with the ApopTag Fluorescein In Situ Apoptosis Detection Kit (Millipore). Reactive oxygen species were evaluated by MitoSOX Red (M36008) in vitro and by dihydroethidium staining in snap-frozen tumor sections (D11347) (both Invitrogen). GSH was measured using the GSH-glo Glutathione Assay Kit (Promega, V6911). The ADP/ATP ratio was determined using the ApoSENSOR ADP/ATP Ratio Assay Kit (K255-200) (Biovision).

Constructs

Human G6PD (Open Biosystems) and mouse sXBP-1 were cloned into a pLenti CMV/TO Puro vector. The pBabe-puro mCherry-EGFP-LC3B construct was obtained from Addgene. Lentiviral and retroviral infections were performed as previously described (Johannessen et al., 2005).

Drug Treatment and Dosing Schedule

Animal procedures were approved by the Center for Animal and Comparative Medicine in Harvard Medical School in accordance with the NIH Guild for the Care and Use of Laboratory Animals and the Animal Welfare Act. IPI-504

(E) (Top 4 panels) Immunocytochemistry using a PML antibody (green) on tumors treated for 7 hr as indicated. (Bottom 2 panels) Dihydroethidium staining (red) of frozen MPNST tumor tissue depicting an increase in ROS levels in response to Rap/IPI-504 after 7 hr of treatment.

(F) Kinetics of ROS induction in S462 cells in response to IPI-504/Rap.

(G) Kinetics of the ratio of ADP/ATP in S462 cells in response to IPI-504/Rap. Note that ROS production precedes the increase in ADP/ATP levels (decrease in ATP).

(H) SREBP1 mRNA levels in tumors from animals that were treated for 7 hr as indicated.

(I) Immunoblots showing expression of FASN, ACC, and G6PD in tumors from animals treated for 7 hr as indicated. Actin serves as a loading control.

(J) G6PD mRNA levels in individual tumors treated as described in (I).

(K) Relative levels of reduced glutathione (GSH) in tumors treated with vehicle or rapamycin/IPI-504 (n-6).

(L) Relative levels of cell death caused by IPI-504 in cells ectopically expressing G6PD or a GFP control plasmid. Immunoblot demonstrating G6PD protein levels in MPNSTs used in the left panel. (See also Figure S5.)

(100 mg/kg) was administered once or twice weekly. Thapsigargin (0.2 mg/kg) and tunicamycin (0.2 mg/kg) were administered twice a week. Rapamycin was administered daily at 5 mg/kg (Johannessen et al., 2008). Compounds given in combination were administered sequentially. Mice were treated daily with 40 mg/kg vitamin C by oral gavage before IP injections of rapamycin and IPI-504.

Tumor Volume Measurements

MPNST Model:

Mice were enrolled in the study when tumor size reached 300–700mm^3. Tumor size was measured every 2–3 days by Vernier calipers. Tumor volume was calculated using the standard formula $L \times W^2 \times 52$. Tumor volume and log2 of fold growth versus day 0 were calculated and graphed.

Lung Cancer Model:

Mice were infected with Adenoviral Cre (University of Iowa) by nasal instillation (Jackson et al., 2005). Tumor burden was determined by MRI 8 weeks after inhalation and again 1 week later (Engelman et al., 2008). Nine weeks after inhalation, tumor-bearing mice were divided into cohorts and were treated with single or double agents for 2 weeks. Lung tissues were harvested for histopathology after the last MRI. Fixed lung tissues were stained by H&E; tumor burden was subsequently analyzed using the ImageJ software (NIH).

EM

Tumor tissues were fixed for EM after 7 and 16 hr of a single dose and further processed for standard EM techniques (Barth et al., 2010).

Statistics

All statistical analysis was performed using SYSTAT 12 software. For each dataset, basic statistical values (mean and standard deviation) were calculated and normality determined (Shapiro-Wilk normality test); all datasets were normally distributed. Thapsigargin and IPI-504 were compared with vehicle-treated tumors; rapamycin/thapsigargin and rapamycin/IPI-504 were compared with rapamycin-only-treated tumors all by Student's t test. Survival analysis was analyzed using the Mandel method. For the comparison of lung tumor burden in the lung cancer model we performed an ANOVA test, followed by Student's t test.

SUPPLEMENTAL INFORMATION

Supplemental Information includes six figures and can be found with this article online at doi:10.1016/j.ccr.2011.08.014.

ACKNOWLEDGMENTS

We thank Wade Harper, Steve Elledge, Nathanael Gray, Heather Harding, and Hugues de Thé for helpful discussions. This work was supported by the NCI KC: (CA129814) and the Ludwig Center at DF/HCC; KWW: (CA122794, CA140594). TD is a recipient of the Young Investigator Award of the Children's Tumor Foundation. OM is a Postdoctoral Fellow of the Research Foundation Flanders (FWO).

Received: December 7, 2010
Revised: May 27, 2011
Accepted: August 12, 2011
Published: September 12, 2011

REFERENCES

TCGA Consortium; Cancer Genome Atlas Research Network. (2008). Comprehensive genomic characterization defines human glioblastoma genes and core pathways. Nature *455*, 1061–1068.

Barth, S., Glick, D., and Macleod, K.F. (2010). Autophagy: assays and artifacts. J. Pathol. *221*, 117–124.

Belsey, M.A. (1973). The epidemiology of favism. Bull. World Health Organ. *48*, 1–13.

Cawthon, R.M., Weiss, R., Xu, G.F., Viskochil, D., Culver, M., Stevens, J., Robertson, M., Dunn, D., Gesteland, R., O'Connell, P., et al. (1990). A major segment of the neurofibromatosis type 1 gene: cDNA sequence, genomic structure, and point mutations. Cell *62*, 193–201.

Cichowski, K., Shih, T.S., Schmitt, E., Santiago, S., Reilly, K., McLaughlin, M.E., Bronson, R.T., and Jacks, T. (1999). Mouse models of tumor development in neurofibromatosis type 1. Science *286*, 2172–2176.

Dancey, J.E., Curiel, R., and Purvis, J. (2009). Evaluating temsirolimus activity in multiple tumors: a review of clinical trials. Semin. Oncol. *36* (*Suppl 3*), S46–S58.

Dasgupta, B., Yi, Y., Chen, D.Y., Weber, J.D., and Gutmann, D.H. (2005). Proteomic analysis reveals hyperactivation of the mammalian target of rapamycin pathway in neurofibromatosis 1-associated human and mouse brain tumors. Cancer Res. *65*, 2755–2760.

DeClue, J.E., Papageorge, A.G., Fletcher, J.A., Diehl, S.R., Ratner, N., Vass, W.C., and Lowy, D.R. (1992). Abnormal regulation of mammalian p21ras contributes to malignant tumor growth in von Recklinghausen (type 1) neurofibromatosis. Cell *69*, 265–273.

Denoyelle, C., Abou-Rjaily, G., Bezrookove, V., Verhaegen, M., Johnson, T.M., Fullen, D.R., Pointer, J.N., Gruber, S.B., Su, L.D., Nikiforov, M.A., et al. (2006). Anti-oncogenic role of the endoplasmic reticulum differentially activated by mutations in the MAPK pathway. Nat. Cell Biol. *8*, 1053–1063.

Ding, L., Getz, G., Wheeler, D.A., Mardis, E.R., McLellan, M.D., Cibulskis, K., Sougnez, C., Greulich, H., Muzny, D.M., Morgan, M.B., et al. (2008). Somatic mutations affect key pathways in lung adenocarcinoma. Nature *455*, 1069–1075.

Douglas, M., Lim, A.R., Porter, J.R., West, K., Pink, M.M., Ge, J., Wylie, A.A., Tibbits, T.T., Biggs, K., Curtis, M., et al. (2009). The antiproliferative activity of the heat shock protein 90 inhibitor IPI-504 is not dependent on NAD(P)H:quinone oxidoreductase 1 activity in vivo. Mol. Cancer Ther. *8*, 3369–3378.

DuPage, M., Dooley, A.L., and Jacks, T. (2009). Conditional mouse lung cancer models using adenoviral or lentiviral delivery of Cre recombinase. Nat. Protoc. *4*, 1064–1072.

Düvel, K., Yecies, J.L., Menon, S., Raman, P., Lipovsky, A.I., Souza, A.L., Triantafellow, E., Ma, Q., Gorski, R., Cleaver, S., et al. (2010). Activation of a metabolic gene regulatory network downstream of mTOR complex 1. Mol. Cell *39*, 171–183.

Efferth, T., Schwarzl, S.M., Smith, J., and Osieka, R. (2006). Role of glucose-6-phosphate dehydrogenase for oxidative stress and apoptosis. Cell Death Differ. *13*, 527–528, author reply 529–530.

Engelman, J.A., Chen, L., Tan, X., Crosby, K., Guimaraes, A.R., Upadhyay, R., Maira, M., McNamara, K., Perera, S.A., Song, Y., et al. (2008). Effective use of PI3K and MEK inhibitors to treat mutant Kras G12D and PIK3CA H1047R murine lung cancers. Nat. Med. *14*, 1351–1356.

Hailey, D.W., Rambold, A.S., Satpute-Krishnan, P., Mitra, K., Sougrat, R., Kim, P.K., and Lippincott-Schwartz, J. (2010). Mitochondria supply membranes for autophagosome biogenesis during starvation. Cell *141*, 656–667.

Hanahan, D., and Weinberg, R.A. (2000). The hallmarks of cancer. Cell *100*, 57–70.

Hayashi-Nishino, M., Fujita, N., Noda, T., Yamaguchi, A., Yoshimori, T., and Yamamoto, A. (2009). A subdomain of the endoplasmic reticulum forms a cradle for autophagosome formation. Nat. Cell Biol. *11*, 1433–1437.

Healy, S.J., Gorman, A.M., Mousavi-Shafaei, P., Gupta, S., and Samali, A. (2009). Targeting the endoplasmic reticulum-stress response as an anticancer strategy. Eur. J. Pharmacol. *625*, 234–246.

Hölzel, M., Huang, S., Koster, J., Ora, I., Lakeman, A., Caron, H., Nijkamp, W., Xie, J., Callens, T., Asgharzadeh, S., et al. (2010). NF1 is a tumor suppressor in neuroblastoma that determines retinoic acid response and disease outcome. Cell *142*, 218–229.

Hotamisligil, G.S. (2010). Endoplasmic reticulum stress and the inflammatory basis of metabolic disease. Cell *140*, 900–917.

Jackson, E.L., Olive, K.P., Tuveson, D.A., Bronson, R., Crowley, D., Brown, M., and Jacks, T. (2005). The differential effects of mutant p53 alleles on advanced murine lung cancer. Cancer Res. *65*, 10280–10288.

Jeanne, M., Lallemand-Breitenbach, V., Ferhi, O., Koken, M., Le Bras, M., Duffort, S., Peres, L., Berthier, C., Soilihi, H., Raught, B., and de Thé, H. (2010). PML/RARA oxidation and arsenic binding initiate the antileukemia response of As2O3. Cancer Cell *18*, 88–98.

Johannessen, C.M., Johnson, B.W., Williams, S.M., Chan, A.W., Reczek, E.E., Lynch, R.C., Rioth, M.J., McClatchey, A., Ryeom, S., and Cichowski, K. (2008). TORC1 is essential for NF1-associated malignancies. Curr. Biol. *18*, 56–62.

Johannessen, C.M., Reczek, E.E., James, M.F., Brems, H., Legius, E., and Cichowski, K. (2005). The NF1 tumor suppressor critically regulates TSC2 and mTOR. Proc. Natl. Acad. Sci. USA *102*, 8573–8578, Epub 2005 Jun 8573.

Karapetis, C.S., Khambata-Ford, S., Jonker, D.J., O'Callaghan, C.J., Tu, D., Tebbutt, N.C., Simes, R.J., Chalchal, H., Shapiro, J.D., Robitaille, S., et al. (2008). K-ras mutations and benefit from cetuximab in advanced colorectal cancer. N. Engl. J. Med. *359*, 1757–1765.

Kim, I., Xu, W., and Reed, J.C. (2008). Cell death and endoplasmic reticulum stress: disease relevance and therapeutic opportunities. Nat. Rev. Drug Discov. *7*, 1013–1030.

Klionsky, D.J., Abeliovich, H., Agostinis, P., Agrawal, D.K., Aliev, G., Askew, D.S., Baba, M., Baehrecke, E.H., Bahr, B.A., Ballabio, A., et al. (2008). Guidelines for the use and interpretation of assays for monitoring autophagy in higher eukaryotes. Autophagy *4*, 151–175.

Luo, J., Solimini, N.L., and Elledge, S.J. (2009). Principles of cancer therapy: oncogene and non-oncogene addiction. Cell *136*, 823–837.

Malhotra, J.D., and Kaufman, R.J. (2007). Endoplasmic reticulum stress and oxidative stress: a vicious cycle or a double-edged sword? Antioxid. Redox Signal. *9*, 2277–2293.

Marcu, M.G., Doyle, M., Bertolotti, A., Ron, D., Hendershot, L., and Neckers, L. (2002). Heat shock protein 90 modulates the unfolded protein response by stabilizing IRE1alpha. Mol. Cell. Biol. *22*, 8506–8513.

Martin, G.A., Viskochil, D., Bollag, G., McCabe, P.C., Crosier, W.J., Haubruck, H., Conroy, L., Clark, R., O'Connell, P., Cawthon, R.M., et al. (1990). The GAP-related domain of the neurofibromatosis type 1 gene product interacts with ras p21. Cell *63*, 843–849.

Massey, A.J., Schoepfer, J., Brough, P.A., Brueggen, J., Chène, P., Drysdale, M.J., Pfaar, U., Radimerski, T., Ruetz, S., Schweitzer, A., et al. (2010). Preclinical antitumor activity of the orally available heat shock protein 90 inhibitor NVP-BEP800. Mol. Cancer Ther. *9*, 906–919.

McGillicuddy, L.T., Fromm, J.A., Hollstein, P.E., Kubek, S., Beroukhim, R., De Raedt, T., Johnson, B.W., Williams, S.M., Nghiemphu, P., Liau, L.M., et al. (2009). Proteasomal and genetic inactivation of the NF1 tumor suppressor in gliomagenesis. Cancer Cell *16*, 44–54.

Meister, A., and Anderson, M.E. (1983). Glutathione. Annu. Rev. Biochem. *52*, 711–760.

N'Diaye, E.N., Kajihara, K.K., Hsieh, I., Morisaki, H., Debnath, J., and Brown, E.J. (2009). PLIC proteins or ubiquilins regulate autophagy-dependent cell survival during nutrient starvation. EMBO Rep. *10*, 173–179.

Ozcan, U., Ozcan, L., Yilmaz, E., Düvel, K., Sahin, M., Manning, B.D., and Hotamisligil, G.S. (2008). Loss of the tuberous sclerosis complex tumor suppressors triggers the unfolded protein response to regulate insulin signaling and apoptosis. Mol. Cell *29*, 541–551.

Pandolfi, P.P., Sonati, F., Rivi, R., Mason, P., Grosveld, F., and Luzzatto, L. (1995). Targeted disruption of the housekeeping gene encoding glucose 6-phosphate dehydrogenase (G6PD): G6PD is dispensable for pentose synthesis but essential for defense against oxidative stress. EMBO J. *14*, 5209–5215.

Pankiv, S., Clausen, T.H., Lamark, T., Brech, A., Bruun, J.A., Outzen, H., Øvervatn, A., Bjørkøy, G., and Johansen, T. (2007). p62/SQSTM1 binds directly to Atg8/LC3 to facilitate degradation of ubiquitinated protein aggregates by autophagy. J. Biol. Chem. *282*, 24131–24145.

Parsons, D.W., Jones, S., Zhang, X., Lin, J.C., Leary, R.J., Angenendt, P., Mankoo, P., Carter, H., Siu, I.M., Gallia, G.L., et al. (2008). An integrated genomic analysis of human glioblastoma multiforme. Science *321*, 1807–1812.

Porstmann, T., Santos, C.R., Griffiths, B., Cully, M., Wu, M., Leevers, S., Griffiths, J.R., Chung, Y.L., and Schulze, A. (2008). SREBP activity is regulated by mTORC1 and contributes to Akt-dependent cell growth. Cell Metab. *8*, 224–236.

Ramanathan, R.K., Egorin, M.J., Eiseman, J.L., Ramalingam, S., Friedland, D., Agarwala, S.S., Ivy, S.P., Potter, D.M., Chatta, G., Zuhowski, E.G., et al. (2007). Phase I and pharmacodynamic study of 17-(allylamino)-17-demethoxygeldanamycin in adult patients with refractory advanced cancers. Clin. Cancer Res. *13*, 1769–1774.

Ron, D., and Walter, P. (2007). Signal integration in the endoplasmic reticulum unfolded protein response. Nat. Rev. Mol. Cell Biol. *8*, 519–529.

Sreedhar, A.S., Mihály, K., Pató, B., Schnaider, T., Steták, A., Kis-Petik, K., Fidy, J., Simonics, T., Maraz, A., and Csermely, P. (2003). Hsp90 inhibition accelerates cell lysis. Anti-Hsp90 ribozyme reveals a complex mechanism of Hsp90 inhibitors involving both superoxide- and Hsp90-dependent events. J. Biol. Chem. *278*, 35231–35240.

Sydor, J.R., Normant, E., Pien, C.S., Porter, J.R., Ge, J., Grenier, L., Pak, R.H., Ali, J.A., Dembski, M.S., Hudak, J., et al. (2006). Development of 17-allylamino-17-demethoxygeldanamycin hydroquinone hydrochloride (IPI-504), an anti-cancer agent directed against Hsp90. Proc. Natl. Acad. Sci. USA *103*, 17408–17413.

Szeinberg, A., Asher, Y., and Sheba, C. (1958). Studies on glutathione stability in erythrocytes of cases with past history of favism or sulfa-drug-induced hemolysis. Blood *13*, 348–358.

Taipale, M., Jarosz, D.F., and Lindquist, S. (2010). HSP90 at the hub of protein homeostasis: emerging mechanistic insights. Nat. Rev. Mol. Cell Biol. *11*, 515–528.

Tang, Y.C., Williams, B.R., Siegel, J.J., and Amon, A. (2011). Identification of aneuploidy-selective antiproliferation compounds. Cell *144*, 499–512.

Whitesell, L., and Lindquist, S.L. (2005). HSP90 and the chaperoning of cancer. Nat. Rev. Cancer *5*, 761–772.

Xu, Y., Zhang, Z., Hu, J., Stillman, I.E., Leopold, J.A., Handy, D.E., Loscalzo, J., and Stanton, R.C. (2010). Glucose-6-phosphate dehydrogenase-deficient mice have increased renal oxidative stress and increased albuminuria. FASEB J. *24*, 609–616.

Ylä-Anttila, P., Vihinen, H., Jokitalo, E., and Eskelinen, E.L. (2009). 3D tomography reveals connections between the phagophore and endoplasmic reticulum. Autophagy *5*, 1180–1185.

Young, A., Lyons, J., Miller, A.L., Phan, V.T., Alarcón, I.R., and McCormick, F. (2009). Ras signaling and therapies. Adv. Cancer Res. *102*, 1–17.

Appendix C: Supplementary Materials For Chapter 2

This appendix contains supplementary materials for Chapter 2. The figures here were originally published as presented here in the following manuscript:

Defining key therapeutic signaling nodes and therapeutic biomarkers for *NF1*-mutant cancers.

Clare F. Malone*, Jody A. Fromm*, Ophélia Maertens, Thomas DeRaedt, Rachel Ingraham, Karen Cichowski. *Cancer Discovery*. Vol 4 (9) pp. 1062-1073. September 2014. *co-first authors

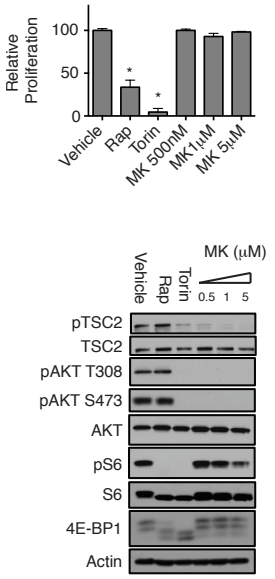

Figure C–1. AKT inhibitors do not slow proliferation of MPNST cells 90-8TL cells were treated with the rapamycin (Rap) at 100nM, Torin1 at 250nM or MK- 2206 (concentration indicated). Bar graph represents the relative change in cell number from day 0 to 96 hours as compared to vehicle treated control cells. Data points show triplicate averages ± SD. Immunoblots show pAKT T308, pAKT S473, pTSC2 T1462, pS6, and 4E-BP1 levels in the presence of the specified inhibitors. AKT, TSC2, S6, and actin serve as controls. * indicates $p<0.00001$

Table C–1. Reported *in vitro* Isoform Specificities of PI3K Inhibitors. Reported *in vitro* isoform specificities of PI3K inhibitors. The IC50 (nM) reported in the literature for each PI3K inhibitor against Class IA catalytic isoforms in *in vitro* binding assays is shown. The source for each data set is listed. A66-(S) is termed a p110α-specific inhibitor, AZD-6482 is classified as a p110β-specific inhibitor, and CAL-101 shows selectivity for p110δ. GDC-0941 does not show significant isoform selectivity.

	Reported *in vitro* IC50 (nM)			
Drug	p110α	p110β	p110δ	Source
A66-(S)	32	>12500	>1250	Jamieson et. al. 2011
AZD-6482	1200	21	80	Nylander et. al. 2012
CAL-101	820	565	2.5	Lannutti et. al. 2010
GDC-0941	3	33	3	Folkes et. al. 2008

Table C–2. Two Class Comparison Between Combination Treated Samples and Controls for other GLUT Proteins and Hexokinase Family. Two class comparison between combination treated samples and controls for the other GLUT proteins and hexokinases. The log2 of fold (combination/control) expression for each gene in the GLUT and hexokinase family are shown, such that negative values indicate a decrease in the combination relative to control, and positive values represent an increase. The p-value for the difference in expression between classes is shown.

Gene Name	Gene Symbol	Log2 of Fold Change	P-value
Glut2	*SLC2A2*	-0.03	0.73
Glut3	*SLC2A3*	-0.07	0.78
Glut4	*SLC2A4*	-0.03	0.87
Glut5	*SLC2A5*	0.15	0.51
Glut6	*SLC2A6*	-0.01	0.97
Glut7	*SLC2A7*	0.06	0.58
Glut8	*SLC2A8*	0.14	0.15
Glut9	*SLC2A9*	0.14	0.30
Glut10	*SLC2A10*	0.43	0.48
Glut12	*SLC2A12*	-0.12	0.59
Glut13	*SLC2A13*	-0.23	0.42
Hexokinase 1	*HK1*	-0.03	0.87
Hexokinase 2	*HK2*	-0.16	0.49
Hexokinase 3	*HK3*	-0.12	0.48